11-3-2008

Elemental Analysis of Biological Matrices by Laser Ablation High Resolution Inductively Coupled Plasma Mass Spectrometry (LA-HR-ICP-MS) and High Resolution Inductively Coupled Plasma Mass Spectrometry (HR-ICP-MS)

Waleska Castro
Florida International University, wacaro@hotmail.com

DOI: 10.25148/etd.FI10022505

FLORIDA INTERNATIONAL UNIVERSITY

Miami, Florida

ELEMENTAL ANALYSIS OF BIOLOGICAL MATRICES BY LASER ABLATION HIGH RESOLUTION INDUCTIVELY COUPLED PLASMA MASS SPECTROMETRY (LA-HR-ICP-MS) AND HIGH RESOLUTION INDUCTIVELY COUPLED PLASMA MASS SPECTROMETRY (HR-ICP-MS)

A dissertation submitted in partial fulfillment of the

requirements for the degree of

DOCTOR OF PHILOSOPHY

in

CHEMISTRY

by

Waleska Castro

2008

To: Dean Kenneth Furton
College of Arts and Sciences

This dissertation, written by Waleska Castro, and entitled Elemental Analysis of Biological Matrices by Laser Ablation High Resolution Inductively Coupled Plasma Mass Spectrometry (LA-HR-ICP-MS) and High Resolution Inductively Coupled Plasma Mass Spectrometry (HR-ICP-MS), having been approved in respect to style and intellectual content, is referred to you for judgment.

We have read this dissertation and recommend that it be approved.

Rosemary Hickey-Vargas

Yong Cai

Bruce McCord

Stanislaw Wnuk

José R. Almirall, Major Professor

Date of Defense: November 3, 2008

The dissertation of Waleska Castro is approved.

Dean Kenneth Furton
College of Arts and Sciences

Dean George Walker
University Graduate School

Florida International University, 2008

DEDICATION

To Jorge, Matthew, family, and friends who I love so much.

ACKNOWLEDGMENTS

I acknowledge my family and friends for their support during this journey of doing the PhD.

I would also like to express my gratitude to the graduate committee: Dr. José R. Almirall, Dr. Yong Cai, Dr. Bruce McCord, Dr. Stanislaw Wnuk, and Dr. Rosemary Hickey-Vargas for their guidance and support during my research. Special thanks to Dr. Almirall for giving me the opportunity of doing science. All these experiences allowed me to grow as a scientist and as a person. I would also have to thank Tatiana Trejos for all the help with the ICP-MS and the SEM/EDS instrumentation, and for her advice.

I would like to acknowledge FIU, the Chemistry and Biochemistry Department, the International Research Forensic Institute, the Dean's office, and the Graduate Student Association for all the support and funding for traveling to the different scientific conferences I had attended to. FIU Graduate School granted me with the 2008 Dissertation Year Fellowship, which allowed me to complete the dissertation work during the last year of my PhD studies. The NITE-CRIME organization provided with the bone standards and with financial support for traveling to the NITE-CRIME workshop in Sitges, Spain. The iron detection limits study was supported by the National Institute of Justice (NIJ), grant 2005-IJ-CX-K069. The HR-SF-ICP-MS was acquired with a National Science Foundation (NSF) Major Research Instrumentation (MRI) award 0420874 to Florida International University.

All this work would not be possible without samples, and for that I'll have to thank Sardiaa Plaud and Dr. Andrew Tyrrell at the JPAC Central Identification Laboratory in Hawaii for the bone samples and for some financial support with the

analytical work of this research. The teeth samples were donated by Major Laura A. Regan, Ph.D., Office of the Armed Forces Medical Examiner.

Last but not least, I would like to thank Tatiana Trejos, María A. Mendoza, Benjamin Naes, Monica Joshi, Patricia Guerra, Hanh Lai, Erika Cahoon, María A. Pérez, Dr. Cleon Barnett, Joseph Gaganon, Dr. Jeannette Perr, Sayuri Umpierrez, and Yisenny Delgado for their friendship.

ABSTRACT OF THE DISSERTATION

ELEMENTAL ANALYSIS OF BIOLOGICAL MATRICES BY LASER ABLATION HIGH RESOLUTION INDUCTIVELY COUPLED PLASMA MASS SPECTROMETRY (LA-HR-ICP-MS) AND HIGH RESOLUTION INDUCTIVELY COUPLED PLASMA MASS SPECTROMETRY (HR-ICP-MS)

by

Waleska Castro

Florida International University, 2008

Miami, Florida

Professor José R. Almirall, Major Professor

The need for elemental analysis of biological matrices such as bone, teeth, and plant matter for sourcing purposes has emerged within the forensic and geochemical laboratories. Trace elemental analyses for the comparison of materials such as glass by inductively coupled plasma mass spectrometry (ICP-MS) and laser ablation ICP-MS has been shown to offer a high degree of discrimination between different manufacturing sources. Unit resolution ICP-MS instruments may suffer from some polyatomic interferences including $^{40}Ar^{16}O^{+}$, $^{40}Ar^{16}O^{1}H^{+}$, and $^{40}Ca^{16}O^{+}$ that affect iron measurement at trace levels. Iron is an important element in the analysis of glass and also of interest for the analysis of several biological matrices. A comparison of the analytical performance of two different ICP-MS systems for iron analysis in glass for determining the method detection limits (MDLs), accuracy, and precision of the measurement is presented. Acid digestion and laser ablation methods are also compared. Iron polyatomic interferences were reduced or resolved by using dynamic reaction cell and high resolution

ICP-MS. MDLs as low as 0.03 μg g^{-1} and 0.14 μg g^{-1} for laser ablation and solution based analyses respectively were achieved. The use of helium as a carrier gas demonstrated improvement in the detection limits of both iron isotopes (^{56}Fe and ^{57}Fe) in medium resolution for the HR-ICP-MS and with a dynamic reaction cell (DRC) coupled to a quadrupole ICP-MS system.

The development and application of robust analytical methods for the quantification of trace elements in biological matrices has lead to a better understanding of the potential utility of these measurements in forensic chemical analyses. Standard reference materials (SRMs) were used in the development of an analytical method using HR-ICP-MS and LA-HR-ICP-MS that was subsequently applied on the analysis of real samples. Bone, teeth and ashed marijuana samples were analyzed with the developed method.

Elemental analysis of bone samples from 12 different individuals provided discrimination between individuals, when femur and humerus bones were considered separately. Discrimination of 14 teeth samples based on elemental composition was achieved with the exception of one case where samples from the same individual were not associated with each other. The discrimination of 49 different ashed plant (cannabis) samples was achieved using the developed method.

TABLE OF CONTENTS

LIST OF TABLES

TABLE PAGE

LIST OF FIGURES

FIGURE PAGE

LIST OF ABBREVIATIONS AND ACRONYMS

ANOVA	Analysis of Variance
DRC	Dynamic Reaction Cell
FGS	Float Glass Standard
LA-HR-ICP-MS	Laser Ablation—High Resolution- Inductively Coupled Plasma-Mass Spectrometry
LASER	Light Amplification by the Stimulated Emission of Radiation
MDL	Method Detection Limits
Nd:YAG	Neodymium: Yttrium Aluminum Garnet
NIST	National Institute of Standards and Technology
DNA	Deoxyribonucleic acid
RSD	Relative Standard Deviation
SEM-EDS	Scanning Electron Microscopy–Energy Dispersive Spectrometer
SRM	Standard Reference Materials
XRF	X-Ray Fluorescence
ICP-AES	Inductively Coupled Plasma Atomic Emission Spectrometry
STD mode	Standard mode
ASTM	American Society for Testing Materials
ESA	Electrostatic Analyzer
TRXRF	Total Reflection X-ray Fluorescence
WD	Working distance
AAS	Atomic Absorption Spectrometry

NAA	Neutron Activation Analysis
LIBS	Laser Induced Breakdown Spectroscopy
CDA	Canonical Discriminant Analysis
PCA	Principal Component Analysis
LA	Laser Ablation

1 INTRODUCTION

Biological matrices such as bone, teeth, and plant material are matrices of interest for forensic scientists, since they are commonly found in crime scenes and/or massive burials, and they could provide with valuable information to solve a case or for discrimination purposes.

1.1 Significance of the Study

Human remains identification is typically based on DNA analysis and/or by comparison of the individual's dental records. The absence of DNA in deteriorated samples and the unavailability of dental records could affect the individuals' identification process. On the other hand, the elemental composition of such matrices can provide key information of environmental exposure at working places, heavy metal poisoning, discrimination between individuals, and to associate an individual to a geographical region. Strontium and light isotope ratios composition of these materials has been used in the past to follow the trail of dietary habits of the inhabitants of a region and/or to associate the individual to a geographical region [1-3]. Trace elements content in bones and teeth could contribute with additional information for the discrimination of individuals with a faster and less complicated method. Recent applications of elemental composition of such matrices to human authentication have been reported in the literature [4, 5]. Similarly, the elemental composition of plants such as marijuana may be used for discrimination purposes.

Elemental analysis of glass by ICP-MS and LA-ICP-MS has previously shown to provide a very high degree of discrimination between different sources of manufactured

materials [6-8]. There has also been an interest in the application of elemental analysis by these sensitive methods to the analysis of biological matrices. The development and application of robust analytical methods for the detection and quantification of trace elemental analysis will lead to a better understanding of the potential utility of these measurements in forensic chemical analyses. A suitable technique for the analysis of biological matrices will require been capable of analyzing highly complex matrices, resolving interferences, analyzing a wide concentration range of elements (ng g^{-1} – %wt), and offering the possibility of reducing cumbersome sample preparation procedures and the contamination of the sample. ICP-MS is one of the preferred techniques for elemental analysis since it can provide excellent sensitivity, accuracy and precision of the analysis. The use of a HR-ICP-MS system offers the resolution of polyatomic interferences improving the detection of trace elements in complex matrices such as bone, teeth, and plant materials in addition to improving the detection limits over a quadrupole based ICP-MS device. By coupling a laser ablation (LA) system for solid sampling, the sample preparation steps and the destruction of the sample are reduced significantly.

The primary aim of this research involves developing an analytical method for the analysis of bone, teeth and plant material using HR-ICP-MS and LA-HR-ICP-MS. Dissolution work in ICP-MS is well known, thus it will helps in establishing the feasibility of using trace elements in bone and teeth matrices regardless of the high concentration of Ca and P, and will provide a point of reference for the laser ablation work. For laser ablation method development the use of calcium as internal standard was evaluated for bone, teeth and plant matrices. An element menu for discrimination was assessed based on their discrimination capabilities (Chapters 3 and 4).

Buried bones are exposed to different environmental conditions that can affect their natural elemental composition. A strategy was developed to decrease the possibility of including those parts of bones affected by diagenesis in elemental analysis for discrimination purposes. Although the approach to avoid using the diagenetic signal in elemental analyses is been reported before [9-12], there is an improvement in the capabilities of detecting elements at the low trace level by using LA-HR-ICP-MS, which also will allow for the use of more elements for possible discrimination between samples from different origin. With this method it is possible to assess the biogenic signal on buried bone samples when no soil or information of the environmental conditions have been provided to evaluate diagenesis effects in the samples.

Iron (an element of interest in bones, teeth, and plant material) presents polyatomic interferences due to the plasma conditions and matrix composition. Standard ICP-MS measurements commonly include the detection of ^{57}Fe, which has a low abundance of 2.2% vs 91.72% for ^{56}Fe. The polyatomic interferences and the low abundance of this element are challenges for standard ICP-MS measurements that affect the detection of iron at trace and ultratrace levels. The capabilities of using HR-ICP-MS and DRC-ICP-MS for the analysis of iron in terms of limits of detection, accuracy and precision were evaluated using glass matrix with the purpose of evaluate the possibility of including $^{56}Fe^{+}$ in forensic analysis of the aforementioned matrices (Chapter 2). This detection limits study with both ICP-MS systems is been reported for the first time providing to the scientific community the opportunity to evaluate iron in glass and implement it on routinely analysis based on their own capabilities.

1.2 Bone, Teeth and Plant Material: Elemental Composition

The elemental composition in bones and teeth varies in concentrations from wt% to ng g^{-1} depending on the intake from diet. Some elements are essential for the human bone development. Exogenous contribution could increase the concentration of elements such as iron, aluminum, and magnesium and could come from the environmental conditions surrounding the remains [5, 13, 14].

The inorganic phase in human bones is mostly hydroxyapatite and it contains elements in minor and trace concentration such as iron, magnesium, zinc, chromium, copper, and manganese that are associated to bone development [15]. Cortical bone is preferred for elemental analysis due to its dense structure, slow regeneration process, and its low susceptibility to environmental changes [15-19]. Isotopic information of cortical bones may provide with information of the individual's latest years of life.

The enamel is the hardest material in teeth with ~ 96% inorganic phase in from of hydroxyapatite [20]. The enamel is completely formed around the adolescence and it doesn't experience a fast degradation as compact bone which makes it suitable to determine elemental composition from childhood [15]. The dentine layer on the other hand has a faster regeneration than enamel, therefore providing information of elemental composition related to more recent events.

Plant mineral content is mainly influenced by the soil and water where it has grown-up. The concentration range of these elements in plant material varies form %wt to ng g^{-1}. The elemental composition of plants could be associated to a geographical region since they absorb nutrients from the soil environment and also to discriminate between different plants of the same species.

2 ANALYTICAL CAPABILITIES OF HR-ICP-MS AND DRC-ICP-MS FOR THE ANAYSIS OF IRON IN GLASS

Iron is a common element found in bone, teeth and plant material. The accurate detection of this element in complex matrices requires the resolution of polyatomic interferences created during the ionization process inside the plasma. ICP-MS has demonstrated to be one of the most effective analytical methods for the comparison of trace elements in small glass fragments due to its multi-element capability, excellent sensitivity, high sample throughput and the capability to provide isotopic information. Elemental analysis of glass by ICP-MS and LA-ICP-MS has previously shown to provide a very high degree of discrimination between different sources of manufactured materials [6-8, 21-24]. Therefore, glass was chosen to evaluate the capabilities of these ICP-MS techniques in detecting iron.

2.1 Iron Content in Glass Matrix

Variations in elemental profiles within glass populations are due to differences in elemental composition of the raw materials used and/or those assosicatedto the manufacturing processes. Although some of the raw materials used in glass manufacturing are relatively pure, a glass product may contain impurities, such as iron oxide, that could produce undesirable color and alter furnace temperatures. Only one-part-per-thousand of iron oxide in sand can impart a green color on the glass and therefore manufacturers usually use discoloring agents to remove or mask the tint. Iron oxide is typically present at concentrations that range from 0.07 to 0.16% wt in float glass, 0.03 to .015 %wt in containers, 0.05% wt in borosilicate glass, and 0.01%wt in lead

crystal glass while in optical and insulating lead glasses, iron oxide content is reduced to trace levels [25].

2.2 Elemental Analysis of Iron in Glass Matrix

The elements used for the discrimination of glasses by ICP-MS had been critically selected from previous studies in which precision, accuracy and discrimination potential of these elements were evaluated at major, minor and trace levels [23, 24]. Iron has been identified in previous studies as an excellent discriminating element and it has been successfully used for classification and discrimination of glasses by X-ray fluorescence [21, 22, 26] and ICP-AES [21, 26]. Nevertheless, the concentration of iron in some glass populations may be close to or lower than the limits of detection of XRF and ICP-AES. Although standard ICP-MS methods provide better sensitivity than the aforementioned techniques, the analytical performance of iron represents a challenge due to inherent interferences. In 2000, Duckworth *et al*. reported that elements measured by ICP-MS without good bias (≤10%) and precision (≤10%RSD) were closely inspected before using them as discriminating elements in a database for float glass. In this study iron presented a bias and precision higher than 10% [27]. The poor precision and accuracy of iron measurements in glass standards do not allow its use in glass databases and limits its use in casework.

The analytical challenges of iron in glass by ICP-MS are the result of polyatomic isobaric interferences such as $^{40}Ca^{16}O^{+}$ and $^{40}Ar^{16}O^{+}$ on $^{56}Fe^{+}$, and $^{40}Ca^{16}O^{1}H^{+}$, $^{40}Ar^{16}O^{1}H^{+}$, and $^{41}K^{16}O^{+}$ on $^{57}Fe^{+}$, respectively. Fortunately, these interferences can be suppressed or resolved by using either DRC or HR ICP-MS systems [28-30]. A solution

based analysis using DRC-ICP-MS reports a comparison of MDLs in 2% HNO_3, in rain water/ HNO_3/HF matrix and the reporting limits generated by Frontier Geosciences Laboratories (Seattle, WA) with detection limits as low as 9 ng L^{-1} for the 2% HNO_3 and 383 ng L^{-1} in the rainwater sample [31]. Balcaen *et al.* performed determinations of Fe in $AgNO_3$ solutions with isotope dilution using the DRC-ICP-MS with NH_3 as a reactant gas. They reported lower iron detection limits with the isotope dilution (0.013 μg g^{-1}) than with external calibration (1.2 μg g^{-1}) [32]. In 2001 Günther *et al.* reported a comparison of detection limits of $^{56}Fe^+$ and $^{57}Fe^+$ using the STD mode and the DRC mode with hydrogen and neon as reactant and buffer gases respectively for laser ablation experiments. The limits of detection were determined for a spot size of 40μm using the gas blank and the ablation of the SRM NIST 610 glass. In this study, the limits of detection were improved from 5.9 μg g^{-1} in standard (STD) mode to 2.1 μg g^{-1} using DRC mode for $^{57}Fe^+$, while for $^{56}Fe^+$ the limits of detection were reported to be 0.3 μg g^{-1}[33].

A study of trace elements in quartz by LA-HR-ICP-MS using an external calibration with the three SRMs NIST 612, NIST 614, and NIST 616 reported limits of detection for $^{56}Fe^+$ of 2.6 μg g^{-1} in medium mass resolution [34]. Iron detection limits in the order of pg g^{-1} were reported for analyses of water, plant, tissue, and rock samples in medium mass resolution by a HR-ICP-MS. The MDLs for iron in oyster tissue/tomato leaves and rock sample digestion blanks were reported to be 113 pg g^{-1} and 3940 pg g^{-1} for $^{56}Fe^+$, and 580 pg g^{-1} and 10600 pg g^{-1} for $^{57}Fe^+$ respectively [35].

Although there are reports of iron detection limits with both ICP-MS systems, at the present there is no existing data that compares the detection limits for $^{56}Fe^+$ and $^{57}Fe^+$ in glass samples using those techniques utilizing both laser ablation and solution

introduction methods. The capability of resolving or reducing the iron polyatomic interferences by using the DRC and high resolution systems will allow for a more optimized use of Fe for the discrimination of glass and the potential use for discrimination in bone, teeth, and plant matrices.

This work was conducted to evaluate the method detection limits (MDL) that can be achieved for Fe using the different ICP-MS systems (Quadrupole, Dynamic Reaction Cell and High Resolution) for solution and laser ablation sampling introduction methods using the glass standard reference materials (SRMs). This work also includes the assessment of precision and accuracy for iron measurements to evaluate the possibility of including iron in forensic analyses of glass and in biological matrices by ICP-MS.

2.3 Methodology

2.3.1 Experimental

2.3.1.1 Laser Ablation Analyses

Glass standard reference material (SRM) NIST 612 (National Institute of Standards and Technology, Gaithersburg, MD, USA) was used for laser ablation analyses with both ICP-MS systems using all configurations. SRM NIST 610 (National Institute of Standards and Technology, Gaithersburg, MD, USA) and the FGS glass standards, described elsewhere [36], were used as external calibrators for some experiments using a NewWave UP 213 laser ablation system (Fremont, CA, USA) and argon as the carrier gas. Method detection limits were calculated for $^{56}Fe^{+}$ and $^{57}Fe^{+}$ using SRM NIST 612. SRMs NIST 1831, NIST 614 and the FGS standards were analyzed to evaluate the

accuracy and precision of the method. For a proper assessment of LA experiments using the ELEMENT 2 high resolution ICP-MS (Thermo Electron Co. Bremen, Germany) and the ELAN DRC II (PerkinElmer, LAS, Shelton, CT, USA), other SRMs were used in place of SRM 612 since the former was used as an external calibrator in the data reduction analyses. For practical purposes only the results of the SRM FGS1 will be presented for all the laser ablation ICP-MS systems.

2.3.1.2 Solution Based Analyses

High purity standards (CPI International, Santa Rosa, California, USA) were used for the preparation of the external calibration curves. Optima grade nitric acid (HNO_3), hydrofluoric acid (HF), and hydrochloric acid (HCl) [Fisher Scientific Pittsburg, USA] were used for the digestion of glass samples. High purity deionized water (>18MΩcm^{-1}) and 0.8M Optima grade nitric acid (Fisher Scientific Pittsburg, USA) were used for the dilutions. Rhodium was used as an internal standard for all solutions analyzed.

SRMs NIST 612, NIST 1831, NIST 614 (National Institute of Standards and Technology, Gaithersburg, MD, USA), and the standards FGS1 and FGS2 were digested following the ASTM E2330-04 standard method for trace elemental analysis of glass using ICP-MS to determine the accuracy and precision of the analysis[37]**.**

2.3.2 Instrumentation

2.3.2.1 ICP-MS Description and Operation Principles

The ICP-MS instrument includes the following basic components: (a) sample introduction device, (b) inductively coupled plasma (ICP) torch, (c) mass spectrometer

interface, (d) ion optics, (f) mass separation device, and (g) ion detector (Figure 1). This technique is based on the ionization of the sample in a sustained plasma created in a torch under an intense radio frequency induced field. The ionized sample is carried by a gas (generally argon) through the mass spectrometer interface under high vacuum (~10^{-6} Torr). The ions are directed through the ion optics and then a complete separation is achieved at the mass separation device and finally detected by the detector.

There are two common sample introduction devices: flow injector nebulizer and laser ablation (LA) of the sample. In the flow injector device the liquid sample is pumped into the nebulizer (usually at 1 mL/min) using a peristaltic pump. The sample is carried out through the nebulizer with an argon flow of ~ 1L/min to create droplets. These drops (which are about 1-2% of the sample) get separated from the larger droplets through the spray chamber. Only the very small droplets (mist) come out from the spray chamber and get introduced into the plasma torch by the sample injector. With LA the solid is placed onto a 3D mobile stage inside the ablation chamber. The ablation chamber is continuously purged with a gas (generally argon). The sample surface is ablated and an aerosol of particles is produced. Then the particles are carried by helium gas stream into the plasma torch.

The plasma torch is surrounded by a coil with current that produces enough radiofrequency to create an induced magnetic field. Argon gas flows around the torch to stabilize and isolate the plasma from the outer tubes and to carry the sample through the torch. A spark of high voltage electrons interact with the ions carried by the gas to creates a very hot plasma (~10,000 K) with positively charged ions at the end of the torch. These positively charged ions are directed into the ion optical lenses. Different voltages are

applied to each set of lenses and the ions get separated by their potential differences. Then they are directed to the mass separation device.

Two common mass separation devices are: (1) quadrupole and (2) magnetic sector field system. The quadrupole has four cylindrical or hyperbolic rods with the same diameter (~1 cm) and length (8-12 cm). The four rods are perfectly aligned in such a way they produce a very uniform and stable field. By applying a direct current (+) and a radiofrequency field (-) to the rods, ions with a specific masses and charge pass through the middle of the four rods and then get detected. Ion with mass to charge ratio different from the selected mass will be ejected between the rods spaces. On the other hand, the magnetic sector field device consists of an electrostatic analyzer (ESA) and a magnetic sector analyzer. Ions exiting from the lenses enter into the magnetic field produced by the magnet. The ions will get dispersed by their energy and mass until they reach an intermediate slit. Then a direct current is applied to the ESA inner an outer plates making the inner plate negatively polar attracting the positive ions, while the outer plate (positive polarity) repels them. The ions are directed towards the ESA to get dispersed with respect to their energy and focused to the exit slit into the detector [38-40].

In the ICP-MS with the DRC, the interferences are removed by a chemical reaction between a reactant gas and the sample [29, 41-45]. The quadrupole (reaction cell) is located between the ion lenses and the quadrupole analyzer. Chemical resolution is achieved by introducing a reactive gas into a cell placed in the ion path. The cell is pressurized with a reactive gas, which can convert interferences to different ions that do not interfere with the analyte, or convert the analyte of interest into a new species that is interference-free. The chemistry involved in the conversion of the interference into a

different ion depends on the reaction gas and the bandpass settings. Bandpass acts as guard wall by allowing only the analyte to pass and enter into the mass analyzer. Iron polyatomic interferences were chemically removed by using methane as a reactant gas [45]. Methane is often used as reactant gas for the removal Fe interferences. Preliminary results in our laboratory showed better sensitivity on the detection of $^{56}Fe^{+}$ with methane as reactant gas. The removal of the refractory interference CaO^{+} was improved significantly with methane than with other gases in glass matrix. It seems that methane works better for the removal of $^{56}Fe^{+}$ interference CaO^{+} in Ca–rich matrices. Additionally for safety reasons it is more convenient to work with methane than with ammonia gas. Equations 1a and 1b describe the chemical reactions occurred in the reaction cell of the $^{56}Fe^{+}$ interferences with the reactant gas (CH_4). For comparison purposes this instrument was also used in STD mode.

$$CH_4 + {}^{40}Ar^{16}O^{+} \rightarrow CH_4^{+} + {}^{40}Ar + {}^{16}O \qquad \text{Eq.1a}$$

$$CH_4 + {}^{40}Ca^{16}O^{+} \rightarrow CH_4^{+} + {}^{40}Ca + {}^{16}O \qquad \text{Eq.1b}$$

2.3.2.2 ICP-MS Systems

The ICP-MS instruments used for this study were an ELAN DRC II ICP-MS (PerkinElmer, LAS, Shelton, CT, USA) and a HR-SF-ICP-MS ThermoFinnigan ELEMENT 2 (Thermo Electron Co. Bremen, Germany). The DRC-ICP-MS was equipped with a quartz cyclonic spray chamber and a concentric tube pneumatic nebulizer. The sample intake rate into a concentric nebulizer and cyclonic spray chamber (ELAN system) was 1 mL min^{-1}. An ASX 510 autosampler (CETAC Technologies, Omaha, NE, USA) was coupled to the ICP-MS for the solution analyses. For laser

ablation analyses, the laser systems were connected to the torch intake of the ICP-MS. The DRC-ICP-MS was operated in STD mode and DRC mode. The removal of $^{56}Fe^{+}$ polyatomic interferences was achieved by using methane as a reactant gas in the DRC mode. For solution analyses the HR-SF-ICP-MS sample introduction setup included a quartz cyclonic spray chamber with a microflow PFA-ST nebulizer (400 µL min^{-1} intake flow) [ESI Scientific, NE, USA] and a 1.5 mm quartz injector connected to a quartz torch CD-type for removable injector (ESI Scientific, Omaha, NE, USA). The laser systems were connected to a 1.75 mm quartz injector inserted into the torch. The HR-SF-ICP-MS system was used in the three mass resolutions available: low (~ 300), medium (~ 4000) and high (~10000).

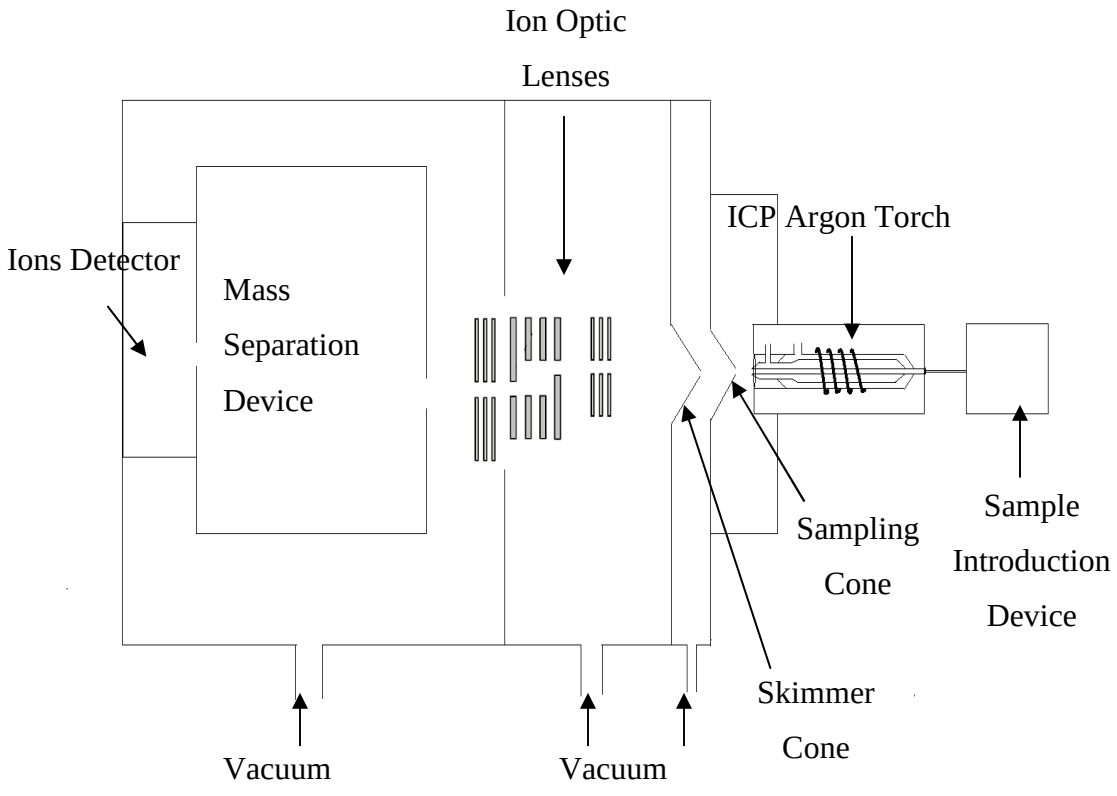

Figure 1. Schematic diagram of the basic components of an ICP-MS.

Before conducting each experiment, the instruments were optimized for sensitivity (maximum counts per second) and for doubly charged species (≤3%) and oxides (≤0.3%). An additional optimization in LA analyses of the ratio U/Th on SRM 612 was also conducted as a measure of fractionation levels (with 1 ± 0.2 determined to be acceptable).

2.3.2.3 Laser Ablation Description and Operation Principles

A typical laser consists of an active laser medium and a resonant optical cavity. The active laser medium is made of a pure material with a specific size and concentration that allows the amplification of the beam by means of stimulated emission. An external energy source energizes the active laser medium where the electrons of an atom or molecule get excited to a high energy level for a short period of time before returning to their original energy level releasing photons during the decay process. The emission of these photons can occur spontaneously or by stimulation. The spontaneous decay of electrons will produce the release of photons at random directions while the stimulation decay is caused by the interaction of the spontaneous decaying electrons with other exited electrons that will cause their return to the original ground state. The photons released during the stimulated decay will travel in phase with the same wavelength and direction of the incident photon. When the photons have the same direction as the optical axis they go back and forth through the resonant optical cavity. Then the light energy is amplified until enough energy is built up to produce a laser light that will be transmitted through a partially reflecting mirror [46].

To achieve the amplification the active laser medium must have at least one exited metastable state in which population inversion can occur. In order to obtain the population inversion there must be more electrons in the high energy level than in the lower energy level. In a four level laser system (Figure 2) the electrons are excited to a high energy level where they decay rapidly in a non-radiative transition to the upper metastable energy level. The transition of electrons from the upper metastable energy level to a lower energy level has a lifetime greater than the transition from the exited to the upper metastable level. Therefore there is a significant accumulation of electrons in the upper metastable energy level causing the population inversion. Then the decay from the upper metastable energy level occurs by means of either spontaneous or stimulated emission into the lower energy level (Figure 2). Then a fast non-radiative decay to the ground state occurs [46]. Most of the practical lasers are based on a four level system because it requires the excitation of few atoms to the upper metastable energy level to form a population inversion, thus it is more efficient than in a three level system.

There a several types of laser and they could be classified according to the physical state of the active laser medium (solid, liquid or gas laser), by the wavelength of emitted radiation (infrared, visible, ultraviolet, and x-ray lasers) or by their operation mode (continuous wave or pulse mode) [47]. In the continuous wave mode laser the population inversion is continually sustained by the source of energy and the output of the laser is continuous with the time. On the other hand in the pulse mode the laser operates with short pulses varying in time. For laser ablation, the pulses must be short enough to avoid melting of the material and allowing an efficient removal of particles from the surface.

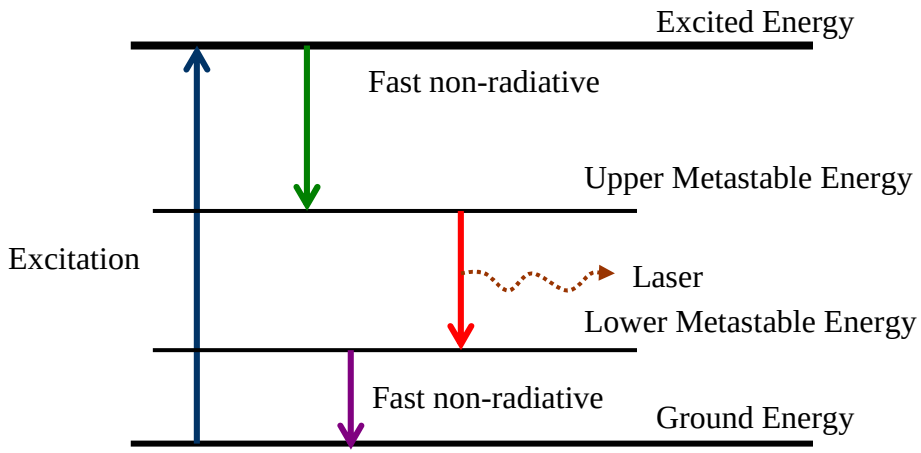

Figure 2. Four level laser energy diagram [46].

One of the most common solid state lasers is the Nd:YAG laser since it is relatively simple and less expensive than other solid lasers, and its properties favors the laser operation. The Nd:YAG (neodymium-doped yttrium aluminum garnet; Nd:$Y_3Al_5O_{12}$) is a crystalline structure that works as the active laser medium. The YAG host possesses several characteristics for the favorable laser operation. The host is a hard structure with good optical quality, high thermal conductivity, and its structure is stable on a wide range of temperatures up to the melting point, thus no change is expected to occur in the solid state. In the Nd:YAG about 1% of the Y^{3+} is replaced by Nd^{3+} [48]. The Nd:YAG laser is a four level system and commonly emits at 1046nm wavelength, although with optical modifications it can emit in the 213nm, 266nm, and 532nm wavelengths. These lasers can operate in the pulse or continuous mode. Typically the Nd:YAG pulsed lasers are operated in a Q switch mode in which an optical switch is located at the resonant optical cavity. When the optical switch is in operation, the light leaving the laser active medium is not been amplified, thus the laser emission can not

occur. This attenuation produces a low Q factor (quality factor) of the resonant optical cavity. The population inversion occurs but there is no amplification and as consequence the laser operation does not happens yet. The energy then is stored in the medium until it reaches a maximum level where the medium is said to be gain saturated. At this point the Q switch changes rapidly from low to high Q factor allowing the amplification by stimulated emission. Due to the large amount of energy stored in the medium, the amplification of the light occurs almost as fast as the energy been depleted in the active laser medium. As a result, a short pulse laser of light is released from the laser with very high peak intensity [49, 50].

The Nd:YAG lasers have found applications in ophthalmology, cutting and engraving metals, in the cosmetic industry, and in analytical techniques such as in laser ablation ICP-MS.

Laser ablation is a technique used to remove material from a solid with a laser beam, although lately it has found some applications in liquid materials. The ablation of the material from the surface occurs by means of melting, fusion, sublimation, erosion, vaporization, and explosion. The ablation process is affected by the ability of the material to absorb energy. To remove an atom from the solid with the laser pulse, an energy exceeding the binding energy of the atom must be applied. To remove the same amount of material from the solid with a short laser pulse the laser intensity should be inversely proportional to the duration of the pulse. For example a laser ablation with 30-100 ns pulse requires intensities ~10^{8}-10^{9} W cm^{-2} [51, 52].

The ablation process could involve thermal or non-thermal ablation mechanisms depending on the lasers wavelength. In a thermal process, melting and vaporization of the

material occurs as result of the direct absorption of the laser light by the electrons. The absorbed energy then is transferred to the atomic lattice. A strong fractionation could result from the thermal mechanism due to the different phase transition of the elements, whereas when the energy of the photon is higher than the bonding energy of the atoms in the solid, the laser radiation can break the atomic lattice resulting in the ejection of ions and atoms without suffering of heating effects (non-thermal ablation process) [53, 54].

In a non-thermal ablation four thresholds are occurring at different time lines, which are presented in Figure 3. The particles removed during this process directly represent the sample composition. At the femtosecond level the absorption of light and electronic excitation occurs. At this stage if the laser wavelength is not the correct one, a plasma shielding effect could happen. When the laser beam interacts with the already growing plasma plum the laser energy can be absorbed or reflected by the plasma. Typically the plasma absorption is more prominent with larger wavelengths. On the other hand a more efficient bond breaking process happens with shorter laser wavelengths. The efficiency in the bond breaking is a result of a better penetration of the laser beam into the plasma leading to less fractionation [55-57]. During the picosecond time frame the emission of electrons from the surface of the material occurs, while at the nanosecond timeline the plasma is formed where radiation, ionization (shock wave), vaporization, convection and melting are taking place. Finally, at the microsecond level the particles are ejected from the surface by means of normal evaporation and explosive boiling [58].

A typical laser ablation system for ICP-MS includes an ablation cell mounted on a platform with X-Y-Z axis translational capabilities and an optical lens. The laser beam is focused on the surface of the material by means of a CCD camera aligned with the optical

lens and through an aperture system that allows spot sizes of 10 to 200 μm. To assist with the imaging the laser system may have reflected light and/or transmitted light, a dual polarizer and a real time image acquisition. A schematic representation of a typical laser system is shown in Figure 4.

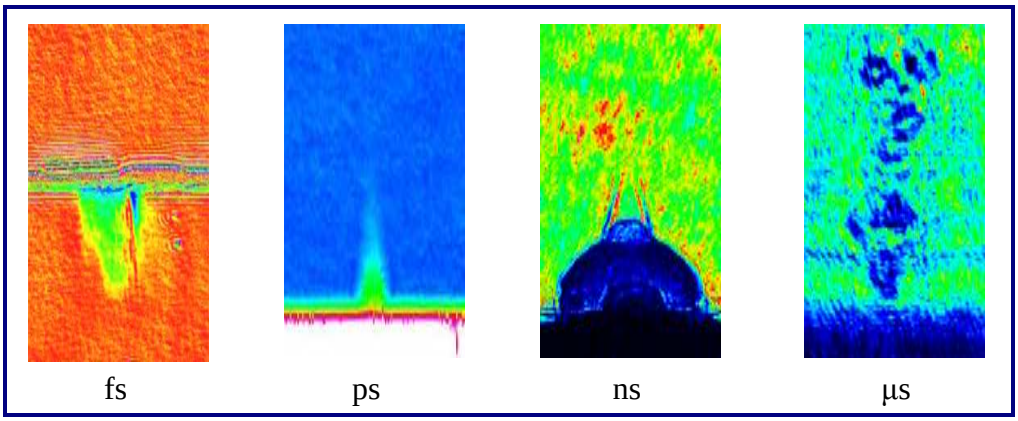

Figure 3. Ablation process time scale [58].

Different ablation modes such as depth profile, special profile, surface and bulk analyses can be achieved depending on the time between individual pulses and the platform movement capabilities. A carrier gas system is integrated to the ablation cell to efficiently transport the particles into the ICP system and to avoid the plasma collapsing. The purging system usually includes a three-way valve system to avoid the introduction of air in the ICP between sample analyses. Typically, argon and/or helium are used for purging the cell and for particle transportation. It has been found the use of helium as carrier gas improves the ablation process and the transportation rate [59-62].

The coupling of laser ablation with ICP-MS allows for the direct analysis of the sample, reducing the sample preparation and analysis time, the use of reagents, sample consumption, and the possible contamination with other sources [63, 64]. The main

disadvantage of ICP-MS is that it requires a matrix matched standard for quantitative analysis, although non-matrix matched calibration using glass SRMs (NIST 612 and NIST 610) have provided satisfactory results [65-67]. LA-ICP-MS also may suffer from potential fractionation during the ablation or sample transportation [64, 68]. The fractionation phenomenon occurs when the ablated products are not stoichiometrically representative of the bulk of the sample composition [69]. Fractionation in LA-ICP-MS limits the accuracy of the quantitative analysis, but it can be solved by following the response of a reference element with the same concentration in the standards and samples [70, 71], by using a matrix matched standard with the sample [72, 73] and by using short wavelength lasers [74]. It is been reported that for quantification in elemental analysis of forensic glass the fractionation effect is negligible [75].

There is no standardized calibration method for the quantitative analysis for all solid samples [76-79]. Glass matrix reference materials such as NIST 612 has been used for optimization and for quantitative analysis of several solid materials including glass [7], plant material (cannabis) [80], and teeth [81-83] samples analyzed by LA-ICP-MS. The general method for LA quantitative analysis includes normalizing the element intensities relative to an element (internal standard) of known concentration and whose concentration variation within samples of the same matrix is virtually unchanged. Other reference materials (matrix related to the samples) are measured with the samples for verification purposes.

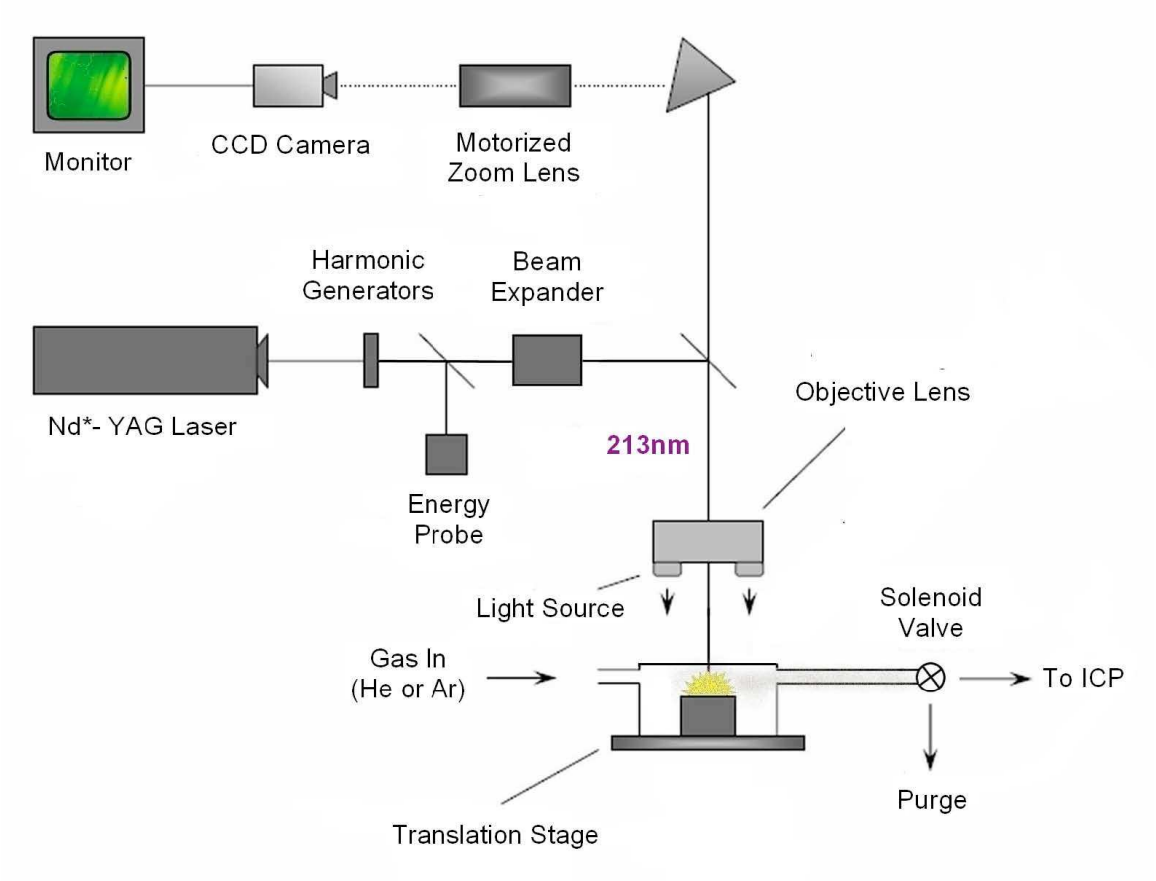

Figure 4. Schematic of the UP213 New Wave Laser System (New Wave Research, Fremont, CA, USA**)**

2.3.2.4 Laser Ablation Systems

Two different Nd:YAG laser units were used for this work: 1) a *New Wave UP-213* operating at 213nm (New Wave Research, Fremont, CA, USA) and 2) a *CETAC LSX 200+* (CETAC Technologies, Omaha, NE, USA) operating at 266nm. Laser ablation parameters are further described in Table 1. The laser ablation systems were operated under different parameters using both helium and argon as a carrier gas, and different ablation cell volumes. The experimental parameters were optimized for each system.

2.3.3 Sample Preparation

2.3.3.1 Laser Ablation

The glass SRMs were rinsed with high purity deionized water and dried overnight prior the LA analysis.

2.3.3.2 Solution

The samples were washed first in methanol for 10 minutes, then with HNO_3 1.6 mol L^{-1} for 30 minutes, followed by rinsing with high purity water (>18 MΩ cm^{-1}). After rinsing, they were left to dry overnight. Glass samples were crushed and weighed to approximately 2 mg ± 1 μg into 5 mL polypropylene tubes. Trace elemental grade (optima grade) nitric (HNO_3), hydrofluoric acid (HF) and hydrochloric acid (HCl) [Fisher Scientific Pittsburgh, USA] were used for the digestion of glass. Samples were sonicated for 2 hours and then dried in a heating block (Dry Digital Bath Incubator, Boekel Scientific, Feasterville, PA, USA). After the samples were taken to complete dryness, they were reconstituted with 0.8mol L^{-1} HNO_3, the internal standard and high purity water. Dilutions of the reconstituted digested glass samples were prepared and measured along with seven reagent blanks that were treated in the same way as the glass samples.

The glass samples were measured against an external calibration curve made from single element high purity standards (1000 μg g^{-1}) [CPI International, Santa Rosa, California, USA]. Rhodium was added as internal standard to a final concentration of 3 ng g^{-1}, 3 ng g^{-1} and 50 ng g^{-1} for the HR-SF-ICP-MS, DRC mode ICP-MS and standard mode ICP-MS calibration curves respectively. Calibration curves had seven calibration points in a range of 0-10 ng g^{-1} for the ELEMENT 2 and ELAN DRC Mode, and from 0-

100 ng g^{-1} for ELAN standard mode analyses. Two control verification checks (at 3 and 5 ng g^{-1} for ELEMENT 2 and ELAN DRC mode and at 7 and 25 ng g^{-1} for the ELAN standard mode) were run with samples in order to evaluate drift and precision over time. All sample preparations and analyses were performed in a normal laboratory environment.

Table 1. Instrumental parameters of laser and ICP-MS systems.

LASER SYSTEMS			**ICP-MS SYSTEMS**			
Parameters	***CETAC LSX 200+***	***New Wave UP 213***	**Parameters**	***ELAN DRC II (STD mode)***	***ELAN DRC II (DRCmode)***	***ELEMENT 2***
Wavelength	266 nm	213 nm	**Auxiliary Gas**	1.1 L min^{-1}	1.0 L min^{-1}	0.8 L min^{-1}
Spot Size	100 μm	100 μm	**Ablation Cell Carrier gas**	0.90 L min^{-1} (laser, He) 0.80 L min^{-1} (laser, Ar)	0.90 L min^{-1} (laser, Ar)	0.60-0.72 L min^{-1} (laser, Ar) 1.0-1.1 L min^{-1} (laser, He)
Energy Output	4.8 mJ	2.4 mJ	**Nebulizer Flow**	1.0 L min^{-1} (solution) 0.98 L min^{-1} (laser)	1.0 L min^{-1} (solution) 0.98 L min^{-1} (laser)	1.0 L min^{-1} (solution) 0.62-0.70 L min^{-1} (laser)
Repetition Rate	10 Hz	10 Hz				
Carrier gas	Ar or He	Ar or He	**RF Power**	1500 W (solution) 1550 W (laser)	1501 W (solution) 1550 W (laser)	1300 W (solution) 1350 W (laser)
Ablation Cell Volume	50.2 mL	30.0 mL	**Reaction Gas**	-	CH_4	-
			Reaction Gas Flow	-	0.5 L min^{-1}	-
			RPq	-	0.5 (laser) 0.6 (solution)	-
			Resolution Modes	-	-	Low, Medium and High

-Not applicable.

2.3.4 Data Analysis

2.3.4.1 Concentration and MDLs using Laser Ablation

The total analysis time was of approximately 170 seconds. During the first 55 seconds the laser was blocked (via the use of a shutter) and the signal of the “blank” was

acquired in order to account for the background level. The laser was then fired for 60 seconds, but only the middle-latter 40 seconds of the ablation signal were used for measurements because of the inherent instability caused when the laser first interacts with a sample. Following these 60 seconds the laser was turned off and the signal was recorded for an additional 55 seconds to purge any signal carryover between samples. Seven sample replicates of either SRM NIST 612 on two non-consecutive days were used to determine the MDLs of LA analyses. Figure 5 shows the transient signal of $^{56}Fe^{+}$ during a typical analysis. The Glitter software (GLITTER, GEMOC, Macquarie University, Australia) was used for data reduction to determine concentration and the MDLs. Glittter software enables plotting the transient signal collected from the LA analysis and to select the background and signal intervals for data reduction. To determine the concentration the Glitter software uses Equation 2, where $conc_{ni}$ is the concentration of element **i** in analysis **n**, cps_{nij} is the mean count rate (background subtracted) of isotope **j** of **i** in analysis **n**, $abundance_j$ is the natural abundance of isotope **j**, and $yield_{ni}$ is the cps per ppm of element **i** in analysis **n**. The $yield_{ni}$ is calculated using Equation 3, where $yield_{ns}$ is the cps per ppm of the internal standard **s** in analysis **n**, $Int(yield_{ni}/yield_{ns})^{std}$ is the ratio of the yield of element **i** in analysis **n** to the yield of the internal standard **s** in analysis **n** interpolated over the standard analyses.

$$conc_{ni} = (cps_{nij} / abundance_j) / (yield_{ni}) \qquad \text{Eq.2}$$

$$yield_{ni} = yield_{ns} * Int(yield_{ni} / yield_{ns})^{std} \qquad \text{Eq.3}$$

Glitter software uses Equation 4 to calculate the limits of detection with 99% confidence level based on Poisson counting statistics. In the Equation 4, B is the total

counts in the background interval. The LA data analysis was performed using SRM NIST 612, SRM 610 or the standard FGS2 as a single point external calibrator. For all the analytical determinations ^{29}Si was used as the internal standard, except for the DRC experiments where ^{24}Mg was chosen as the internal standard.

$$MDL = 2.3 * \sqrt{2B} \qquad \text{Eq. 4}$$

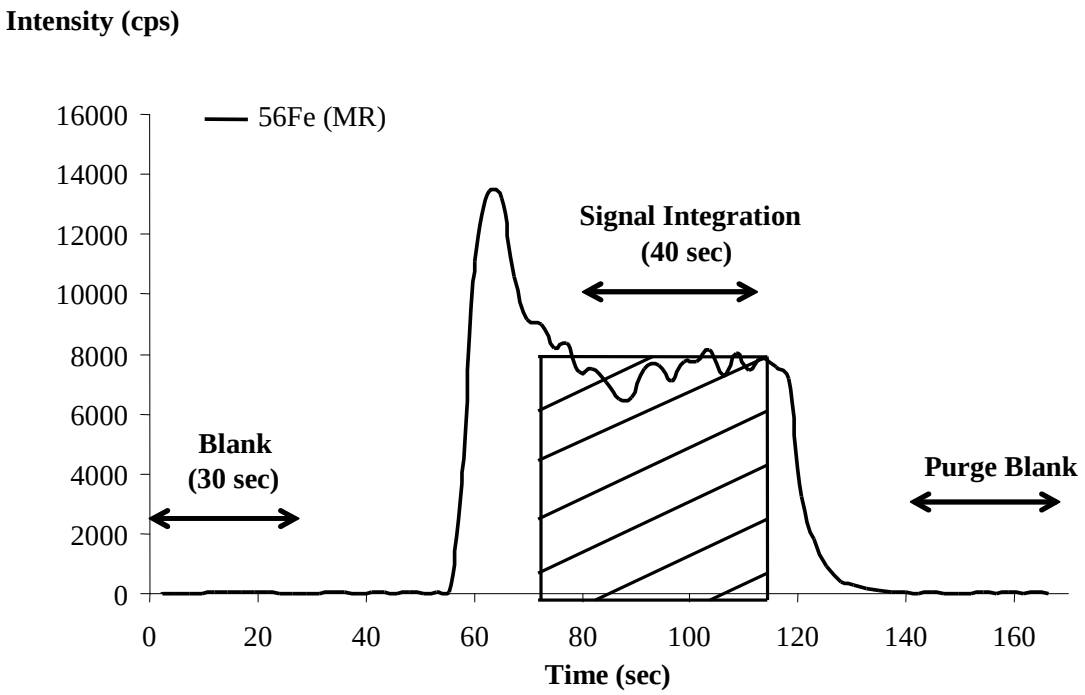

Figure 5. A typical laser ablation transient signal of iron in SRM NIST 612 analyzed with the ELEMENT 2.

2.3.4.2 Concentration and MDLs using Solution Analysis

The glass samples were measured against an external calibration curve. The intensities (cps) for the standards and samples were normalized to the rhodium (internal standard) signal (cps). A lineal regression line was determined from the plot of the

normalized signal (cps) against the concentration of the correspondent standard. Then the concentrations in the samples were determined by using the slope and intercept of this equation.

The iron MDLs on solution analyses for SRM NIST 612 were determined by Equation 5 where σ is the standard deviation of the blank's signal and m is the slope of the curve. MDLs were determined with at least 7 replicates of reagent blanks measured in two non-consecutive days in order to account for inter-day variations.

$$MDL = \frac{3\sigma_{blank}}{m} \qquad \text{Eq. 5}$$

To compare the MDLs obtained from laser and solution work, the MDLs for solution are referred to the concentration on glass assuming and average weight of 2mg of glass diluted into 4mL after acid digestion [37]. Therefore, MDL obtained in $\mu g\ L^{-1}$ were multiplied by a factor of 2 to be reported in $\mu g\ g^{-1}$ on glass.

2.3.4.3 Precision and Accuracy of LA and Solution Analyses

The accuracy of the analyses was determined by comparing the SRMs NIST 612, NIST 1831, standards FGS1 and FGS2 experimental values of iron with the certified and/or consensus values. Precision was determined by calculating the relative standard deviation (%RSD) of 5 sampling replicates on each glass sample. The method was evaluated with an accuracy of ≤10% bias from the consensus or certified, and a precision of ≤10% RSD.

2.4 Results and Discussion

Three main ICP-MS configurations were used to evaluate the method detection limits of iron in glass analysis: ICP-MS STD mode, ICP-MS DRC mode and HR-SF-

ICP-MS, where the latter two were used to reduce the polyatomic interferences associated with Fe measurements. MDLs were evaluated with laser ablation and solution modes since these are the two major sampling introduction methods routinely used in forensic laboratories for elemental analysis. Two laser systems were operated with helium and argon in order to account for the effects of laser wavelengths and carrier gases on the sensitivity. Table 1 shows the experimental parameters used for each ICP-MS configuration.

Both isotopes $^{56}Fe^{+}$ and $^{57}Fe^{+}$ were analyzed, however the target isotope in this study was $^{56}Fe^{+}$ since it has a greater abundance than $^{57}Fe^{+}$ (91.72% vs 2.2%). Iron interferences represent an analytical challenge for standard ICP-MS systems because polyatomic interferences containing argon (a property of the ICP) and calcium (a major component in glass) are present at very high levels.

2.4.1 Method Evaluation for Solution Based and LA Analyses

2.4.1.1 Analytical Performance of DRC vs. STD Mode

Analytical performance of the method was evaluated in terms of limits of detection, accuracy and precision. For solution analysis in STD mode, $^{57}Fe^{+}$ concentration on the standard FGS1 was considerably high compared to the consensus value meaning the interferences produced were not efficiently removed in this mode possibly due to high abundances of argon hydroxide interferences. This effect of the interferences in standard mode is more pronounced at low concentration levels of iron such as in the case of SRM 612 were iron is only present at 56.3 $\mu g\ g^{-1}$. By using the DRC mode, the iron interferences were properly reduced leading to an accurate

measurement of $^{56}Fe^{+}$ when compared to the consensus value (580 ± 60 μg g^{-1}) with a bias and a precision of less than 10 % (Table 2). Iron of mass 57 was not measured in the DRC mode since the target mass to reduce interferences on DRC mode with methane was mass 56, therefore the effect on reducing the main interferences on mass 57 was not optimized. In the LA analyses with the STD mode and different carrier gases, $^{57}Fe^{+}$ produced better accuracy than in solution based analyses. This is because in LA mode, a dry plasma contains much less hydroxide interferences such as $^{40}Ca^{16}O^{1}H^{+}$, $^{40}Ar^{16}O^{1}H^{+}$. For the analysis of $^{56}Fe^{+}$ in the DRC Mode the interferences were efficiently reduced leading to a good accuracy of <10% bias and a precision of the measurements of < 10%RSD (Table 3).

Table 2. Results of accuracy (%bias) and precision (%RSD): solution based analyses for standard FGS1.

	ELAN STD Mode			ELAN DRC Mode		
Isotope	**[a]Ave ± σ**	**%RSD**	**[b] %Bias**	**[a]Ave ± σ**	**%RSD**	**[b] %Bias**
^{57}Fe	699 ± 9	1.3	21	-	-	-
^{56}Fe	-	-	-	554 ± 58	10	5

	E2 in MR			E2 in HR		
Isotope	**[a]Ave ± σ**	**%RSD**	**[b] %Bias**	**[a]Ave ± σ**	**%RSD**	**[b] %Bias**
^{57}Fe	544 ± 52	10	6	529 ± 13	3	9
^{56}Fe	542 ± 61	11	7	521 ± 10	2	10

[a] Average (Ave) concentration in μg g^{-1}

[b] Bias was determined using the consensus value of Fe: 580 ± 60 μg g^{-1} [27]

-Not determined.

2.4.1.2 Analytical Performance of HR-ICP-MS

Interferences of $^{57}Fe^{+}$ were not properly resolved for solution analyses with the ELEMENT 2 in low resolution mode hydroxides are present in wet plasma. Although oxide levels were optimized to less than 0.3%, the oxides could be transformed into

hydroxide species $^{40}Ca^{16}O^{1}H^{+}$ and $^{40}Ar^{16}O^{1}H^{+}$ with the water in solution causing a significant increase in the concentration measurement of $^{57}Fe^{+}$ in LR compared to the consensus value of iron in the standard FGS1, therefore it was not reported. The accuracy and precision of $^{57}Fe^{+}$ measurements were improved in medium resolution (MR) and high resolution (HR) with less than 10 % bias and less than 10 % RSD for precision (Table 3).

Table 3. Results of accuracy (%bias) and precision (%RSD): LA analyses for standard FGS1.

(ELAN DRC II -New Wave UP213 laser)

	ELAN STD Mode (He)			ELAN STD Mode (Ar)			ELAN DRC Mode (Ar)		
Isotope	**Average ± σ**	**%RSD**	***%Bias**	**Average ± σ**	**%RSD**	***%Bias**	**Average ± σ**	**%RSD**	***%Bias**
^{57}Fe	526 ± 6	1	9	526 ± 9	2	9	-	-	-
^{56}Fe	-	-	-	-	-	-	543 ± 13	3	6

(ELEMENT 2 -New Wave UP213 laser)

	E2 in LR (Ar)			E2 in MR (Ar)			E2 in HR (Ar)		
Isotope	**[a]Ave ± σ**	**%RSD**	**[b] %Bias**	**[a]Ave ± σ**	**%RSD**	**[b] %Bias**	**[a]Ave ± σ**	**%RSD**	**[b] %Bias**
^{57}Fe	557 ± 25	5	4	619 ± 5	1	7	630 ± 8	1	9
^{56}Fe	-	-	-	629 ± 11	2	8	636 ± 22	3	10

(ELEMENT 2 -New Wave UP213 laser)

	E2 in LR (He)			E2 in MR (He)			E2 in HR (He)		
Isotope	**[a]Ave ± σ**	**%RSD**	**[b] %Bias**	**[a]Ave ± σ**	**%RSD**	**[b] %Bias**	**[a]Ave ± σ**	**%RSD**	**[b] %Bias**
^{57}Fe	631 ± 15	6	9	602 ± 17	3	4	561 ± 39	3	3
^{56}Fe	-	-	-	609 ± 23	2	5	556 ± 8	2	4

(ELEMENT 2 -CETAC LSX 200+)

	E2 in LR (Ar)			E2 in MR (Ar)			E2 in HR (Ar)		
Isotope	**[a]Ave ± σ**	**%RSD**	**[b] %Bias**	**[a]Ave ± σ**	**%RSD**	**[b] %Bias**	**[a]Ave ± σ**	**%RSD**	**[b] %Bias**
^{57}Fe	613 ± 14	2	6	650 ± 13	2	12	565 ± 4	1	3
^{56}Fe	-	-	-	641 ± 3	0.5	11	648 ± 5	1	12

(ELEMENT 2 -CETAC LSX 200+)

	E2 in LR (He)			E2 in MR (He)			E2 in HR (He)		
Isotope	**[a]Ave ± σ**	**%RSD**	**[b] %Bias**	**[a]Ave ± σ**	**%RSD**	**[b] %Bias**	**[a]Ave ± σ**	**%RSD**	**[b] %Bias**
^{57}Fe	561 ± 16	3	3	613 ± 22	4	6	544 ± 40	7	6
^{56}Fe	-	-	-	547 ± 16	3	6	636 ± 12	2	10

[a] Average (Ave) concentration in μg g^{-1}

[b] Bias was determined using the reference value of Fe: 580 ± 60 μg g^{-1} [27]

-Not determined.

For most of the laser ablation experiments using HR-SF-ICP-MS with the three mass resolutions, the polyatomic interferences of $^{56}Fe^{+}$ and $^{57}Fe^{+}$ were properly resolved providing accurate concentration measurements of iron in the standard FGS1. Accuracy and precision of the analyses in all the mass resolutions were within the acceptable parameters (≤10% bias and ≤10% RSD) (Table 3).

In general, solution based and laser ablation accuracy and precision results with the different ICP-MS configurations were in agreement. The results showed improved accuracy on the DRC and HR-SF ICPMS being medium resolution the optimum resolution mode for iron since it resolves the interferences without sacrificing sensitivity. The method was properly assessed giving validity to the MDLs results obtained during these experiments.

2.4.2 MDL of Solution Based and LA Analyses

The iron method detection limits in DRC mode were significantly lower than in standard mode (0.03 vs 9.5 µg g^{-1} for laser ablation and 0.33 vs 1.9 µg g^{-1} for solution based analyses). This demonstrates the ability of DRC with eliminating interferences, reducing the limits of detection and allowing for more certainty in iron determinations in glass matrices. Higher background levels in solution and laser ablation analyses in the STD mode contribute to higher detection limits of $^{57}Fe^{+}$.

The use of a high resolution sector field ICPMS resolved the polyatomic interferences in iron. Low MDLs for both iron isotopes were achieved in laser ablation analyses using the ELEMENT 2, particularly in medium resolution for $^{56}Fe^{+}$. Higher MDLs in HR could be attributed to the increase in resolution, which decreases the

sensitivity, therefore affecting the limits of detection (Table 4). When comparing the MDLs results in MR and HR using the two laser systems, higher detection limits were observed with the NW UP213 laser system. The differences in the ablation process (i.e. amount of mass ablated) associated with the lasers energies could contribute to these variations. Regardless, the MDL values are comparable (Table 4). In the low resolution mode, high background levels contributed to the increase in the detection limits. This pattern was also observed for the STD mode in the quadrupole instrument.

Table 4. MDLs for SRM NIST 612 laser ablation analyses of $^{56}Fe^{+}$ and $^{57}Fe^{+}$ using the different ICP-MS configurations.

MDLs ± σ for Laser Ablation Analyses in µg g^{-1} (ELEMENT 2 -LSX 200+ laser)

Isotope	E2 in LR (Ar)	E2 in MR (Ar)	E2 in HR (Ar)	E2 in LR (He)	E2 in MR (He)	E2 in HR (He)
^{57}Fe	2.3 ± 0.1	0.40 ± 0.04	1.5 ± 0.5	2.4 ± 0.1	0.23 ± 0.06	1.2 ± 0.6
^{56}Fe	-	0.055 ± 0.003	0.15 ± 0.01	-	0.037 ± 0.003	0.11 ± 0.03

MDLs ± σ for Laser Ablation Analyses in µg g^{-1} (ELEMENT 2 -New Wave UP213 laser)

Isotope	E2 in LR (Ar)	E2 in MR (Ar)	E2 in HR (Ar)	E2 in LR (He)	E2 in MR (He)	E2 in HR (He)
^{57}Fe	8.3 ± 0.9	0.9 ± 0.4	3.6 ± 0.6	3.5 ± 0.3	0.8 ± 0.2	3.9 ± 1.2
^{56}Fe	-	0.12 ± 0.01	0.3 ± 0.1	-	0.085 ± 0.007	0.29 ± 0.05

MDLs ± σ for Laser Ablation Analyses in µg g^{-1} (ELAN DRC II -New Wave UP213 laser)

Isotope	ELAN STD mode (He)	ELAN STD mode (Ar)	ELAN DRC mode (He)	ELAN DRC mode (Ar)
^{57}Fe	9.5 ± 1.0	9.6 ± 2.0	-	-
^{56}Fe	-	-	[a] 0.025 ± 0.003	0.6 ± 0.2

[a] Data published from a previous study [21]
-Not determined.

The solution based analyses with the HR-SF-ICP-MS showed an improvement in the MDLs of both iron isotopes in medium and high resolutions vs. low resolution (Table 5). In the quadrupole system the use of DRC allowed to achieve MDLs of 0.30 µg g^{-1} for $^{56}Fe^{+}$. In MR and HR, the interference signals are properly separated from the iron signals, while in the DRC mode; the polyatomic interferences are significantly reduced by chemical reaction but may not be completely removed.

In solution based analyses higher MDLs for $^{56}Fe^{+}$ were obtained than with laser ablation. Differences in the MDLs could be attributed to the dilution factor and the possible increase in background contribution due to the digestion process in solution analyses.

Table 5. MDLs results for solution analyses of $^{56}Fe^{+}$ and $^{57}Fe^{+}$ using the different ICP-MS systems.

MDLs ± σ for Solution Analyses in μg g^{-1} (ELEMENT 2)

Isotope	E2 in MR	E2 in HR
^{57}Fe	0.19 ± 0.12	0.58 ± 0.10
^{56}Fe	0.14 ± 0.06	0.62 ± 0.11

MDLs ± σ for Solution Analyses in μg g^{-1} (ELAN DRC II)

Isotope	ELAN STD mode	ELAN DRC mode
^{57}Fe	1.9 ± 1.2	-
^{56}Fe	-	0.33 ± 0.41

-Not determined.

2.4.3 Carrier Gas Effect on Laser Ablation MDLs

MDLs for both iron isotopes obtained with the CETAC LSX 200+ laser coupled to the HR-SF-ICP-MS were not significantly different at low and high resolutions when argon or helium were used as the carrier gas. Slightly lower MDLs were obtained for $^{56}Fe^{+}$ and $^{57}Fe^{+}$ when helium carrier gas was used in medium resolution. Experiments performed with the New Wave UP 213 laser coupled to the HR-SF-ICP-MS showed similar MDLs for $^{57}Fe^{+}$ and $^{56}Fe^{+}$ with helium and argon carrier gases in medium and high resolution. In the low resolution mode, higher MDLs were obtained when using argon as carrier gas because of the higher background produced with this laser of lower energy (2.4mJ vs. 4.8mJ for the CETAC LSX 200+).

With the ELAN DRC II, the carrier gas effect was more significant. Lower detection limits are achieved when helium was used as the carrier gas. MDLs determined for iron isotopes in the ELAN DRC II with both carrier gases were comparable with what was observed in MR with the ELEMENT 2 with both laser ablation systems/carrier gas combinations. For laser ablation analysis in glass matrix, helium as carrier gas has proven to increase the sensitivity in the detection of elements. The improvement in sensitivity is attributed to a more efficient particle removal and transportation into the ICP-MS [59-62]; therefore lower detection limits are achievable.

2.5 Conclusions

Polyatomic interferences for iron were significantly reduced or resolved with both DRC-ICP-MS and HR-ICP-MS. Method limits of detection as low as ~0.03 $\mu g\ g^{-1}$ were achieved with both DRC and the SF instruments using laser ablation mode in glass matrices. DRC-ICP-MS provided an excellent tool to achieve low MDLs for Fe in both laser ablation and solution analyses, but it is limited to the analysis of few elements in the DRC mode since the suppression of interferences is chemically dependent and other interferences could be formed in the cell that affect the analysis. From a practical point of view, this limitation requires separate measurements for Fe and for the other elements typically used in glass comparisons, especially when LA is involved since the transition from DRC to non-DRC mode is not fast enough for transient signals. The need of performing separate analysis for Fe and for the rest of the elements used in glass analysis is not only time consuming but also requires more sample. An advantage of DRC-ICP-MS over HR-ICP-MS is its lower costs and ease of use.

HR-ICP-MS allowed for the resolution of iron interferences in both medium and high resolutions. In laser ablation, the lower MDLs were achieved using medium resolution since in high resolution the sensitivity is significantly reduced, affecting the detection limits. In solution analyses, the HR-ICP-MS system at MR provides lower detection limits than DRC-ICP-MS. Advantages of HR-ICP-MS vs. DRC-ICP-MS instruments include its capability to achieve lower MDLs for Fe (particularly in laser ablation introduction method) and its capability to conduct multielemental analysis using laser ablation. Nevertheless, the fast transient signal measured in laser ablation does not allow to switch from different resolution modes in the same method, therefore the analysis with LA is limited one resolution in the sector field instrument.

Solution and LA analyses with the different ICP-MS instrumental setups provide accurate and precise measurements of the iron isotopes. The accuracy and precision in a multielemental analysis could be affected when the DRC-ICP-MS is used. The reactant gas could react with other isotopes of interest within the glass matrix causing problems in their detection. Although similar MDLs can be achieved with helium or argon as carrier gas in the LA-HR-ICP-MS systems, lower detection limits could be obtained with helium.

This work demonstrates the capabilities of these ICP-MS systems and setups to resolve and/or reduce polyatomic interferences allowing for accurate and precise measurements of iron isotopes in glass matrices. Although there were some differences in MDLs for each of the LA setups and ICP-MS systems, these results open the possibilities of doing elemental analysis, which includes the use of iron isotopes in routine casework analysis of glass and possibly for the analysis of bone, teeth and plant materials.

3 HR-ICP-MS AND LA-HR-ICP-MS FOR THE ELEMENTAL ANALYSIS OF BONE AND TEETH

Bone and teeth are calcified tissues in the human body where mineral in the form of hydroxyapatite is the predominant constituent. Trace elements are commonly found in the mineral phase of these calcified tissues, although some elements could be associated to the organic phase. Light and heavy isotope ratios have been used in anthropology for determining dietary lifestyles of populations and for provenance purposes as mentioned previously. On the other hand, the elemental composition on these matrices may act as a fingerprint as well as allowing identification of an individual from commingled samples.

Several factors could influence the concentration of trace elements in bone and teeth, especially in buried samples. Factors affecting bone and teeth trace element content (additionally to the diet intake) includes: remodeling process [84], bone diseases [84-86] or tooth cavities [87-89], and direct exposure from contaminated materials [90, 91]. In bone buried samples, soil conditions such as temperature, pH, and water exposure can cause changes in the mineral composition of bones leading to exchange of ions with the environment [92]. Therefore diagenesis needs to be assessed in order to distinguish the biogenic from the diagenetic signal. In order to better asses the elemental composition of these matrices it is important to know how trace elements are related and associated to these calcified tissues. A comprehensive background about bones and teeth matrices development, their constituents and elemental composition is described below.

Elemental analysis of glass and paint by ICP-MS and LA-ICP-MS has shown previously to provide a very high degree of discrimination between different sources of manufactured materials as mentioned in previous chapters. There has also been an

interest in the application of elemental analysis by these sensitive methods to the analysis of bones and teeth. Since these biological matrices play an important role in the forensic analysis of a crime scene and in massive burials, the development and application of robust analytical methods for the detection and quantification of trace elemental analysis will lead to a better understanding of the potential utility of these measurements in forensic chemical analyses. Among the instruments used to study these biological materials are Neutron Activation Analysis (NAA) [93, 94], Atomic Absorption Spectrometry (AAS) [95-100], X-Ray Fluorescence (XRF) [86, 101], Inductively Coupled Plasma-Atomic Emission Spectrometry (ICP-AES) [102], Laser Induced Breakdown Spectroscopy (LIBS) [103-106] and Inductively Coupled Plasma-Mass Spectrometry [3, 107, 108]. These techniques have some considerations such as analyzing highly complex matrices, resolution of spectral interferences capabilities, a wide concentration range of analysis (ng g^{-1} – %wt), cumbersome sample preparation procedures and possible contamination of the sample. Inductively Coupled Plasma Mass Spectrometry is one of the preferred techniques for elemental analysis since it can provide excellent sensitivity, accuracy and precision of the analysis. The use of a sector field High Resolution Inductively Coupled Plasma Mass Spectrometry system offers the resolution of polyatomic interferences improving the detection of trace elements in complex matrices such as bone and teeth in addition to improving the detection limits over a quadrupole based ICP-MS device. By coupling a laser ablation (LA) system for solid sampling, the sample preparation steps and the destruction of the sample are reduced significantly. Another advantage of LA is the possibility of doing quantitatively analysis using a non matrix match calibration with internal standardization which is

useful for the analysis of teeth samples where there are no reference standards. Having a general method that works for both matrices (bone and teeth) simplify the analysis. Since reference materials such as NIST 612 and NIST 610 have been used for non matrix match standard analysis successfully [65-67], this study used the same method. Laser ablation also allows for spatial resolution analysis at micron level in the rastering mode which is been used to evaluate elemental composition changes throughout the matrix for several applications [83, 109, 110]. For buried bone samples the LA spatial resolution capabilities provides with a great analytical tool for assessing variations of elemental composition in bone matrix and separate the biogenic form the diagenetic signal.

A method for the analysis of bone and teeth materials was developed by analyzing bone SRMs NIST 1486 and NIST 14000 with LA-HR-ICP-MS is suggested. The analytical technique (LA-HR-ICP-MS) was optimized and compared against dissolution work to confirm and validate the accuracy of the method and to assess the possibility of matrix suppression effect from major elements Ca and P in bone analyses. An element menu was selected for discrimination of bone and teeth samples from different origin based on the following characteristics: (1) the elements should be consistently present in bone and teeth matrix, (2) the concentration of these elements in the matrix should be above instrumental detection limits, (3) the elements should be preferably associated to the inorganic phase of these matrices, and (4) the elements less prone to diagenesis are preferred. A discrimination data analysis was then performed using the chosen element menu. Discrimination analyses bone and teeth samples were carried out.

3.1 Bone Matrix

The human skeleton is composed of over 200 bones each of them varying in size, shape, and function. Bones are divided by gross structure and shape. There are two groups of bones based on the gross structure: (a) cortical or compact bone and (b) trabecular or spongy bone [4]. Compact bone is a dense structure located at the outer layers of bones while trabecular bones are less dense with a honeycomb-like structure located at the inner layers of the bones. Variations in the annual turnover rate of bones are related to the type of bone and the age. For young adults and children the bone turnover rate is higher when compared with adults. The annual turnover rate for compact bone in general is approximately 2.5% while the trabecular bone is approximately 10% [4]. Therefore the elemental composition in human bones is time dependent. Recent exposure events could be assessed by analyzing trabecular bones, while information of more extended periods could be evaluated with compact bone.

At the shape level, the bones are classified in three types: (a) long bones, (b) flat bones, and (c) irregular bones. The long bones are found in the limbs and have an elongated diaphysis with epiphyses at the ends. Long bones are located in the arms, legs, hands, feet, fingers and toes that include femurs, tibias, fibulas, radii, humerus, ulna, metacarpals, metatarsals, and phalanges. The external layer of the long bones is covered with connective tissue (periosteum). The outer layer of the long bones consists of compact bone while the inner layer is trabecular bone containing the red bone marrow. The flat bones provide with extensive protection and a large surface for muscular attachment. Flat bones are broad and flat plates shape such as the skull, pelvis, sternum, rib cage, and scapula. They are composed of two thin layers of compact bone with an

internal layer of trabecular bone where the bone marrow is located. Flat bones include the occipital, parietal, frontal, nasal, lacrimal, vomer, scapula, os coxæ (hip bone), sternum, and ribs. The irregular bones have a distinctive shape different from long and flat bones. The functions of these bones include protection of nervous tissue, anchor points for muscle attachment, and maintain support of some other parts. Irregular bones are made of trabecular bone between two thin layers of compact bone. Vertebræ, sacrum, coccyx, temporal, sphenoid, ethmoid, zygomatic, maxilla, mandible, palatine, inferior nasal concha, and hyoid are irregular bones.

It is been reported by Sillen in 1989 [111] that compact bone of the shaft of long bones are often chosen for elemental analysis since they are less susceptible to experience environmental contamination and been affected by diagenetic processes, although other bones such as rib, clavicle, and ulna have shown good results [112]. For the purpose of this study compact bone fragments of the epiphyses regions (proximal and distal) of long bones were analyzed.

In general, bones are composed of approximately 70% mineral phase, 20% collagen, 8% of water and 2% of other components [4]. The mineral portion of bones is primarily calcium phosphate in the amorphous and crystalline forms; been the crystalline the dominant form in adult's bones. The crystalline hydroxyapatite is represented by the unit cell formula $Ca_{10}(PO_4)_6(OH)_2$. About 40% of the compact bone mineral phase is in the amorphous form, which can spontaneously transform into the crystalline form in the presence of water. Therefore most of the archeological bone samples are in the crystalline form [15].

The calcification process in bones refers to the mechanisms involved in the deposition of amorphous and crystalline hydroxyapatite in an organic matrix. Posner in 1978, suggested three main factors involved in the calcification process of bones: (1) increasing the production of (Ca^{2+}) x (PO_4^{2-}) solution ion in an optimal level so that a spontaneous precipitation of the mineral occurs, (2) availability of substances that create nucleating sites or eliminate anything that interferes with the sites, and (3) the removal of substances that prevent mineral formation or turned to inactive to allow the calcification [113]. The enzyme alkaline phosphatase it is found to hydrolyze phosphate esters producing an excess of free inorganic phosphate ions, thus increasing the (Ca^{2+}) x (PO_4^{2-}) at specific calcification centers enough to cause apatite precipitation. This enzyme is used as an indicator of active bone metabolism. The calcium-binding proteins are suggested to be associated to the formation of apatite by increasing of the (Ca^{2+}) x (PO_4^{2-}) product. These enzymes seem to raise the calcium phosphate supersaturation allowing the apatite to form. Nucleation is the process that allows for the precipitation of a minimum amount of salts ions. Nucleation in bone is considered to be heterogeneous since it is highly dependent on the availability of nucleating substrate. Collagen, carbohydrate protein complexes (glycoproteins), matrix vesicles (osteoblasts and chondrocyte), and the calcium storage in osteoblasts and chondrocytea have been found to provide with nucleating sites for the calcification of bone. Magnesium is an intracellular ion present at high concentrations in bone matrix that prevents the formation the crystalline apatite from the amorphous form in the matrix vesicles. The proteoglycans in cartilage and pyrophosphates are also related to slows down or inhibit the calcification process of bones. It is been suggested that the pyrophosphates are regulators of the calcification of

soft and hard tissues. The precipitation of calcium phosphate has shown to be inhibited by the pyrophosphate in solution of crystals and in presence of apatite crystals forms. Also the presence of pyrophosphate slows the transformation of the amorphous form into crystalline apatite [113].

The crystalline hydroxyapatite is formed by repetitions of the unit cell $Ca_{10}(PO_4)_6OH_2$. Hydroxyapatite is a right rhombic prism that arranges in such a way that forms a hexagonal lattice [113]. The crystals have three zones: (1) crystal interior, (2) crystal surface, and (3) the hydration shell. All the zones provide with a surface for ions exchange. A rapid exchange of ions is expected to occur in the hydration shell and in the crystal surface, while the exchange in the crystal interior is probably slower. Ions such as Fe, Cu, Pb, Mn, Sn, Al, Sr, and B have been detected at trace levels in bones, although hydroxyapatite itself have shown to vary with age [113]. Elements such as Sr, Na, and Pb are known to substitute Ca in apatite, while elements that cannot be accommodated in the apatite lattice (e.g. potassium) are likely to be absorbed on the surface.

The amorphous apatite is distributed throughout the bone matrix, although in the mineral phase of an adult human femur, close to 40% is in amorphous apatite form. The amorphous phase has been found to decline with time. The distribution of the ions in the amorphous phase is unknown because the amorphous calcium phosphates have not a rigidly defined chemical composition. The rate at which the amorphous form transforms into the crystalline apatite depends mainly on the apatite product rather than the amorphous precursor. Chemical species such as pyrophosphates, diphosphonates, adenosine triphosphate, ATP and Mg can either stabilize the amorphous calcium phosphate formation or prevent it to transforms into the crystalline form.

The movement of ions in bones has been extensively studied. Recently the use of radioactive tracers has been implemented for a better understanding of the movements of ions into and out of the human skeleton. The behavior of some alkaline earths with respect to calcium has been studied. These studies were performed with respect to calcium since the total mass of bone in a standard man of 70 kg is 5000g and the total body calcium is 1000 g. From the total amount of calcium, about 0.4% is in soft tissues and 0.03% is in the blood, therefore the large amount of calcium could be involved in the transfer of ions in and out of the skeleton. Calcium, strontium, barium, and radium are similarly distributed in the skeleton throughout the bone mineral. Although they have similarities in the absorption, excretion, and skeleton deposition, there are some differences in how they are retained. The movement of ions in the skeleton depends greatly of the bone type. In a study where the four radionuclides (^{47}Ca, ^{85}Sr, ^{133}Ba, and ^{233}R) indicated that the turn over rates in bone are similar although differences in the late retention is attributed to the differences in clearance from labile body pools.

Trace elements found in human bones are listed in Table 6 [114]. These trace elements are essential in different metabolic processes associated with the bone growth in the mineral and the organic parts, and most likely involve the interaction with proteins and enzymes. They can be bound to the organic component of bone or be absorbed by the mineral portion without forming a separate mineral [114]. Elements such as Mn, Cu, and Zn are required for the development of healthy bones [114]. Elements that with toxicity effects to humans are Pb and Cd. Lead, strontium, barium and zinc are likely to be integrated in the mineral structure because they are still present in the mineral phase after removal of the organic portion [115]. On the other hand most of the Al, Cu, Fe and a

minor part of Zn seems to be bonded to the organic portion since they have been found in high concentrations in the tendon as well [114].

The distribution of some trace elements throughout the skeleton seems to vary according to the bone structural and functional conditions [116, 117]. Bratter *et al.* reported that the concentration of Br, F, Pb, Sr, and Zn in different parts of the skeleton varied within a single bone and in other parts of the skeleton. It was also found higher concentrations of trace elements in the epiphyseal areas of long bones than in the shaft. Also higher concentration of some elements is found in the trabecular bone than in compact bone [116].

Table 6. Concentration ranges of trace elements detected in human bones [105].

Element	**[a] Concentration Range (μg g^{-1})**	**Element**	**[a] Concentration Range (μg g^{-1})**
Li	1-26	*As*	0.011 ± 0.0005
Be	0-4	*Se*	0.1-21
B	2-4	*Br*	1-5
Al	3-241	*Rb*	0.3-0.7
Si	3-40	*Sr*	75-150
S	[b] 0.69-1.83	*Zr*	0.3-6
Ti	0.1-2	*Mo*	0-0.1
V	0.04-8	*Ag*	1-19
Cr	0.1-6	*Cd*	1-8
Mn	0.2-26	*Sn*	3-13
Fe	3-120	*Sb*	0-3
Co	0-0.4	*Ba*	20-5940
Ni	2-18	*Hg*	0.012 ± 0.0003
Cu	1-3860	*Pb*	10-50
Zn	50-280	*Rare Earths*	0.001-2.2

[a] Concentration in Dry Weight

[b] Concentration in wt%

Carvalho *et al*. in 2004 performed studies of trace element in post-mortem bone samples from an archeological place using total reflection x-ray fluorescence (TRXRF) [118]. They determined the elemental profile of the trace elements Mn, Fe, Cu, Zn, Sr,

Ba, and Pb in the femur cortical and trabecular bones of a man and woman buried on the same grave in Portugal. In general Sr and Zn are relatively constant throughout the compact bone, which confirmed previous studies suggesting these elements concentration are not likely to be affected by diagenesis. There were variations in concentration in the inner portion (layer exposed to the trabecular bone) and in the external surface exposed to the soil. The differences in concentration at the inner and outer layers of compact bone were attributed to the soil contamination and the deposition of elements in the pores and voids of the trabecular bone that is in contact to the inner layer. Enrichment of Mn, and Fe in both compact and trabecular bone were observed, although their concentration was more prominent in the trabecular bones due to the larger pores and voids that will allow the accumulation of these elements. The dense structure of compact bone makes it less susceptible for the accumulation of Fe and Mn. The Fe and Mn concentration in trabecular bone agreed with the concentration found in soil suggesting environmental contamination with these elements. It was demonstrated that manganese, iron, and copper from the soil penetrated easily in the bone especially at the periosteum and trabecular bone. Lead concentrations in the inner and outer layers of compact bone were consistent with the concentration in soil suggesting port-mortem accumulation of this element from the environment. On the other hand lead concentrations in the inner layer of compact bone are related mostly to the intake prior burial.

To better understand the elemental composition of bone it is important to comprehend the chemistry of trace elements involved somehow with the bone matrix, bone growing mechanism, the storage of elements in the skeleton, and knowing the origin of these trace elements occurring in *in vivo* bone tissue. Although there is many trace

elements found in bone matrix (Table 6), there are only few that are of importance or related to bone regardless its function in the skeleton. Among these elements are: iron, aluminum, strontium, lead, zinc, barium, copper, magnesium, and manganese. When dealing with buried samples diagenesis is an important consideration in bone elemental composition, especially when the former is used for sourcing or determining dietary habits of individuals and/or populations.

3.1.1 Trace Elements in Bone Matrix: In Vivo

3.1.1.1 Zinc

Zinc concentration in the human body is 3 mg/100g of body weight. Skeletal abnormalities in fetal and postnatal development are strongly related with Zn deficiency. Zinc is essential for proper functioning of over a hundred enzyme systems in almost every tissue in the body, protein synthesis, carbohydrate metabolism, and bone formation. Studies on Zn in bone tissue culture demonstrated that Zn was involved in the increase of protein synthesis, the activity of the enzyme alkaline phosphatase, and in the bone collagen content [119, 120]. It is been found that Zn concentrates in the layer of osteoid before calcification takes place, which corresponds to the greatest concentration of alkaline phosphatase. This enzyme uses Mg as cofactor and an excess of Zn will inhibit the enzyme if Mg is displaced. Another enzymes essential in bone formation and remodeling is the collagenasa, which is Zn dependent. Studies in chick demonstrated the inhibition of this enzyme with the deficiency of Zn [121]. Zinc is also located in the bone mineral phase, most likely in hydroxyapatite in the form of a complex with F. This complex Zn-F may improve the crystalline structure of the apatite [122].

3.1.1.2 Copper

Several studies have reported that a diet deficient in Cu inhibits the bone growth and with pathological changes related to osteoporosis [123-125]. Copper has structural and functional roles in several important enzyme systems including the mitochondrial cytochromes, lysyl oxidase, superoxide dismutase, ceruloplasmin, and copper binding protein (CuBP) of intestinal mucosal cell cytosol. Copper works as an electron acceptor in the electron transport chain that allows the normal intracellular activity within the metabolic active bone cells. Once the copper is absorbed in the gastrointestinal mucosa, it is transported to albumin and to ceruloplasmin. Eight Cu atoms are in the ceruloplasmin molecule from which 4 are exchangeable and are part of the transportation mechanism; and the other 4 atoms are part of the structure. Bone mineral metabolism seems to not be directly affected by Cu, although its been found it plays a role in the cartilaginous phase as a cofactor in lysyl oxidase [126]. The liver and brain are the primary Cu storage organs since they store copper in ceruloplasmin. Bones do not make ceruloplasmin but still need it for Cu storage. Therefore bone overexposure to Cu has no physiological impact. In the mineral phase Cu is likely to be intergraded in the crystal lattice as any other divalent cation.

3.1.1.3 Magnesium

Magnesium is one of the most abundant cations found in the skeleton. It is found in all living tissue as an intracellular ion and it is an activator of many enzymes especially the ones related to the calcification of the skeleton (alkaline phosphatase and pyrophosphatasa) [113]. The use of Mg is essential for any enzyme catalyzed by ATP.

Magnesium also can inhibit the formation of calcium apatite within matrix vesicles. Around 60% of the magnesium in the human body is found in the skeleton and approximately 1% of the total body magnesium is extracellular [15]. Close to 30% of the magnesium in bone is absorbed on the crystals apatite surface to be exchangeable while the other 70% is been found to be integrated in the crystalline apatite by replacing Ca. [15, 113]. Magnesium concentration has been found to be constantly higher in trabecular bone than in compact bone.

3.1.1.4 Iron

It is been reported that the iron in the skeleton is associated to the organic phase rather than in the mineral portion. The iron in human bone ranges from 0.04-1.1 mmol kg^{-1}dry weight. The iron from the diet intake comes from plant and animal sources, which are associated to the two forms of iron: the heme that is derived from the myoglobine and hemoglobine, and the nonheme that come mainly from the plants. The iron present in bone tends to depend on the bone retention capabilities. The absorption of the heme iron is less affected by other dietary constituents while the nonheme absorption could be increased by vitamin C and alcohol [15]. Trace metals such as Ca, Cd, Cu, and F can also affect the absorption of iron in bone [127]. Histochemical and radionucleid studies of iron overload in the skeleton have shown the capabilities of iron to be absorbed by compact and trabecular bone. Also iron it is been found at the trabecular and endosteal surfaces, in mineralized bone at the junction of osteoid, and deposited into osteoclasts, osteocytes, and osteoblasts [127]. Contamination with iron from the soil is typically questioned especially when analyzing ashed bone. Since iron is mostly bound to the organic phase

(collagen) and this phase is less susceptible to exchange reactions than the mineralized bone, the contribution of iron from the soil could be minimal [15].

3.1.1.5 Strontium

Strontium shares many of calcium's chemical properties. One of these properties includes the replacement capabilities with calcium in different metabolic processes. Around 99% of the strontium in the body is located at the skeleton therefore the analysis of bone mineral has been used to follow up feeding habits [15]. The distribution of strontium in bone is similar to calcium, although bone and other organs such as kidney and the intestine prefer calcium over strontium. The discrimination is mainly attributed to the presence of living cells although also occurs at the crystal formation level [113]. The strontium levels in human bones vary with diet. The strontium concentration in a human ulna, was higher in the diaphysis than in the epiphyseal region, which may indicate differences in Sr concentration in trabecular and compact bone [118]. It is been reported that high Sr intake resulted in defective bone formation and mineralization [128-130].

3.1.1.6 Manganese

The skeleton is one of the main manganese storage locations. Most of the manganese is associated to the mineral phase with a small portion linked to the organic matrix [15]. Concentrations ranging from 1 to 4 ppm in bone ash were reported previously [131]. Manganese plays as a co-factor of a variety of enzymes such as pyruvate kinase, superoxide dismutase and carboxylases. A deficiency of manganese is been correlated to retarded bone growth, and skeletal abnormalities producing deformity in long bones and joint in mammalians. In a study with a Mseleni population of South

Africa it was reported that a deficiency in manganese diet could be a consequence of a disorder of mineralization and epiphyseal dysplasia [132].

3.1.1.7 Aluminum

Most of the aluminum ingested is eliminated in the faces but some small portion is absorbed in the gastrointestinal wall allowing accumulation in organs such as the liver, the testes, and in bones [114]. Also it is been found that fluorine increases the elimination of aluminum in the feces most likely because of the ability of Al^{3+} to from a complex with F^- ions. Rodriguez *et al.* performed a study with rats and showed a decrease of the osteoblast surface and an increase in the osteoid accumulation after the administration of aluminum, causing a cessation of bone formation [133]. These results suggest that bone formation is inhibited by the reduction of osteoblast activity, the osteoid mineralization and the matrix formation associated with the increase in aluminum content. Prolongated exposure to aluminum from antiacids and contaminated food and water may lead to a significant accumulation in bone. Other components that could increase or decrease the absorption and deposition of Al include citrate and ascorbate. Citrate in conjunction with the aluminum chloride in water demonstrated an enhancement in the Al absorption in bone of rabbits, while the ascorbate prevented its accumulation enhancing its excretion.

3.1.1.8 Barium

In a human diet, barium is not considered as an essential element in nutrition [134], although at some extent exposure from air, food and water occurs. Particles of barium are found in air due to industrial emissions from combustion of coal and diesel, and incineration processes. Concentration of barium in the ambient has been reported to

range from 0.0015-0.95 mg m^{-3} [135]. On the other hand lower concentrations (<0.002mg g^{-1}) of barium are found in most of the foods such as milk, potatoes, and flour [136]. The average human barium intake ranges from 0.65-1.7mg per day. In a study of barium content in human organs and tissues it was reported a that the total body barium content in a 70kg adult was 22,000μg with 93% of it found in bones and connective tissues [134]. Most of the barium is found associated to the inorganic portion of bone [114]. The incorporation of barium in the bone matrix is similar as calcium but it occurs at a faster rate [137]. In a study the barium retention on dogs bone surfaces have been reported to be longer than the retention of calcium, especially close to the Havarsian canals [138]. It is estimated that the half life of barium in bone lasts for about 50 days [139].

3.1.1.9 Lead

Lead is one a toxic metal to humans, and the skeleton isthe primary storage site for this element. This heavy isotope has a +2 valence that allows its accommodation in the empty spaces destined for cations such as calcium in the hydroxyapatite crystals without altering its functionality, although deforming it [140]. About 90% of the body's lead is located in the skeleton. The deposition of Pb in the skeleton is been described as a protective mechanism against lead toxicity. Since it has the capability of substituting calcium in hydroxyapatite, lead has been denominated as a volume seeker in the skeleton. The transfer of lead into the skeleton is most likely driven by diffusion from the blood supply passing through the skeletal cell layer into the semi-fluid section surrounding the hydroxyapatite crystals [127]. Lead is incorporated into an exchangeable surface and then passes to the non-exchangeable portion where the lead can be released by the change of

some factors such as the bone turnover rate, the surrounding pH, the concentration of the elements calcium, magnesium, and phosphate, and some bone regulating hormones. Lead seems to affect the functionality of the osteoblast inhibiting the bone formation by diminishing the collagen production and the bone growth. The mineralization process is also affected by the presence of lead by causing a decrease in calcium content, which is enough to produce rickets. The removal of lead from the skeleton will increase its presence in the blood stream, increasing the chances of causing damage to soft tissue and other organs. Under normal circumstances where there was no environmental contamination or exposure to lead the human skeleton levels should be practically zero. Data retrieved from several studies may suggest that there where insignificant differences in lead concentration (in ash weight) among different bones, except for the hard portion of the temporal bone that has been reported to have significantly higher lead concentrations. Lead skeletal content seems to increase in an irregular way with age [141].

3.1.2 Diagenesis in Buried Bones

In archeology the term diagenesis is described as the effect of the chemical, physical and biological conditions affecting the chemical or structural characteristics of buried bones and which determine if the material is destroyed or preserved [142, 143]. The buried bone material suffers from alterations such as molecular loss and substitution, crystallite reorganization, porosity and microstructural changes [144] that could lead to the uptake of cations, exchange of ions, breakdown and leaching of collagen, microbial attack, alteration and/or leaching of the mineral matrix, and infilling with mineral

deposits among other processes which settle the preservation or destruction of the buried bone. Diagenesis pathways are: (1) chemical deterioration of the organic phase, (2) chemical deterioration of the mineral phase, and (3) microbial attack [145].

The gradual loss of the organic phase strongly depends on the temperature and the pH of the environment. At higher temperatures of the organic material in buried bones will degrade at a faster rate. The underground water and its pH will allow for the removal of soluble products while the insoluble ones could be removed by physical means. Fatty products are more likely to be removed by alkaline waters while the more acidic products will be more easily removed at lower pH [92]. Once the organic portion is removed, the porous surfaces become more exposed and therefore susceptible to hydrolytic infiltration that may facilitate the uptake of endogenous and exogenous charged species into hydroxyapatite. The exposed porous bone surfaces will also easy the penetration of microorganisms causing chemical changes in the mineral phase where re-crystallization of hydroxyapatite may lead to the incorporation or substitution of exogenous material [146]. Therefore assessing the effects of diagenesis in buried bone is crucial for interpretation of the elemental composition in this matrix.

To better evaluate the diagenetic signal in buried bones the analysis of the soil associated to the samples is desirable. If the concentration of the elements in the soil and the bones are in agreement, then there is a strong evidence of diagenesis [12, 118].

Additionally to the elemental composition of soil, four diagenetic parameters have been used to assess diagenesis in buried bones: (1) collagen content, (2) histological integrity, (3) porosities (potential of hydrolytic leaching), and (4) crystallinity determined based on the infra-red splitting factor (IRSF). The histological integrity of bone and the

collagen content register the effects of diagenesis while the porosity and at some degree the crystallinity reflect the response of bone to the environmental conditions. Although these factors are useful to assess diagenesis, they are not directly correlated to any degradation process. The increase of these factors indicates a greater degree of diagenetic effects in the bone samples and is dependent on the environmental conditions [146].

When soil and the environmental conditions where the bones were buried are unknown, a different approach may be taken with a simpler strategy that has been recognized to evaluate and separate the biogenic elemental composition of buried bone from the one originated from diagenesis. This procedure is based on the higher solubility of the diagenetically altered material compared to that in biogenic bone mineral. The major component of biogenetic material is hydroxyapatite. Any alteration on hydroxyapatite will be an indication of diagenesis. The assessment of diagenesis in buried bones, the Ca/P ratio is determined. Any deviation from the theoretical Ca/P ratio for native (unchanged) hydroxyapatite (2.15) will indicate the bone has suffered of diagenesis, therefore the elemental composition of the bone samples are not from biogenic origin [10]. The theoretical Ca/P value was corroborated with the results published by Gawlik *et al.* in 1982 [11]. They reported a Ca/P experimental value of 2.17 ± 0.17 for experiments done with bone samples from the iliac crest of 20 individuals [11]. Dickerson in 1962 reported the Ca/P ratio found in femur samples of individuals of different groups' ages with the purpose of determining the changes in the composition of human femur during growth. Results on the analysis of the epiphyses portions of femurs of 5 groups of ages from 2 days old to 12 years old showed an average of Ca/P ratio of 2.10 ± 0.29. Analysis with whole bones of adults between 18 to 35 years old showed a

Ca/P ratio of 1.72 ± 0.22 [9]. Results of Ca/P seemed to vary according to the bone portion analyzed and the age. The Ca/P ratio of young mature bones is found to be below the theoretical value. This is attributed to the turnover or remodeling rate which is faster at this age. The Ca/P ratio in human bone increases with age as the turnover rate becomes slower [114].

It is also been reported that the middle layer of compact bone is less likely to experience diagenetic changes [118]. Analyses of cross-sections of femur compact bone by electron microprobe and total reflection X-ray fluorescence have demonstrated constant concentrations of elements such as Sr, Zn, and Pb between the periosteum and endosteum. The periosteum and endosteum regions showed a drastic change on elemental concentration suggesting that the elemental composition in these areas is from diagenesis or due to the closeness to trabecular bone [12, 118].

For the purpose of this study the area between the periosteum and endosteum of femur and humerus compact bones are analyzed to avoid the diagenetic signal. To corroborate the biogenic signal, the Ca/P ratios in the area of analysis are determined. Since femur and humerus bones were analyzed in this study, the Ca/P ratio reported by Dickerson *et al.* for femur bones (2.10 ± 0.29) will be considered as unchanged hydroxyapatite; therefore the elemental composition should be primarily biogenic [9]. Additionally a spatial resolution analysis of bone layers was performed with LA-ICP-MS to confirm the stability of the biogenic signal between the periosteum and endosteum of the bone samples.

3.2 Tooth Matrix

To understand the mineral nature and the elemental composition of human teeth it is important to know how teeth develop and their constituents. The development of the three principal layers of tooth will be discussed next, although only the elemental composition on enamel and dentine mineral phase will be discussed since these are the main studied layers of tooth for elemental and isotopic analyses in anthropology and forensics.

3.2.1 Tooth Development

The development of human tooth is a complex process that starts its formation from the embryonic cell all the way to eruption in the mouth. The process of tooth formation is mainly separated in the following stages: (1) the bud stage, (2) the cap, (3) the bell, and (4) crown or maturation. All these stages can be appreciated microscopically with different histologic sections of the same developing tooth at each stage [147].

At the bud stage it is evident the appearance of the tooth bud where there is no clear arrangement of cells. During the cap stage the cells start to arrange. The aggregation of ectomesenchymal cells results in what is called the dental papilla. Here the tooth bud grows around this aggregated cells becoming the enamel (or dental) organ. The dental follicle which is a condensation of ectomesenchymal cells will surround the enamel organ and limit the dental papilla. Further development will lead the enamel organ to produce the enamel and the dental papilla to produce the dentine and pulp of the tooth [147]. At the bell stage histodifferentiation and morphodifferentiation occur. Cells surrounding the enamel organ divide in three layers: the outer enamel epithelium (cuboidal cells on the

periphery of the enamel organ), the inner enamel epithelium (columnar cells adjacent to the dental papilla), and the stratum intermedium (cells between the inner enamel epithelium and the stellate reticulum). These layers will eventually from part on the development of the dentine and enamel. Also during the bell stage the initial growth of the crown and maybe other structures such as enamel knots, enamel cords, and enamel niche are observed. In the crown or maturation stage the hard tissues begging their development. Dentine and enamel layers start to develop at this stage, been the dentine formed before the enamel (Figure 6).

3.2.1.1 Dentine

The process called dentinogenesis, which is the first indication of the crown or maturation stage in the tooth, forms the dentine. Several dentine types such as mantle dentin, primary dentin, secondary dentin, and tertiary dentin result from the different stages in dentinogenesis. Odontoblasts are the cells in charge of the formation of dentine and secrete an organic matrix which contains collagen fibers that will surround the area near to the inner enamel epithelium. Then the odontoblast process take place where the odontoblasts move inwards to the center of the tooth, inducing the secretion of hydroxyapatite crystals and the mineralization of the matrix. This layer of mineralization area is known as mantle dentine [148]. The primary dentine forms because of the increase in the size of the odontoblasts that diminishes the availability of extracellular resources to from part of the organic matrix for the mineralization. The increase in odontoblasts size also causes a reduction of collagen secretion, which results in a tightly arranged heterogeneous nucleation during the mineralization process. After the root formation, the

secondary dentine is deposited at a slow rate and is not uniformly distributed along the tooth [149]. The development of the secondary dentine layer occurs throughout life. The tertiary dentine occurs as reparative or restorative measures when the tooth experience attrition of dental caries [149].

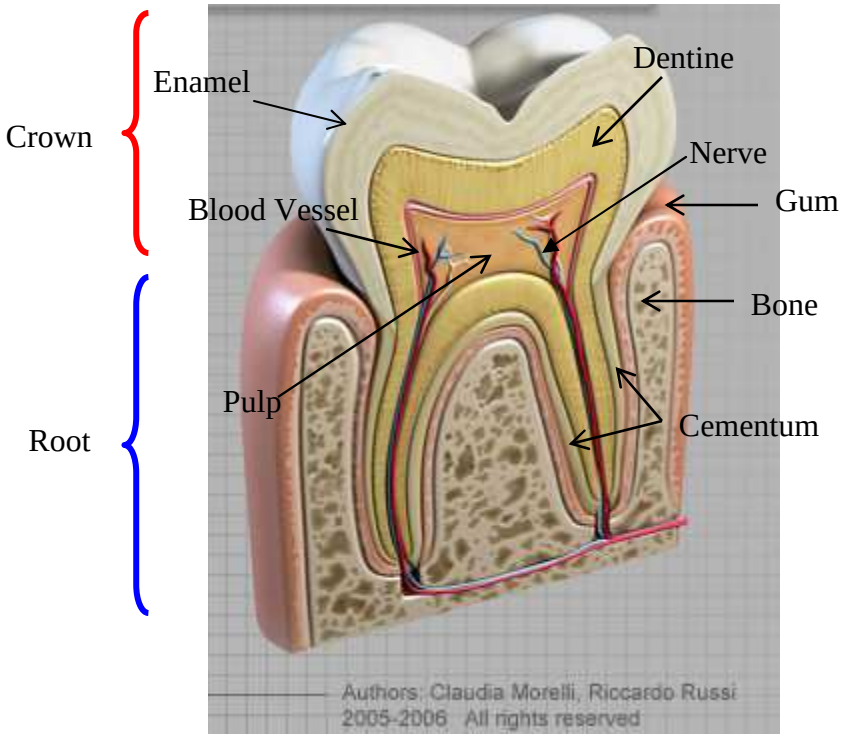

Figure 6. Diagram of a human tooth [150].

3.2.1.2 Enamel

The process by which enamel forms is called amelogenesis. In amelogenesis there is a mutualistic relationship with the dentine growth, where the dentine is the first to be formed. The enamel will form in two stages: (1) the secretory stage and (2) the maturation stage. In the secretory stage enamel proteins are released contributing to the enamel matrix which is partially mineralized by alkaline phosphatase [151]. This partially

mineralized layer is deposited on the dentine. The enamel growth then continues towards the outside and away of the center of the tooth. During the maturation stage some proteins (amelogenins, ameloblastins, enamelins, and tuftelins) [151] are transported to the outside of the enamel by the ameloblasts to complete the mineralization process.

3.2.1.3 Cementum

Cementogenesis is the process by which the cementum in tooth is formed. This process occurs at the latest stages of tooth development. The cells in charge of the cementogenesis are called cementoblasts. During cementogenesis two types of cementum are formed: cellular and acellular from which the former forms first. The acellular cementum is formed from a matrix of proteins and fibers that join the peridontal ligaments as the mineralization occurs. The cellular cementum is developed after most of the tooth is finished [148].

3.2.2 Trace Elements in Tooth Enamel and Dentine

The tooth enamel is approximately 96% by weight mineral, 0.5% by weight (on average) organic matter and the remaining portion is water. Enamel is the hardest calcified tissue in the human body and it is completely formed at 15 years of age. Elemental and isotopic composition of the early ages of life is fixed in the enamel layers. In archeology, the enamel is often the preferred material for determining elemental and isotopic composition because of its hardness and it is also less likely to be affected by diagenesis and environmental contamination. When diagenesis and environmental contamination are not a problem, the analysis of the enamel and cleaned dentine provide with acceptable results for modern forensic investigation [4].

The mineral composition of enamel is mainly hydroxyapatite although some major and minor elements are also found in this phase such as sodium, magnesium, potassium, chlorine, fluorine, zinc, iron, and strontium. Table 7 shows the major and minor elements in the inorganic portion of human enamel. The great differences in concentration of some elements reported in Table 7 in part reflect the biological variations between individuals due to the diet and water supply but also there is some contribution from the sample preparation and the analytical techniques used.

Studies on the different layers of enamel revealed that in rare occasions the trace elements are distributed evenly throughout the enamel. Elements such as Pb, Sr, Ni, Zn, Mn, Cu, Ag, Al, Fe, Cd, and Sn are found in greater concentration at the outer layer of the enamel than in the interior [114]. Cadmium, lead, tin, zinc, strontium, and copper seem to be deposited more intensively during the tooth formation prior eruption. It is been reported that Zn concentration decreases as going into the deeper enamel layers. On the other hand Pd shows a steep change from the outer layers to the inside. Lead concentrations at the inside enamel layers tend to stabilize.

Dentine consists of 70% by weight mineral, 20% by weight organic matter (collagenous proteins), and 10% by weight of water [114, 148]. When compared with the enamel, the dentine is much softer and less mineralized structure, therefore decays more rapidly. Several elements have been reported to be present in the dentine (Table 8). The data presented in Table 8 is a compilation of references from different studies and analytical techniques; therefore the large range of concentrations can be associated to analytical performance as well as with population differences. Regardless it is a good guide of which elements are present in human dentine. Brudevold *et al.* analyzed

different layers of dentine to determine the zinc concentration and they found an even distribution of Zn concentration in the dentine layer at 225 μg g^{-1}. Higher concentrations were found in the layer close to the pulp and in the outermost enamel layer [152].

Table 7. Trace elements present in detectable and quantifiable amounts in human tooth enamel [114].

Element	[a]Concentration Range	Element	[a]Concentration Range
Li	0.05-13.2	Sr	13-1400
Be	<0.01-15.9	Y	<0.01-0.017
B	0.5-190	Zr	<0.02-12
F	8-1000	Nb	<0.1-0.76
Al	1.5-353	Mg	0.6-39
Si	3-1400	Ag	0.005-37
S	0-530	Cd	0.03-74
Ti	<0.1-66	Sn	0.03-93
V	<0.01-0.28	Sb	<0.01-3
Cr	0.003-18	I	0.01-9.9
Mn	0.08-63	Cs	<0.02-0.10
Fe	0.8-759	Ba	0.8-190
Co	0.0002-45	Ce	0.02-0.19
Ni	0.1-13	Pr	<0.01-0.07
Cu	0.1-81	Nd	<0.02-0.09
Zn	9-1200	W	<0.08-0.4
As	<0.001-0.008	Au	<0.02-0.30
Se	0.012-18	Hg	0.005-16
Br	0.32-33	Pb	<0.1-1000
Rb	0.15-30	Bi	<0.02-0.07

[a]Dry weight in μg g^{-1}

Other elements such as Rb, Li, Ba, and Sr were analyzed in the coronal dentine on some tooth sections. Petersson *et al.* found no dependence of these elements concentration with the depth in the dentine layers although Rb, and Ba appeared to have higher concentrations in the layer closer to the pulp [153]. Higher concentrations of Pb, Fe, Ni, Cu and Zn were found in the pulpal wall than in the coronal middle dentine [154].

The elemental composition in teeth matrix is very similar to bones. Trace elements in hydroxyapatite matrix can be determined using the same method as in bone analysis. An element menu similar to the one chosen for bone is been selected accordingly to the following criteria: presence of the element in the hydroxyapatite matrix and the availability of the element's concentration above the instrumental detection limits. For the purpose of this study the following elements will be considered in tooth analysis: Mg, Mn, Fe, Cu, Zn, Rb, Sr, Ba, and Pb. After optimization of the laser ablation analysis, the same analytical method is been applied for both calcified tissues.

Table 8. Range of concentration or mean concentration of trace elements detected in human dentine [114].

Element	[a]Concentration Range	Element	[a]Concentration Range
B	[b]present	As	[b]present
F	2-1000	Se	0.1-0.3
Al	65-150	Br	4-115
Si	[b]present	Rb	5.6 ± 1.9
S	706	Sr	70-250
Ti	[b]present	Mo	[b]present
V	[b]present	Ag	0.005-3
Cr	0.005-2	Sn	[b]present
Mn	0.04-6	Sb	0.69 ± 0.41
Fe	2-110	I	3.7 ± 0.4
Co	0.0003-32	Ba	129 ± 55
Ni	5-30	W	2.6 ± 1.1
Cu	0.2-50	Au	0.03-0.07
Zn	100-700	Pb	2-44

[a]Dry weight in μg g^{-1}

[b]When there are no reliable quantitative data, the element is noted as present

3.3 Methodology

3.3.1 Suggested NITE-CRIME Method

3.3.1.1 Solution Based Analyses

Bone standard reference materials (SRMs) NIST 1486 (bone meal) and NIST 1400 (bone ash) [National Institute of Standards and Technology, Gaithersburg, MD, USA] were used to evaluate the method. Two digestion methods and a matrix suppression study from major elements calcium and phosphorus were assessed by measuring the SRMs against an external calibration curve. For the matrix suppression study the external calibration curve was modified in such a way that resembled the calcium and phosphorus concentration in bone samples. The suppression study allowed determining the whether the trace elements could be use for the elemental analysis of bone and teeth matrices by the HR-ICP-MS. The ICP-MS instrumental parameters for solution based analyses are shown in Table 9.

Table 9. Optimized experimental parameters for solution based and laser ablation analyses using the HR-ICP-MS system

		Laser Ablation Analyses	
Instrumental Parameters	*Solution Based Analyses*	*Pre-Ablation Parameters*	*Ablation Parameters*
Sample Gas Flow (L min^{-1})	1.07	[a]---	[a]---
Makeup Gas Flow (L min^{-1})	[a]---	0.70-0.80	0.70-0.80
Carrier Gas Flow (L min^{-1})	[a]---	Ar: 0.80-0.95 He: 0.90-1.10	Ar: 0.80-0.95 He: 0.90-1.10
Rf Power (W)	1300-1380	1300-1400	1300-1400
Plasma Gas Flow (L min^{-1})	16.00	16.00	16.00
Spot Size (µm)	[a]---	200	100
Laser Energy (mJ)	[a]---	1.16 (40%)	2.8 (100%)
Frequency (Hz)	[a]---	10	10
Ablation Mode	[a]---	Rastering	Single Spot
Ablation Time	[a]---	75 µm sec^{-1}	60 sec

[a]Not applicable

3.3.1.1.1 Digestion Procedures

Bone SRMs NIST 1400 and NIST 1486 (National Institute of Standards and Technology, Gaithersburg, MD, USA) were dried overnight under vacuum and weighed (about 0.150 g). The dried standards were placed into a 50 mL plastic disposable digestion tubes (Environmental Express Inc., Mt. Pleasant, South Carolina, USA) for open vessel digestion (OPD) and in the microwave vessels HP-500 Plus high pressure digestion vessels (CEM, Matthews, North Carolina, USA) for microwave assisted digestion (MAD). Three milliliters of 0.8M optima grade nitric acid (Fisher Scientific Pittsburg, USA) and 1 mL 30% ultrapure hydrogen peroxide (J.T. Baker, Phillipsburg, NJ, USA) were added to the digestion tubes.

Open Vessel. A condensation disc was placed on top of the digestion tubes to avoid excessive evaporation of the solution. After acids reaction (1-2 hours), the digestion tubes were placed on a heating block (Environmental Express Inc., Mt. Pleasant, South Carolina, USA) at 45 °C for one hour. The temperature was increased to 80 °C for 12 hours. After the tubes were cooled down and closed with a lid they were stirred for 0.5-1 min each. The final solution was quantitatively transferred to 25 mL volumetric flasks and completed to the mark with ultrapure deionized water (>18 MΩ cm^{-1}). Dilutions of the concentrated solutions were prepared with rhodium as internal standard for analysis.

Microwave Assisted. The microwave vessels were properly closed and put into the microwave oven MARS XS (CEM, Matthews, North Carolina, USA). The microwave was set with a ramp temperature program of 200°C at 14.6°C/min rate and hold at 200°C

for 30 minutes. Once the vessels were cooled down they were transferred quantitatively to 100 mL volumetric flasks and completed to the mark with ultrapure deionized water (>18 MΩ cm^{-1}).

Dilutions from the concentrated solutions were prepared with rhodium as internal standard. The solutions were measured against an external calibration curve containing elements of interest in the bone matrix. Certified values from some of the elements were provided by NIST and were used to assess the accuracy of the method. Acceptable accuracy results were considered to be 10 % bias from the certified or reference values and the precision of the measurements was evaluated with a 10% relative standard deviation (%RSD) of four sample replicates.

3.3.1.1.2 External Calibration Curve

Single element stock solutions of 1000 mg L^{-1} of each element were used to prepare the calibration curve. The following isotopes were measured for quantification: ^{25}Mg, ^{27}Al, ^{55}Mn, ^{56}Fe, ^{57}Fe, ^{64}Zn, ^{66}Zn, ^{85}Rb, ^{88}Sr, ^{137}Ba, and ^{208}Pb.

All solutions were prepared using high purity deionized water (>18 MΩ cm^{-1}) and 0.8M optima grade nitric acid (Fisher Scientific Pittsburg, USA). Elements were measured against normal ICP-MS calibration where the calibration levels were from 0 to 10 ng g^{-1}. Rhodium was added as internal standard to a concentration of 5ng g^{-1}.

Control verification checks (at 5 ng g^{-1}), including a secondary source standard to validate external calibration, were run with samples in order to evaluate drift and precision over time.

3.3.1.1.3 External Calibration Curve with Ca and P

Fresh bone SRMs were taken into solution by the open vessel digestion method aforementioned and measured against a modified calibration curve prepared with the addition of aliquots from a 10000 μg g^{-1} of calcium and phosphorus single stock standards (CPI International, Santa Rosa, California, USA) to each of the calibration standards in order to simulate the concentration of these elements in the bone SRMs (~32% Ca and ~15% P). Different dilutions of the bone SRMs were measured against this calibration curve to measure major, minor and trace elements. The elements concerned with this study were: ^{25}Mg, ^{27}Al, ^{55}Mn, ^{57}Fe, ^{66}Zn, ^{85}Rb, ^{88}Sr, ^{137}Ba, and ^{208}Pb.

3.3.1.2 Laser Ablation Analyses

3.3.1.2.1 Assessment of calcium as internal standard

In order to use calcium as internal standard, the calcium concentration of five bone and teeth samples respectively was determined by using a Scanning Electron Microscope (SEM) Philips XL30 with an Energy Dispersive X-ray Spectroscopy (EDS) detector (FEI Company, Hillsboro, Oregon, USA) in three different regions of each sample.

3.3.1.2.2 Laser ablation method optimization

Bone SRMs were prepared as pellets in a stainless steel manual pellet press (CARVER Inc., Wabash, IN, USA) with a 13 mm die. The pellets were compressed at approximately 2000psi for 1.5 minutes under vacuum. Pre-ablation of the surface was performed with the conditions showed in Table 9 to eliminate any press contamination.

The pellets were analyzed using the glass matrix SRM NIST 612 (National Institute of Standards and Technology, Gaithersburg, MD, USA) as calibrant and ^{42}Ca as internal standard since calcium is consistently found in bone samples at high percentage levels. The samples were ablated under the conditions shown in Table 9. A background signal was collected during the first 30 seconds of analysis. Then, the laser was fired for 60 seconds from which the middle 30 were used for signal integration. Another additional 30 second were analyzed to verify the return of the signal to the background levels and to purge before the next analysis. The total analysis time was 120 seconds. The pellets were sampled in replicates of four.

The ablation mode (single spot vs. scan line), frequency (5Hz vs. 10Hz), carrier gas (helium vs. argon) and gas flows parameters were compared for the method. A spot size of 100µm was selected for laser ablation analysis to increase the amount material removed for better representation of the sample. Helium was tested as carrier gas since in previous studies with other matrices have shown improvement in sensitivity due to a more efficient particle removal and transportation into the ICP-MS [61, 62].Doubly charged species, oxides and the U/Th fractionation were optimized to 3%, 3%, and about 1 respectively. The elements of interest in these analyses were: ^{25}Mg, ^{27}Al, ^{55}Mn, ^{56,57}Fe, ^{63}Cu, ^{64,66}Zn, ^{85}Rb, ^{88}Sr, ^{137}Ba, and ^{208}Pb. Most of these elements were chose because they are commonly found in bone matrix at concentrations above the detection limits, some of these elements are found in the inorganic phase, some elements have possible applications for work monitoring and environment exposure events, and after using statistical analysis these elements provided good discrimination between individuals.

3.3.2 Instrumentation

A high resolution (HR)-ICP-MS ELEMENT 2 (Thermo Electron Co. Bremen, Germany) was used for solution based and laser ablation analysis of the bone SRMs. The HR-ICP-MS system was used in the three mass resolutions low (~300), medium (~4000), and high (~10,000) for solution based analyses. The HR-ICP-MS was coupled to a Nd:YAG laser unit operating at 213 nm wavelength (New Wave Research, Fremont, CA, USA) for laser ablation experiments. The analyses with laser ablation were performed in medium resolution since the transient signal is gathered and no more than one resolution can be used at the same time. The description and operative principles of the HR-ICP-MS and the LA system were described in Sections 2.3.2.1 and 2.3.2.3 respectively.

3.3.2.1 SEM/EDS operative principles and experimental conditions

The image acquired by the SEM is the result of the interaction of a high energy electron beam with the surface of the material analyzed. These beam electrons interact with the atoms in the sample to release secondary electrons, backscatter electrons and x-rays. These released electrons provide with topographical and composition information of the surface analyzed.

When the electron beam and the sample atoms interact causing shell transitions an emission of x-rays characteristics of the parent element are released. The detection and measurement of these x-rays allows elemental analysis by EDS. With EDS it is possible to do qualitative, semiquantitative, and with the appropriate standards quantitative analysis with a sampling depth of 1 to 2 microns. The x-rays can also be used to map the elemental distribution in the sample surface.

In order to analyze samples by SEM/EDS the sample must be conductive. Biological samples such as bone, teeth and plant are not good conductive materials, thus coating with a thin layer of a conductive material such as carbon or gold may be required to reduce to the minimum the charging effect. Another alternative to reduce the charging effect will be to measure the samples in low vacuum. To avoid altering the material, these samples were measured in low vacuum.

Images and elemental analysis of Ca and P for the bone samples was performed with a SEM Philips XL30 (FEI Company, Hillsboro, Oregon, USA) with an EDS detector. The SEM/EDS conditions for the Ca and P determinations were: voltage of 25 kV, working distance (WD) of 10, spot size of 6, elapsed lifetime of 500 sec, and a magnification of 800x.

3.3.3 Data Analysis

3.3.3.1 Solution Based Analyses

The digested bone SRMs were measured against an external calibration curve. The intensities (cps) for the standards and samples were normalized to the rhodium (internal standard) signal (cps). A linear regression line was determined from the plot of the normalized signal (cps) against the concentration of the correspondent standard. Then the concentrations in the samples were determined by using the slope and intercept of this equation.

3.3.3.2 Laser Ablation Analyses

The transient signal of each element was collected during the ablation and then analyzed with GLITTER software (GLITTER, GEMOC, Macquarie University, Australia). The elements' concentrations were calculated based on a linear fit to ratios using the concentration of ^{43}Ca as internal standard in the bone SRMs and the calibrant SRM NIST 612 (for more details refer to Section 2.3.4.1).

3.3.2 Analysis of Bone and Teeth Samples by LA-HR-ICP-MS

3.3.2.1 Bone samples

3.3.2.1.1 Elemental analysis and discrimination of buried samples

Bone fragments of twelve individuals recovered from World War I (individuals 10-12) and World War II (individuals 1-9) [JPAC Laboratories, Hawaii, USA] were analyzed following the suggested NITECRIME method for laser ablation analyses. These individuals were already identified by mitochondrial DNA and/or from dental records. Soil samples were not provided; therefore the assessment of the possible leaching of elements could not be evaluated. Spatial analysis of the cross-section of 12 bone fragments was performed to identify the biogenetic signal. Analysis of the area between the periosteum and endosteum was performed. To corroborate the biogenic signal the Ca/P ratio was determined using SEM/EDS (Philips XL30, FEI Company, Hillsboro, Oregon, USA). The bone samples included proximal and distal fragments of humerus and femur bones of either hand or leg. Humerus bones from individuals 1 and 4 were not provided.

Thin bone fragments were cut with emery and fiberglass blades. After fragments were cut, the fragments were thoroughly rinsed with high purity deionized water (>18 MΩ cm^{-1}) for 10 minutes and dried overnight on polyethylene weighing boats. The fragments were ablated under the conditions specified in Table 9. The analysis was done in replicates of four spot per sample.

3.3.2.1.2 Crater morphology and estimate of ablated mass

Three ablation spots with the optimized conditions on a bone fragment and the SRMs NIST 1486 (pressed pellet) and NIST 612 (glass disk) were performed at a flat edge of the sample to measure the crater morphology. The UP213 New Wave Laser has a flat beam profile, thus the shape of the crater resembles to a cylinder. By determining the volume of the cylinder with the crater radius (r) and height (h) and the density of the material it is possible to estimate the mass occupied in this crater or the mass removed during the ablation. The r and h dimensions of the craters were determined by measurements done on the images of the craters taken with the SEM Philips XL30 (FEI Company, Hillsboro, Oregon, USA).

3.3.2.2 Teeth samples

Teeth samples were donated by Major Laura A. Regan from her Ph.D. research. The sample collection consisted of a brief survey and tooth donation for analysis of stable isotopes to determine if these isotopes can used as geographical markers for regions of childhood residency. Donations were received from patients that included cadets, active-duty, retirees, and dependents. The samples were comprised molars, canine, and wisdom teeth.

3.3.2.2.1 Elemental analysis of the different tooth layers

A set of teeth samples (Table 10) where the enamel was removed was analyzed to evaluate the elemental composition of the layers within the same tooth. The dentine + cementum portion was ground mix in a high speed micro mill and formed as pellets using the procedures mentioned above. The enamel was already in powder form; therefore the pellets were formed with the same procedure. Pre-ablation of the surface prior analysis was performed using the parameters mentioned in Table 9 to eliminate any possible contamination from the pellet press. Each sample was analyzed by doing three ablation spots in different areas of the pellet.

In addition to assessing the elemental composition on the different layers of tooth, the discrimination power of the elemental composition of enamel and dentine + cementum separately was assessed.

3.3.2.2.2 Elemental analysis of whole tooth

The set of samples presented in Table 11 were used to evaluate the discrimination power of elemental analysis in whole tooth samples. Each tooth was submerged in liquid nitrogen and broken into halves between polyethylene weighing boats in a mortar. The fragment was ground/mix in a high speed micromill and prepared as pellet using the procedures mentioned previously. The laser ablation analysis was carried out under the conditions described in Table 9 in replicates of five ablation spots per sample.

Table 10. List of teeth samples used for the study of the elemental composition on enamel and dentine + cementum portions.

Sample ID	Tooth #	Description	Natal Region
EAFA-139 AFA-139	16	enamel dentine+cementum	Panama, HI, TX, Germany
EAFA-276 AFA-276	32	enamel dentine+cementum	NY
EAFA-034 AFA-034	32	enamel dentine+cementum	WA
EAFA-265 AFA-265	16	enamel dentine+cementum	CO
EAFA-152 AFA-152	16	enamel dentine+cementum	Japan, Germany, SD
EAFA-026 AFA-026	16	enamel dentine+cementum	PA, NC, TX

3.3.2.3 Data processing and discrimination analyses

The data processing for determining concentration of the elements was done following the procedures mentioned in Section 3.3.2.2. The bone data was analyzed using the multivariate statistical analysis called Canonical Discriminant Analysis (CDA), described elsewhere [155], using the SPSS software (SPSS Inc., Chicago, IL, USA). For bone analyses the mean of the elements' concentrations on each bone (humerus and femur) was used for the discrimination analysis. Nested ANOVA analysis was used to assess which elements provide the best discrimination among the bone samples.

Nested-ANOVA statistical analysis was used to determine the elements that showed to provide with the most discrimination with the set of bone samples in this study. The multivariate analysis Principal Component Analysis (PCA) from SYSTAT 11 (Systat Software Inc., Chicago, IL) was used for discrimination of the whole teeth samples and for the discrimination of the different layers of tooth separately.

Table 11. Identification and natal origin information of whole teeth samples

Sample ID	Tooth #	Natal Region
AFA-004	1	IN
AFA-078	1	VT
AFA-093	17	OH
AFA-109	17	Peru
AFA-157	17	NE
AFA-159	32	mixed USA
AFA-199	17	TX
AFA-259	17	CA
AFA-265	17, 32	CO
AFA-277	32	mixed USA
AFA-278	16	NM
AFA-286	32	SC
AFA-289	1, 17, 32	FL
TWN-038	canine (6?)	Taiwan

3.4 Results and Discussion

3.4.1 Suggested NITE-CRIME Method

3.4.1.1 Digestion Methods

Two digestion methods for the analysis of bone SRMs were evaluated with an accuracy of 10% bias from the certified value and a precision of 10%RSD of the replicates of each sample. These have been reported previously as typical results for NAA analyses [156] while for ICP-MS analysis the accuracy and precision varies and the behavior of elements at these levels is still not very well understood in this matrix. Both digestions methods involved an acid digestion with nitric acid and peroxide. Table 12 shows the results of accuracy and precision from both digestion methods for bone SRMs. Elements certified by NIST in the bone SRMs NIST 1400 and NIST 1486 were considered to evaluate the accuracy of the concentration measurements obtained when digested by OVD and MAD. With OVD most of the elements had a recovery of 90% or

higher in both SRMs. For the SRM NIST 1486 the elements Mg, Fe, Mn, Sr, Ba and, Pb were measured with an accuracy of <10%bias while rubidium and zinc had a bias higher than 10%. Zinc experimental concentrations for both isotopes were showed an enrichment of this element suggesting some sort of contamination. Rubidium is not a certified element, therefore is not used to assess accuracy. The results with MAD for the SRM NIST 1486 showed poor accuracy (>10% bias) for Mg, Mn, ^{56}Fe in medium resolution, Zn, Sr, and Ba in low resolution. There was a low recovery of magnesium and for zinc. There was an enrichment of strontium causing a high bias (27%), which suggests a possible contamination with this element. Iron of mass 56 and barium in medium and low resolutions respectively showed a bias slightly higher than 10%, while the same isotopes measured in higher resolutions were within the acceptable parameters. Barium accuracy was determined against a non certified value, but the closeness of the concentration in the other resolutions may indicate this could be close to the real value. The precision of the measurements were below 10%RSD for most of the elements for both digestion methods, except for zinc and lead in the SRM NIST 1486. Although lead concentration was measured with good accuracy (8%bias) the precision of the measurements was very high (~40%RSD). The higher RSDs are attributed to the low recovery of this element in two of the four replicates. As is shown in Table 12 similar results were obtained for the SRM NIST 1400 with the exception of the accuracy of aluminum. The bias of the aluminum concentration was determined using a non-certified value provided by NIST and with both digestions a lower concentration was found when compared with the non certified value. The precision for all the measurements in the SRM NIST 1400 digested by both methods showed to be within the acceptable range

(≤10%RSD). Better results were obtained with the OVD procedure for magnesium, manganese, strontium, barium, and lead. For the other elements both digestion procedures showed to provide similar results.

3.4.1.2 Matrix suppression study

In the matrix suppression study fresh bone SRMs were digested using the open vessel digestion method. For comparison purposes the results with the modified calibration curve, was compared to results of the SRMs measured against a normal ICP-MS external calibration curve (ECC). For both bone SRMs the precision of the measurements were <10%RSD with both external calibrations (Table 13). The accuracy obtained with the modified calibration curve in the SRM NIST 1486 was above 10%bias for manganese, zinc, barium, and rubidium. Since the rubidium and barium values are not certified, they can only work as reference and not necessarily measures the accuracy of the analysis. Aluminum was below detection limits with both ECC's. NIST reported aluminum concentration in both SRMs as a non certified value and for SRM NIST 1486 its reference concentration is <1 $\mu g\ g^{-1}$ therefore it was expected to be close or below the detection limits with both ECC's. Iron, magnesium, zinc and strontium had a percent bias less than 10% for both SRMs which are acceptable values for the method (Table 13). Similar results were obtained with the SRM NIST 1400 with the exception that aluminum was consistently lower with both calibration curves resulting in a bias higher than 10%. For some elements in both SRMs the concentration determined with the modified ECC seems to provide lower values. This behavior may suggest some suppression especially for elements in concentrations close to detection limits and/or could be due to the

instrumental variation since both experiments were performed in different days and with different digested SRMs. Regardless, there is no strong evidence of matrix suppression of the trace elements by the high content of calcium and phosphorus in bone matrix, thus the use of trace elements for elemental analysis is valid.

3.4.1.3 Assessment of calcium as internal standard

For laser ablation analyses it is important to use an internal standard that is present in the matrix at high concentrations and do not vary significantly between samples of the same matrix. Calcium is present at approximately 26 wt% in the SRM NIST 1486 (bone meal) and at ~38 wt% in NIST 1400 (bone ash). To verify the calcium concentration in bone, calcium measurements of four bone samples were measured by detecting the calcium Kα line in the SEM/EDS instrument. The bone SRM NIST 1486 was measured prior the samples to verify the accuracy of the analysis. The accuracy of the analysis was evaluated by determining the %bias of the SRM measurement against the certified value. Typical acceptable values of accuracy and precision for SEM/EDS are within 10-15%bias and 15-20% RSD. The analysis of the SRM NIST 1486 was accepted with 15.2% bias and a precision of 2.4%RSD (Table 14). A correction to the measurement was done since solid oxides were added to the total amount of the SRM. The results for the four bone samples are shown in Table 15. The concentration of calcium in bone samples were similar to the calcium concentration in the SRM NIST 1486, thus for purposes of laser ablation data analyses and to generalize the method, the calcium concentration used was 26.58wt%.

Table 12. Results dissolution of bone SRMs NIST 1400 and NIST 1486 by Open Vessel and Microwave Assisted digestion procedures.

SRM NIST 1486	Concentration ± σ, µg g^{-1}			%Bias		%RSD	
Isotope	[f]MAD	[g]OVD	Reference Value	[f]MAD	[g]OVD	[f]MAD	[g]OVD
^{25}Mg (LR)	3978 ± 38	4190 ± 7	[a] *4660 ±170*	15	10	1	0.2
^{27}Al (LR)	[d]---	[d]---	[b] *<1*	[d]---	[d]---	[d]---	[d]---
^{27}Al (MR)	[d]---	[e]---	[b] *<1*	[d]---	[e]---	[d]---	[e]---
^{55}Mn (LR)	1.32 ± 0.02	1.08 ± 0.01	[b] *1*	32	9	1	1
^{56}Fe (MR)	113 ± 3	93 ± 3	[a] *99 ±8*	14	6	3	3
^{57}Fe (MR)	99 ± 4	92 ± 6	[a] *99 ±8*	0	7	4	7
^{56}Fe(HR)	103 ± 4	[e]---	[a] *99 ±8*	4	[e]---	3	[e]---
^{57}Fe(HR)	102 ± 4	[e]---	[a] *99 ±8*	3	[e]---	4	[e]---
^{64}Zn (MR)	97 ± 14	179 ± 3	[a] *147 ±16*	34	22	14	2
^{66}Zn (MR)	94 ± 13	183 ± 4	[a] *147 ±16*	36	24	14	2
^{85}Rb (LR)	0.34 ± 0.002	0.30 ± 0.01	[c]0.34	0	12	1	3
^{88}Sr (LR)	334 ± 2	248 ± 2	[a] *264 ±7*	27	6	1	1
^{137}Ba (LR)	277 ± 5	289 ± 6	[c]320	13	10	2	2
^{137}Ba (MR)	288 ± 5	[e]---	[c]320	10	[e]---	2	[e]---
^{137}Ba (HR)	290 ± 6	[e]---	[c]320	9	[e]---	2	[e]---
^{208}Pb (LR)	1.4 ± 0.6	1.21 ± 0.05	**1.3 ±0.01*	8	7	42	4
^{208}Pb (MR)	1.4 ± 0.6	[e]---	**1.3 ±0.01*	8	[e]---	41	[e]---

SRM NIST 1400	Concentration ± σ, µg g^{-1}			%Bias		%RSD	
Isotope	[f]MAD	[g]OVD	Reference Value	[f]MAD	[g]OVD	[f]MAD	[g]OVD
^{25}Mg (LR)	6005 ± 88	6516 ± 69	[a] *6840 ±13*	12	5	1	1
^{27}Al (LR)	344 ± 33	218 ± 7	[b] *530*	35	59	10	3
^{27}Al (MR)	371 ± 31	[e]---	[b] *530*	30	[e]---	9	[e]---
^{55}Mn (LR)	17.3 ± 0.6	17.3 ± 0.4	[b] *17*	2	2	4	3
^{56}Fe (MR)	617 ± 18	634 ± 19	[a] *660 ±27*	7	4	3	3
^{57}Fe (MR)	608 ± 18	672 ± 16	[a] *660 ±27*	8	2	3	3
^{56}Fe(HR)	628 ± 25	644 ± 28	[a] *660 ±27*	5	2	4	4
^{57}Fe(HR)	639 ± 28	668 ± 23	[a] *660 ±27*	3	1	4	3
^{64}Zn (MR)	126 ± 13	235 ± 10	[a] *181 ±3*	30	30	10	4
^{66}Zn (MR)	123 ± 10	241 ± 9	[a] *181 ±3*	32	33	8	4
^{85}Rb (LR)	0.50 ± 0.01	0.52 ± 0.02	[c]0.55	9	5	2	5
^{88}Sr (LR)	281 ± 3	246 ± 11	[a] *249 ±7*	13	1	1	5
^{137}Ba (LR)	231 ± 4	267 ± 2	[c]280	18	5	2	1
^{137}Ba (MR)	240 ± 4	259 ± 1	[c]280	14	8	2	1
^{137}Ba (HR)	247 ± 4	[e]---	[c]280	12	[e]---	2	[e]---
^{208}Pb (LR)	9.3 ± 0.1	8.9 ± 0.1	[a] *9.1 ±0.1*	2	2	1	1
^{208}Pb (MR)	9.6 ± 0.2	[e]---	[a] *9.1 ±0.1*	5	[e]---	2	[e]---

[a] Certified Value from NIST

[b] Non certified values provided by NIST

[c]Concensus values are from NITE-CRIME 1st Round Robin

[d] Concentration below detection limits

[e] Not determined

[f] Microwave Assisted Digestion

[g] Open Vessel Digestion

Table 13. Results of the matrix suppression study for SRMs NIST 1486 and NIST 1400.

SRM NIST 1486	Concentration ± σ, µg g^{-1}			%Bias		%RSD	
Isotope	Normal [e]ECC	[e]ECC with Ca and P added	Reference Value	Normal [e]ECC	[e]ECC with Ca and P added	Normal [e]ECC	[e]ECC with Ca and P added
^{25}Mg	4190 ± 7	4266 ± 114	[a] *4660 ± 170*	10	8	0.2	3
^{27}Al	[d]---	[d]---	[b] *<1*	[d]---	[d]---	[d]---	[d]---
^{55}Mn	1.08 ± 0.01	0.88 ± 0.04	[b] *1*	9	12	1	5
^{57}Fe	93 ± 3	91 ± 1	[a] *99 ± 8*	6	8	7	1
^{66}Zn	183 ± 4	125 ± 7	[a] *147 ± 16*	24	15	2	6
^{85}Rb	0.30 ± 0.01	0.25 ± 0.01	[c]0.34	11	26	3	6
^{88}Sr	248 ± 2	255 ± 10	[a] *264 ± 7*	6	4	1	4
^{137}Ba	289 ± 6	286 ± 7	[c]320	10	11	2	3
^{208}Pb	1.21 ± 0.05	[d]---	[a] *1.33 ± 0.01*	7	[d]---	4	[d]---

SRM NIST 1400	Concentration ± σ, µg g^{-1}			%Bias		%RSD	
Isotope	Normal [e]ECC	[e]ECC with Ca and P added	Reference Value	Normal [e]ECC	[e]ECC with Ca and P added	Normal [e]ECC	[e]ECC with Ca and P added
^{25}Mg	6516 ± 69	6449± 131	[a] *6840 ± 130*	5	6	1	2
^{27}Al	218 ± 7	296 ± 9	[b] *530*	59	49	3	3
^{55}Mn	17.3 ± 0.4	15.4 ± 0.03	[b] *17*	2	9	3	2
^{57}Fe	672 ± 16	597 ± 11	[a] *660 ± 27*	2	10	3	2
^{66}Zn	241 ± 9	172 ± 7	[a] *181 ± 3*	33	5	4	4
^{85}Rb	0.52 ± 0.02	0.40 ± 0.01	[c]0.55	5	27	5	4
^{88}Sr	246 ± 11	262 ± 4	[a] *249 ± 7*	1	5	5	2
^{137}Ba	267 ± 11	244 ± 2	[c]280	5	13	1	1
^{208}Pb	8.9 ± 0.1	10.1 ± 0.3	[a] *9.1 ± 0.1*	2	11	1	5

[a] Cetified Value by NIST

[b] Non certified Value provided by NIST

[c] Concensus Value from NITECRIME 1st Round Robin

[d] Below detection limits

[e] External Calibration Curve

Table 14. Calcium concentration in the SRM NIST 1486 measured by SEM/EDS.

Sample ID	Concentration of Ca, wt%	
NIST 1486-1	22	
NIST 1486-2	21	
NIST 1486-3	21	
Average	21	
StDev	0.5	[a]23
%RSD	2	
Certified Value	26.58 ± 0.24	26.58 ± 0.25
%Bias	21	13

[a]Corrected value due to the addition of GeO_2 and Y_2O_3

Table 15. Results of calcium concentration in bone samples by SEM/EDS.

Sample ID	Concentration of Ca, wt%
I06LHD	21
I06LHP	21
I08RHD	22
I09RFP	21
Average	21
StDev	0.3
%RSD	1

3.4.1.4 Laser ablation method optimization

For laser ablation analyses the acceptable parameters of accuracy and precision were ≤10%bias and ≤15%RSD. The acceptable precision is higher than with dissolution work because in LA we are dealing with smaller amount of sample and with a less homogeneous media than with solution; therefore the precision of the LA measurements is expected to be higher.

The optimization with carrier gas was determined with helium and argon gases. This study was performed with single spot ablations of 100μm at a frequency of 10Hz. The frequency and ablation mode parameters were selected at the beginning following the typical setup of glass laser ablation analysis as a reference. The optimization of frequency and ablation mode was corroborated in an additional study that will be explained below. Table 16 shows the results of accuracy and precision with bone SRMs NIST 1486 and NIST 1400. It is clear that when helium was used as carrier gas the accuracy of all elements in SRM NIST 1486 was improved and within the acceptable parameters while the results with argon carrier gas showed to be higher than 10% bias for most of the elements in this matrix. For the SRM NIST 1400 the accuracy of the certified elements Zn and Fe elements resulted with bias higher than 10%. Both elements had lower concentration than the certified value indicating a problem either with the ionization of these elements or with the distribution of the elements in the SRM. When argon was used as carrier gas the concentration determination was not possible because the signal of this element in the calibrant (SRM NIST 612) was not enough sensitive to be detected properly as it was explained in Chapter 2. The iron signal in SRM NIST 612 was improved with helium as carrier gas allowing an accurate determination of iron concentration in the bone SRMs. In terms of precision for both SRMs the %RSDs were ≤15% for most of the elements, although some elements showed lower %RSDs when argon was used as carrier gas. Previous studies with glass have shown an improvement in the removal and particle transportation in laser ablation analyses using helium as carrier gas [61, 62]. Helium is selected as carrier gas for the analysis of bone and teeth matrices due to the improved results obtained with this gas.

Table 16. Results of optimization of carrier gas in laser ablation method development

	Concentration ± σ, µg g-1			%Bias		%RSD	
Isotope	Carrier Gas: Argon	Carrier Gas: Helium	Reference Value	Carrier Gas: Argon	Carrier Gas: Helium	Carrier Gas: Argon	Carrier Gas: Helium
^{25}Mg	5856 ± 44	4327 ± 30	[a] *4460 ±170*	26	7	1	1
^{27}Al	0.88 ± 0.11	1.07 ± 0.04	[b] <1	12	7	13	3
^{55}Mn	1.2 ± 0.3	0.99 ± 0.13	[b] 1	18	1	24	13
^{57}Fe	[d] ---	101 ± 12	[a] *99 ±8*	[d] ---	2	[d] ---	11
^{65}Cu	0.61 ± 0.06	0.74 ± 0.08	[b] 0.8	23	8	9	11
^{66}Zn	75 ± 1	134 ± 2	[a] *147 ±16*	49	9	2	2
^{85}Rb	0.30 ± 0.02	0.35 ± 0.03	[c] 0.34	12	1	6	4
^{88}Sr	265 ± 16	283 ± 14	[a] *264 ± 7*	0.2	7	6	14
^{137}Ba	296 ± 26	289 ± 2	[c] 320	7	10	9	1
^{208}Pb	1.2 ± 0.2	1.4 ± 0.2	[a] *1.33 ±0.01*	10	4	15	11

	Concentration ± σ, µg g-1			%Bias		%RSD	
Isotope	Carrier Gas: Argon	Carrier Gas: Helium	Reference Value	Carrier Gas: Argon	Carrier Gas: Helium	Carrier Gas: Argon	Carrier Gas: Helium
^{25}Mg	7300 ± 518	6382 ± 69	[a] *6840 ±130*	7	7	7	1
^{27}Al	271 ± 103	302 ± 78	[b] 530	49	43	38	26
^{55}Mn	15 ± 2	15.1 ± 0.2	[b] 17	14	11	17	2
^{57}Fe	[d] ---	484 ± 14	[a] *660 ±27*	[d] ---	27	[d] ---	3
^{65}Cu	0.93 ± 0.05	2.1 ± 0.1	[b] 2.3	60	9	5	5
^{66}Zn	119 ± 12	157 ± 8	[a] *181 ± 3*	34	13	10	5
^{85}Rb	0.30 ± 0.02	0.44 ± 0.01	[c] 0.55	45	20	7	2
^{88}Sr	227 ± 5	253 ± 0.8	[a] *249 ± 7*	8.8	2	2	0
^{137}Ba	228 ± 6	254 ± 1	[c] 280	19	9	3	0
^{208}Pb	5.31 ± 0.0.63	8.6 ± 0.2	[a] *9.07 ±0.12*	41	5	12	2

[a] Certified Value by NIST

[b] Non certified values provided by NIST

[c] Concensus value of the First Round Robin of NITE-CRIME Network (unpublished data)

[d] Not determined

The ablation mode and frequency parameters were optimized with the same bone SRMs' pellets. This optimization study was performed using helium as carrier gas and a spot size of 100 µm since it was shown previously to provide desirable results. Two ablation modes (single spot and scan line) and frequency (5 HZ and 10Hz) were evaluated with the acceptable parameters of %bias and %RSDs abovementioned. It is clear on Table 17 that better accuracy and precision was obtained for most of the elements in both SRM's with single spot ablation at 10Hz repetition rate (frequency). The

specific setup of frequency and ablation mode provides with a more efficient particle removal with the non-matrix match standardization using glass as calibrant. The improvement in sensitivity translates in more accurate results.

Table 17. Results of optimization parameters ablation mode and frequency for SRMs NIST 1486 and NIST 1400.

SRM NIST 1486	**Concentration ± σ, µg g^{-1}**									
Optimization Parameter	**^{25}Mg**	**^{27}Al**	**^{55}Mn**	**^{57}Fe**	**^{65}Cu**	**^{66}Zn**	**^{85}Rb**	**^{88}Sr**	**^{137}Ba**	**^{208}Pb**
Single Spot, 5Hz	982 ± 81	1.2 ± 0.5	1.3 ± 0.2	49 ± 10	0.74 ± 0.01	92 ± 13	0.24 ± 0.02	268 ± 18	224 ± 14	0.88 ± 0.16
Single Spot, 10Hz	4327 ± 30	1.0 ± 0.1	1.0 ± 0.1	101 ± 12	0.74 ± 0.08	134 ± 2	0.30 ± 0.01	283 ± 38	289 ± 2	1.4 ± 0.2
Scan Line, 5 Hz	4633 ± 184	1.5 ± 0.2	2.6 ± 0.3	97 ± 12	0.72 ± 0.09	78 ± 2	0.25 ± 0.02	262 ± 5	315 ± 15	1.43 ± 0.06
Scan Line, 10Hz	4081 ± 300	1.3 ± 0.7	1.1 ± 0.1	69 ± 9	0.57 ± 0.05	60 ± 4	0.22 ± 0.02	265 ± 30	277 ± 20	0.81 ± 0.15
Reference Value	***[a]4460 ± 170***	**[b]1**	**[b]1**	***[a]99 ± 8***	**[b]0.8**	***[a]147 ± 16***	**[c]0.34**	***[a]264 ± 7***	**[c]320**	***[a]1.33 ± 0.01***
%Bias										
Optimization Parameter	**^{25}Mg**	**^{27}Al**	**^{55}Mn**	**^{57}Fe**	**^{65}Cu**	**^{66}Zn**	**^{85}Rb**	**^{88}Sr**	**^{137}Ba**	**^{208}Pb**
Single Spot, 5Hz	78	21	26	50	8	38	29	1	30	34
Single Spot, 10Hz	3	4	2	2	8	9	12	7	10	5
Scan Line, 5 Hz	4	50	163	2	10	47	27	1	2	7
Scan Line, 10Hz	8	31	5	30	28	59	36	0.3	13	39
%RSD										
Optimization Parameter	**^{25}Mg**	**^{27}Al**	**^{55}Mn**	**^{57}Fe**	**^{65}Cu**	**^{66}Zn**	**^{85}Rb**	**^{88}Sr**	**^{137}Ba**	**^{208}Pb**
Single Spot, 5Hz	8	45	17	21	1	15	7	7	6	18
Single Spot, 10Hz	1	9	10	11	11	2	4	14	1	11
Scan Line, 5 Hz	4	1	11	13	12	3	10	2	5	4
Scan Line, 10Hz	7	6	5	13	9	7	11	11	7	19

SRM NIST 1400	**Concentration ± σ, µg g^{-1}**									
Optimization Parameter	**^{25}Mg**	**^{27}Al**	**^{55}Mn**	**^{57}Fe**	**^{65}Cu**	**^{66}Zn**	**^{85}Rb**	**^{88}Sr**	**^{137}Ba**	**^{208}Pb**
Single Spot, 5Hz	1671 ± 102	263 ± 109	14 ± 0.6	141 ± 11	1.0 ± 0.1	118 ± 5	0.26 ± 0.04	240 ± 9	190 ± 6	4.96 ± 0.86
Single Spot, 10Hz	6382 ± 69	302 ± 78	15.1 ± 0.2	484 ± 14	2.1 ± 0.1	157 ± 8	0.44 ± 0.01	253 ± 0.8	254 ± 1	8.6 ± 0.2
Scan Line, 5 Hz	6040 ± 343	255 ± 61	16 ± 4	265 ± 79	0.86 ± 0.09	106 ± 9	0.28 ± 0.08	250 ± 10	269 ± 21	5.26 ± 0.49
Scan Line, 10Hz	6041 ± 458	304 ± 43	12 ± 1	285 ± 42	0.98 ± 0.10	128 ± 15	0.28 ± 0.04	252 ± 16	246 ± 16	4.83 ± 0.97
Reference Value	***[a]6840 ± 130***	**[b]530**	**[b]17**	***[a]660 ± 27***	**[b]2.3**	***[a]181 ± 3***	**[c]0.55**	***[a]249 ± 7***	**[c]280**	***[a]9.07 ± 0.12***
%Bias										
Optimization Parameter	**^{25}Mg**	**^{27}Al**	**^{55}Mn**	**^{57}Fe**	**^{65}Cu**	**^{66}Zn**	**^{85}Rb**	**^{88}Sr**	**^{137}Ba**	**^{208}Pb**
Single Spot, 5Hz	76	50	17	79	55	35	52	4	32	45
Single Spot, 10Hz	7	43	11	27	9	13	20	2	9	5
Scan Line, 5 Hz	10	52	7	55	63	41	48	1	4	42
Scan Line, 10Hz	12	43	30	57	58	29	48	1	12	47
%RSD										
Optimization Parameter	**^{25}Mg**	**^{27}Al**	**^{55}Mn**	**^{57}Fe**	**^{65}Cu**	**^{66}Zn**	**^{85}Rb**	**^{88}Sr**	**^{137}Ba**	**^{208}Pb**
Single Spot, 5Hz	6	42	4	10	8	4	14	4	3	17
Single Spot, 10Hz	1	26	2	3	5	5	2	0.3	0.4	2
Scan Line, 5 Hz	6	24	23	23	11	8	29	4	8	9
Scan Line, 10Hz	8	14	9	15	11	12	12	7	6	20

[a] Certified Value by NIST

[b] Non certified values provided by NIST

[c] Concensus value of the First Round Robin of NITE-CRIME Network (unpublished data)

In summary the optimal parameters for the LA analysis of bone SRM's were single spot ablation of 100µm size at a repetition rate of 10HZ using helium as carrier gas. These parameters were used for all laser ablation analyses.

3.4.1.5 Crater morphology and Estimate of the ablated mass

Ablation spots of 100µm radius were created at the edge of the bone matrix under the following laser conditions: repetition rate- 10Hz, laser energy (100%) and in a helium gas environment. The crater morphology in the bone fragment, the SRM NIST 612 and the SRM NIST 1486 pellet varied according to the density. Deeper penetration of the laser was obtained with the SRM NIST 1486 pellet when compared to the bone fragment (Figures 7 and 8). This indicates a difference in density these materials. The crater morphology on the SRM NIST 1486 resembles to that a cylinder with a flat bottom, whereas the craters in the bone fragment showed a non-flat bottom. Regardless, in order to avoid an incorrect analysis all signal integration of the SRMs and samples with the Glitter software do not take into account this last portion of the ablation.

The density of glass was previously reported in our laboratory as 2.4×10^6 g m^{-3}. With the glass density and the volume of the crater, the estimated ablated mass for SRM NIST 612 was 8.2 ± 0.2 µg. For a pellet of 13mm radius, 4mm height, and a mass 1.0020g, the density of the SRM NIST 1486 pressed pellet was 4.72×10^5 g m^{-3}, thus the estimated ablated mass for the craters on the SRM NIST 1486 was 8.8 ± 0.4 µg. Using the density of compact bone (1.9×10^6 g m^{-3}) [157] and volume of the craters the estimated ablated mass was 12 ± 1 µg. The estimated ablated mass of the SRMs NIST 612 and NIST 1486 were very similar, whereas the estimated mass of the bone fragment

is about 1.3 times more than the SRMs. Regardless, the mass ablated under the optimized laser ablation parameters resulted to be very similar.

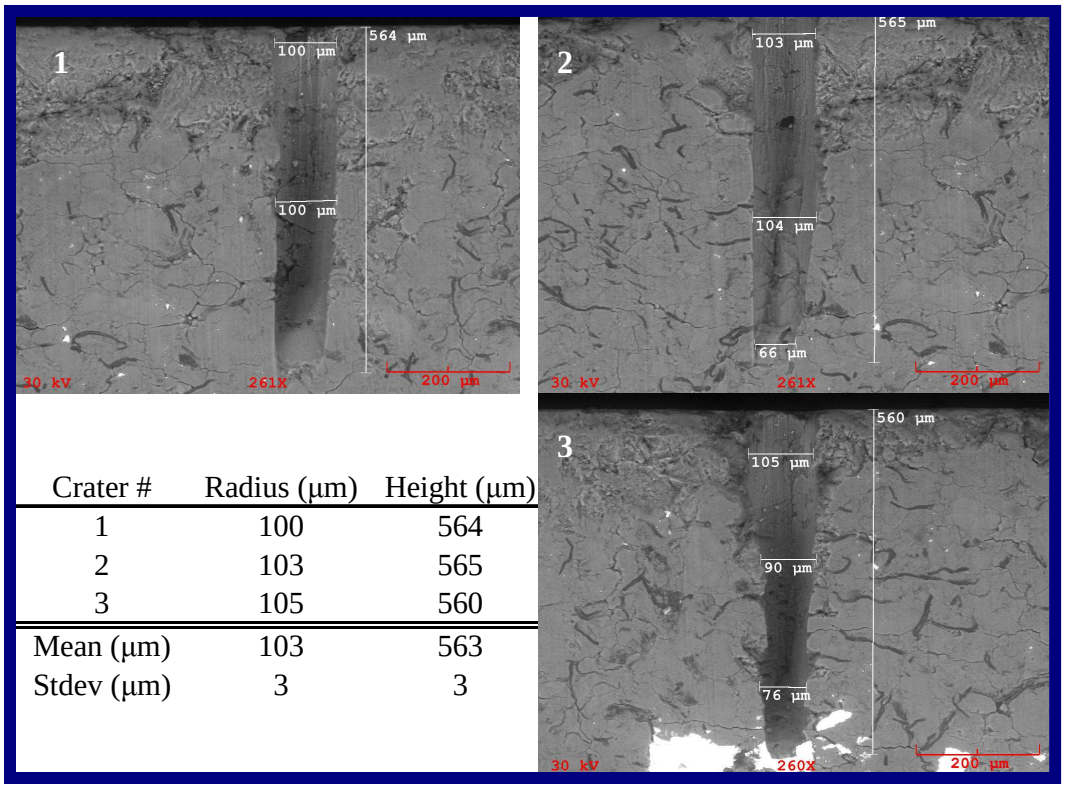

Crater #	Radius (µm)	Height (µm)
1	100	564
2	103	565
3	105	560
Mean (µm)	103	563
Stdev (µm)	3	3

Figure 7. SEM images of the craters on the SRM NIST 1486 pressed pellet and the crater dimensions measurements. (The brightened area in crater 3 is due to residues of C tape)

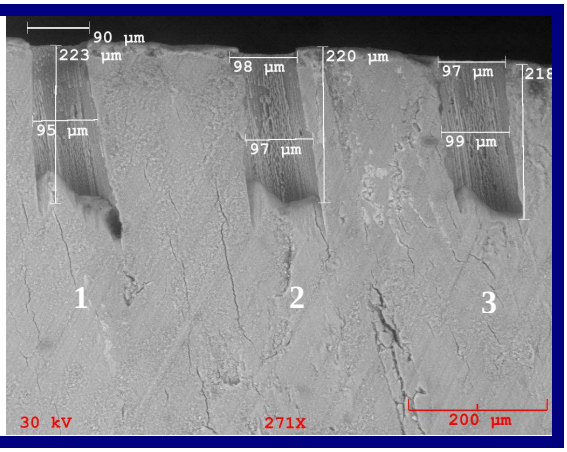

Crater #	Radius (µm)	Height (µm)
1	90	223
2	98	220
3	97	218
Mean (µm)	95	220
Stdev (µm)	4	3

Figure 8. SEM images of the craters on a bone fragment and the crater dimensions measurements.

3.4.2 Analysis of Bone and Teeth Samples by LA-HR-ICP-MS

3.4.2.1 Elemental analysis and discrimination of buried samples

Prior elemental analysis with the optimized LA method, a rastering analysis of the cross-section of 12 compact bone fragments was performed by LA-HR-ICP-MS. The concentration was determined with the LA method from the external layer (exposed to the environment) of the bone through the inner layer (close to trabecular bone) (Figure 9). The rastering was performed using a 100 µm spot size, a frequency of 10 Hz and helium as carrier gas. The scanning time was 15 µm per second. Then, the transient signal was integrated in intervals of 5 seconds of ablation, which represents the concentration in a 75 µm region. This is a relatively fast way to establish constant concentration of the elements of interest in compact bones.

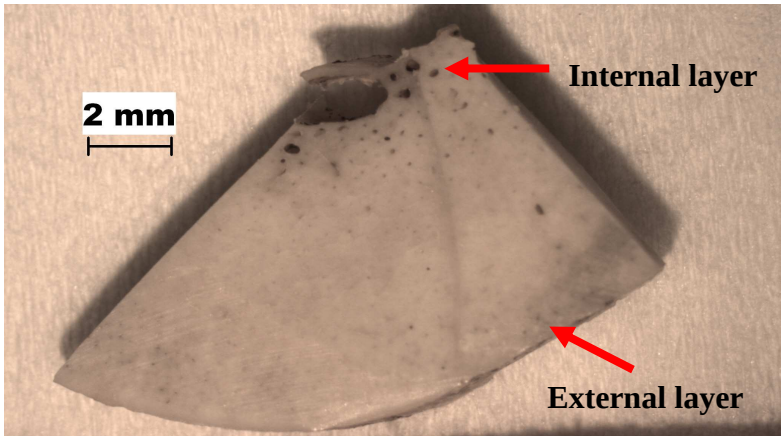

Figure 9. Picture of a typical compact bone fragment.

For practical purposes only data from one of the bone fragment is shown. Elements such as Mn, Sr, Zn, Ba, and Fe showed increased concentration close to the external layer while only Mn and Fe showed increased concentration at both the external and internal layers of the bone (Figures 10). Magnesium on the other hand presented less

concentration at the extremes than in the middle regions. A concentration with relatively small variation was presented at the middle layers (between regions 5 to 8) of the bone. The stabilized signal in the middle layers of bone may indicate that the elemental composition in this region reflects that of the biogenetic signal rather than from the one affected by diagenesis. In general the same results were observed for the 12 bone samples analyzed under the same conditions by LA-HR-ICP-MS. The results suggested that the biogenetic signal in these bones is present in the middle regions of the bone cross-section; therefore the LA analysis should be done within this area.

To confirm the above results the Ca/P ratios was determined in the middle layers of bone using SEM/EDS. Seven random samples and the SRM NIST 1486 were analyzed for this purpose under the optimized SEM/EDS conditions in low vacuum with an energy voltage of 25 kV and a magnification of 800X, which allowed analyzing an area of approximately 300 µm x 300 µm. Areas where the Ca/P ratio lied between 1.81 and 2.39 were considered as an unchanged hydroxyapatite, thus the elemental composition comes mostly from the biogenetic signal. The Ca/P ratio results for the SRM and the seven bone samples are shown in Table 18. All the samples showed a Ca/P ratio between the expected values confirming the biogenetic signal in this preferred area of analysis.

Once the area of biogenetic signal is established, the bone samples were analyzed with the suggested NITE-CRIME LA method using the HR-ICP-MS (Section 3.4.1.4). A wide variety of elements were measured using LA-HR-ICP-MS from which only several elements were selected for discrimination analysis based on the capability to discriminate among samples (Nested ANOVA analysis), the presence of these elements above the instrumental detection limits for LA, and the likeliness of these elements to be in bone.

Table 18. Ca/P ratio of compact bone samples determined by SEM/EDS.

Sample	Ca/P ± σ
SRM NIST 1486	1.91 ± 0.01
I10RDH	2.25 ± 0.02
I08RPH	1.98 ± 0.01
I07LPH	1.96 ± 0.12
I11RDF	2.02 ± 0.02
I12RDF	2.05 ± 0.02
I05RDF	1.82 ± 0.03
I08RDF	1.94 ± 0.01

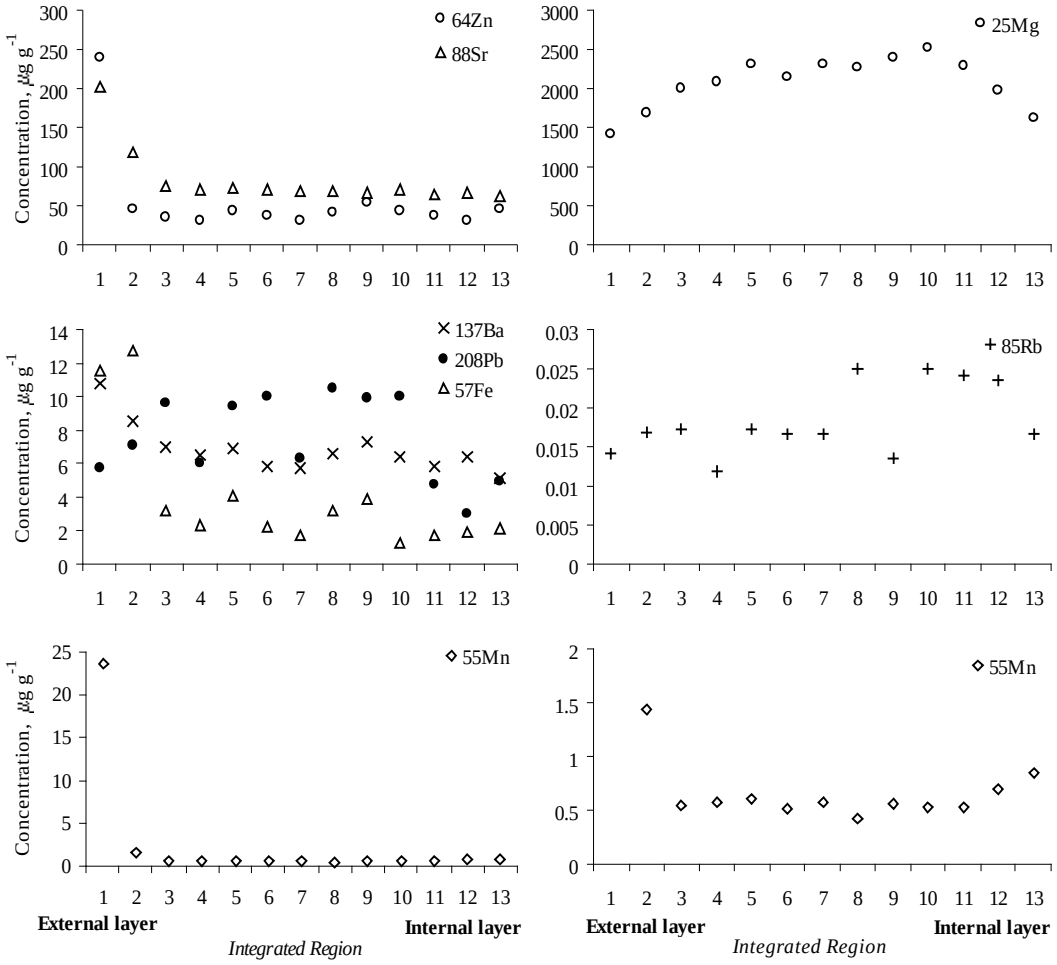

Figure 10. Concentration of Zn, Sr, Pb, Fe, Ba, Rb, Mn, and Mg in the cross-section of the sample I08RPH.

The Nested ANOVA analysis provides with information regarding to significant differences at two levels: between individuals and between bone type (humerus and femur proximal and distal). If the $P_{statistic}$ is <0.05, then the null hypothesis is rejected implying that there are significant differences within a specific level for that specific element. Table 19 shows the Nested ANOVA results for each element measured. It is clear from these results that by looking at Sr, Mg, Rb, Sr, and Fe respectively there are significant differences between individuals. At the second level all elements except Zn showed to significant differences between bone types.

Table 19. Nested ANOVA results for the LA data of all bone samples.

	$P_{statistics}$	
Element	**Between Individuals**	**Between Bone Type (Humerus and Femur)**
Fe	0.02	<<0.001
Cu	0.44	<<0.001
Mn	0.34	<<0.001
Mg	0.004	<<0.001
Sr	<<0.001	<<0.001
Ba	0.82	<<0.001
Pb	<<0.001	<<0.001
Rb	0.03	<<0.001
Zn	0.4	0.06
Al	0.25	<<0.001

Using the Nested ANOVA results and the aforementioned factors, the element menu for discrimination among bones of different individuals includes: Mg, Mn, Fe, Zn, Rb, Sr, Ba, and Pb.

The data were analyzed using the multivariate analysis CDA with the above mentioned discrimination elements. When all bones for individuals 1-9 from World War

II and individuals 10-12 form World War I was used for the multivariate analysis, there was no separation of the individuals by elemental composition (Figure 11). Only a 60.0% of the original cases were correctly classified. Individuals 12 and 7 are largely separated from the rest of individuals suggesting the elemental composition is significantly different. There was an overlap of all other individuals' groups. The samples I03RPF and I10RPH were analyzed as unknown to validate the analysis.

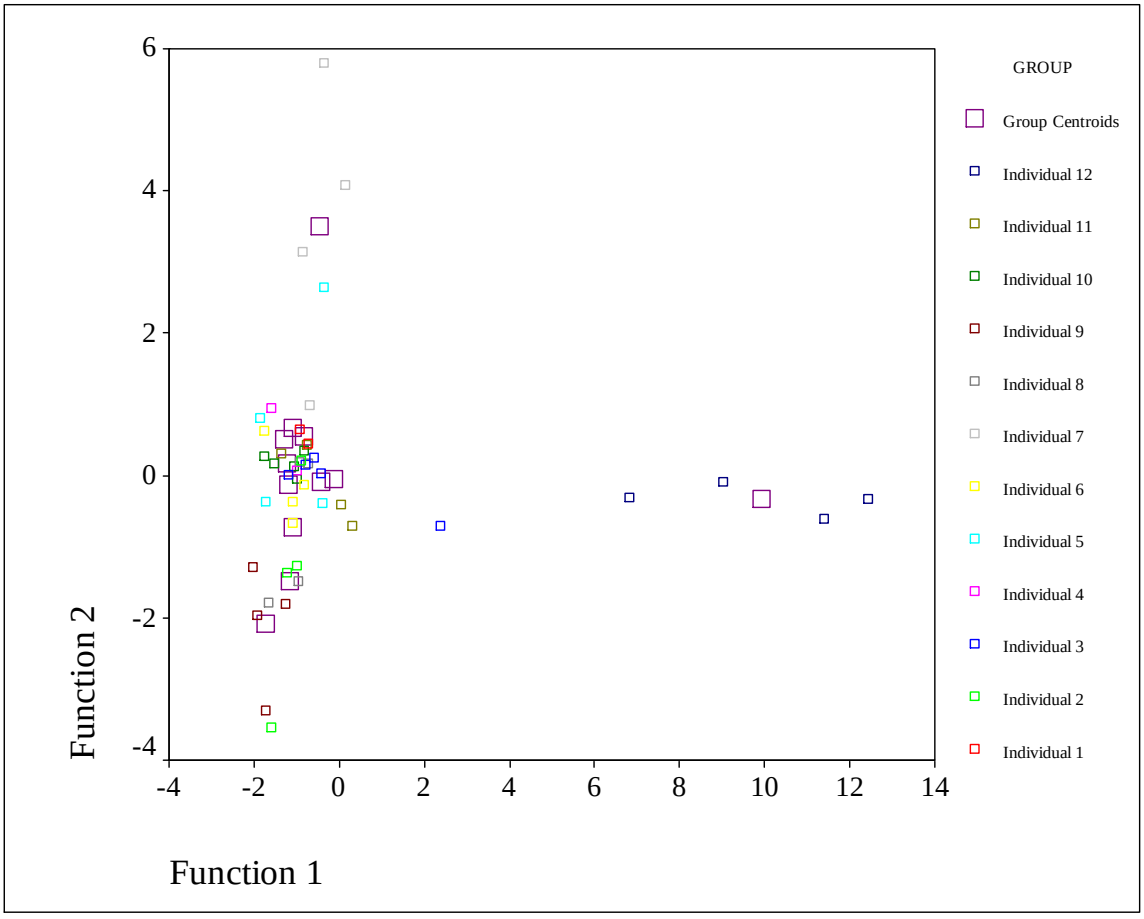

Figure 11. CDA plot of the humerus and femur bones for the 12 individuals.

When the samples were separated by bone type there was an improvement in the discrimination of the individuals by elemental composition. When only the humerus data was used for the CDA, the 90.5% of the original cases were correctly identified. There was an overlapping of the groups of individuals 8 and 10. The group of individual 12 showed to be of very different elemental composition from the other individuals, including the samples coming from the same recovery site (Individuals 10 and 11). The sample measured as an unknown (I10RPH) was correctly groped with Individual 10 group (Figure 12).

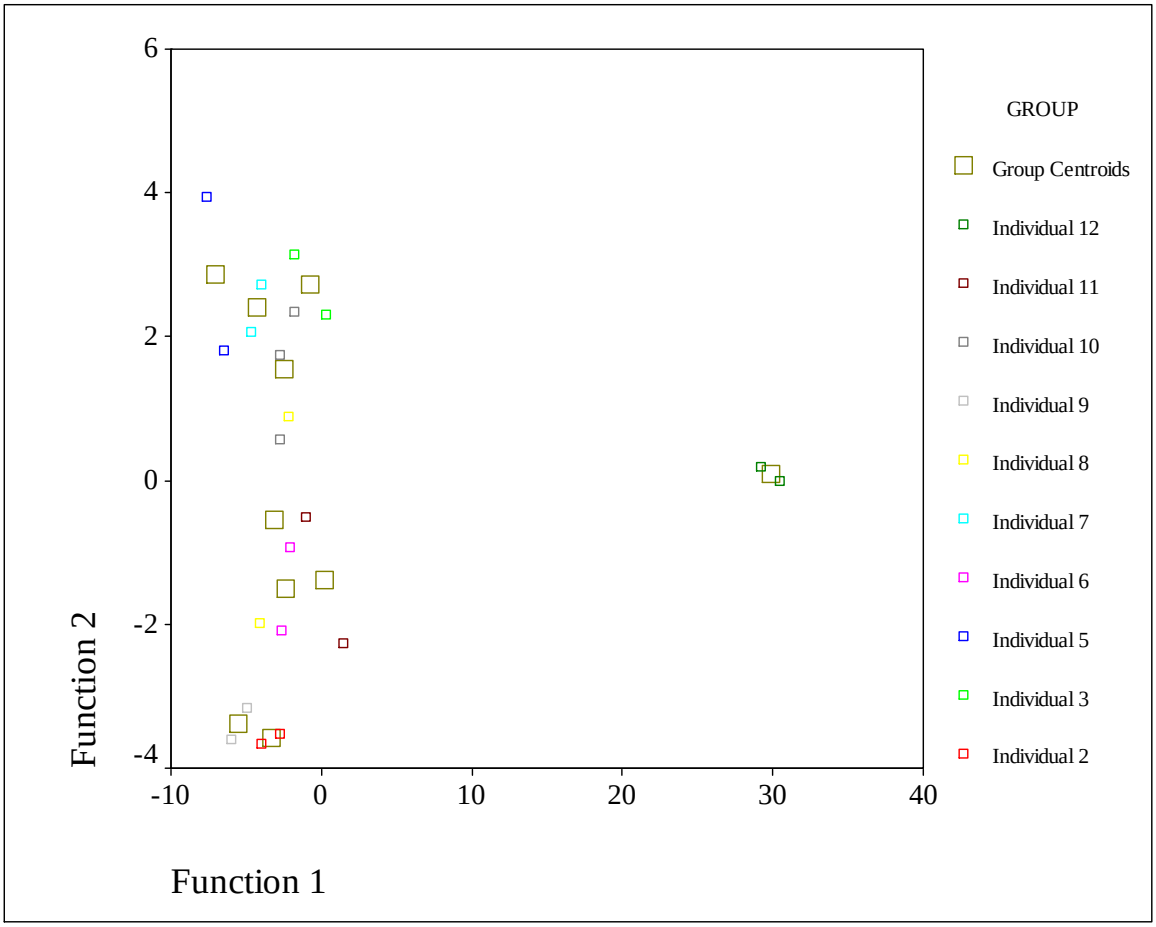

Figure 12. CDA plot of the humerus bones for 10 individuals.

For the CDA of femur bones, only 80.0% of the original case groups were correctly classified. The unknown sample I03RPF was correctly grouped with Individual 3 group, which validates the analysis (Figure 13). Here, as with the CDA of humerus bones, individual 12 is grouped to a very large distance from the rest of the other groups, suggesting a significance difference in elemental composition.

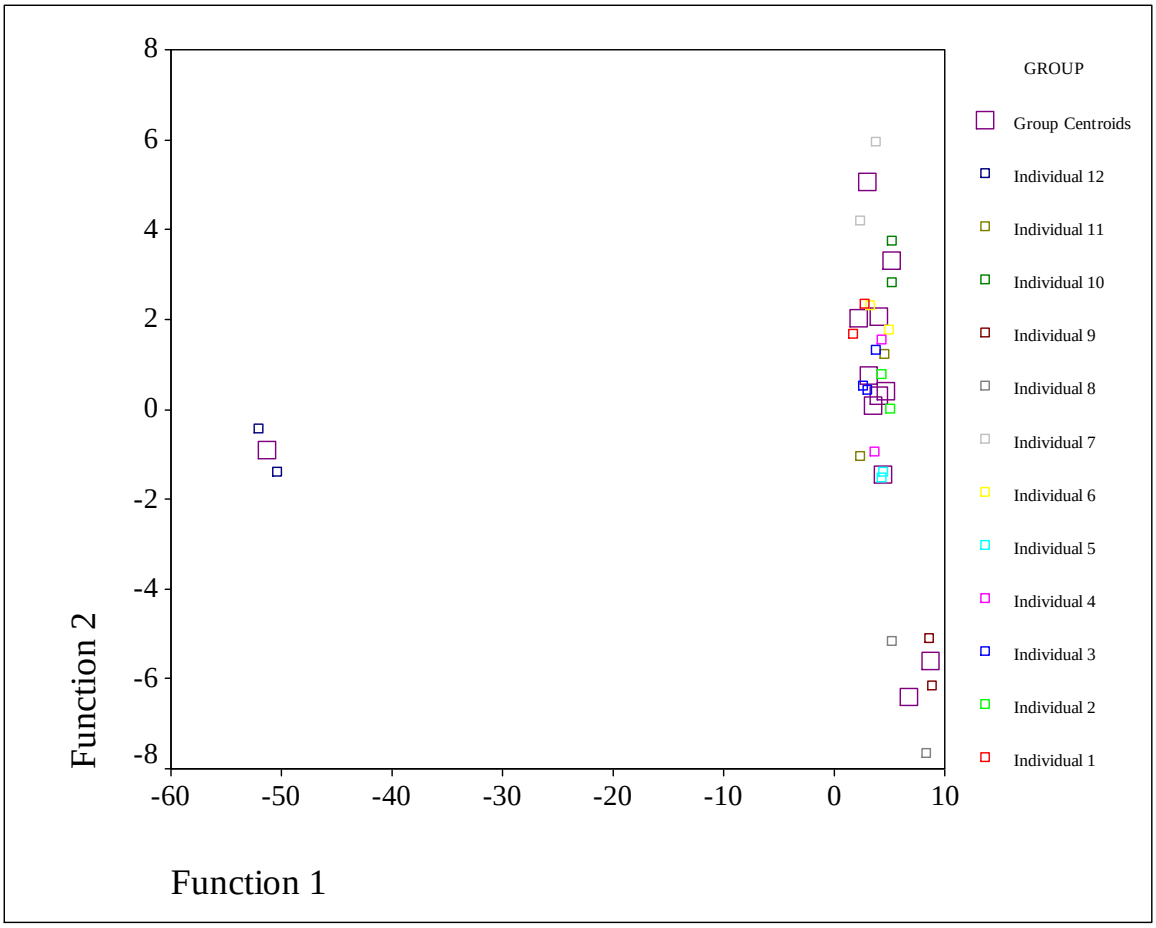

Figure 13. CDA plot of the femur bones for the 12 individuals.

The differences in the discrimination of the analysis of one bone type over the other may be attributed to the differences in elemental composition on bones from different anatomical areas as presented in the abovementioned studies.

3.4.2.3 Teeth

3.4.2.3.1 Elemental composition of the different tooth layers

The elemental composition of the enamel and dentine + cementum of teeth of different individuals were evaluated using the suggested NITE-CRIME method for LA-HR-ICP-MS (Section 3.4.1.4). A similar element menu to that used for bone was selected for discrimination analyses. The concentration of the elements Mg, Mn, Fe, Cu, Zn, Rb, Sr, Ba, and Pb were compared in the enamel and the dentine + cementum layers (Table 20). Some elements such as Mg and Zn tend to be in higher concentrations at the enamel layer than in the dentine + cementum while elements such as Mg, Cu, Rb, Ba, and Pb tend to be in higher concentrations in the dentine + cementum layer than in the enamel. Iron and strontium seemed to be in about the same concentration in both enamel and in dentine + cementum layers. The higher concentration of Zn in the enamel than in the dentine is consistent with what Brodelvold *et al.* [152] reported and the higher concentration of Rb and Ba in dentine than in enamel is been reported by Peterson *et al.* [153]. Differences in concentration of elemental composition within layers within the same tooth are related to the mineral intake in the diet of the individuals, the remodeling rate of the tooth layers and due to the role of these elements in the tooth development.

PCA analyses were performed with the enamel and dentine + cementum elemental composition to asses the discrimination method. Each group represents a different individual. Figure 14 shows the PCA plot of the elemental analysis of the enamel layer of different individuals. Sample EAFA034#32 was analyzed as an unknown the same day to validate the method. As is shown in Figure 15 there was correct grouping

of all the samples although the groups EAFA139#16, EAFA276#32 and EAFA152#16 and the groups EAFA159#17, EAFA034#32, and EAFA034#32[a] were overlapped. The EAFA034#32 and EAFA034#32[a] groups were overlapped as expected since they are the same sample; therefore the analysis is been validated. The groups EAFA026#16 and EAFA265#16 were not overlapped with any other group suggesting the elemental composition of these are significantly different from the others.

Table 20. Results of the elemental analysis of enamel and dentine + cementum in tooth samples. Concentration ± σ is in μg g^{-1}.

Isotope	EAFA276#32	AFA276#32
^{25}Mg	1872 ± 145	7867 ± 383
^{55}Mn	0.71 ± 0.11	0.33 ± 0.03
^{57}Fe	10 ± 4	11 ± 2
^{63}Cu	0.036 ± 0.005	0.11 ± 0.01
^{66}Zn	160 ± 9	85 ± 32
^{85}Rb	0.075 ± 0.004	0.19 ± 0.02
^{88}Sr	69 ± 3	79 ± 4
^{137}Ba	0.92 ± 0.02	2.6 ± 0.1
^{208}Pb	0.20 ± 0.19	1.8 ± 0.3

Isotope	EAFA265#16	AFA265#16
^{25}Mg	1959 ± 57	9303 ± 278
^{55}Mn	0.62 ± 0.14	0.84 ± 0.7
^{57}Fe	6 ± 2	73 ± 28
^{63}Cu	0.05 ± 0.03	0.19 ± 0.02
^{66}Zn	129 ± 11	121 ± 47
^{85}Rb	0.077 ± 0.005	0.20 ± 0.01
^{88}Sr	60 ± 1	78 ± 4
^{137}Ba	0.81 ± 0.03	3.1 ± 0.2
^{208}Pb	0.10 ± 0.01	0.9 ± 0.2

Isotope	EAFA159#17	AFA159#17
^{25}Mg	2139 ± 93	9945 ± 777
^{55}Mn	0.99 ± 0.37	0.46 ± 0.04
^{57}Fe	10 ± 4	53 ± 15
^{63}Cu	0.024 ± 0.003	0.38 ± 0.04
^{66}Zn	123 ± 46	105 ± 48
^{85}Rb	0.081 ± 0.003	0.16 ± 0.02
^{88}Sr	54 ± 2	57 ± 2
^{137}Ba	2.4 ± 0.1	6.2 ± 0.3
^{208}Pb	0.12 ± 0.01	2.2 ± 0.4

Isotope	EAFA152#16	AFA152#16
^{25}Mg	1844 ± 75	7582 ± 245
^{55}Mn	0.72 ± 0.06	0.378 ± 0.004
^{57}Fe	7.6 ± 0.5	8 ± 1
^{63}Cu	0.025 ± 0.005	0.087 ± 0.001
^{66}Zn	161 ± 12	93 ± 5
^{85}Rb	0.074 ± 0.007	0.18 ± 0.01
^{88}Sr	71 ± 2	82 ± 2
^{137}Ba	1.08 ± 0.08	2.6 ± 0.4
^{208}Pb	0.11 ± 0.01	1.7 ± 0.1

Isotope	EAFA026#16	AFA026#16
^{25}Mg	2019 ± 202	8958 ± 382
^{55}Mn	0.94 ± 0.11	0.48 ± 0.05
^{57}Fe	15 ± 9	38 ± 12
^{63}Cu	0.04 ± 0.01	0.13 ± 0.02
^{66}Zn	126 ± 57	76 ± 30
^{85}Rb	0.087 ± 0.27	0.17 ± 0.01
^{88}Sr	32 ± 3	55 ± 3
^{137}Ba	0.89 ± 0.2	2.8 ± 0.2
^{208}Pb	0.11 ± 0.02	0.22 ± 0.09

Isotope	EAFA139#16	AFA139#16
^{25}Mg	1827 ± 119	8875 ± 115
^{55}Mn	3.0 ± 0.7	0.63 ± 0.11
^{57}Fe	9.3 ± 0.4	88 ± 22
^{63}Cu	0.04 ± 0.01	0.27 ± 0.03
^{66}Zn	196 ± 50	150 ± 4
^{85}Rb	0.08 ± 0.01	0.19 ± 0.01
^{88}Sr	77 ± 2	81 ± 1
^{137}Ba	2.1 ± 0.1	3.8 ± 0.2
^{208}Pb	0.22 ± 0.11	0.72 ± 0.03

Isotope	EAFA034#32	AFA034#32
^{25}Mg	1811 ± 68	8714 ± 218
^{55}Mn	0.78 ± 0.08	0.45 ± 0.09
^{57}Fe	9 ± 2	21 ± 3
^{63}Cu	0.029 ± 0.009	0.13 ± 0.02
^{66}Zn	130 ± 32	113 ± 5
^{85}Rb	0.08 ± 0.01	0.15 ± 0.01
^{88}Sr	47 ± 3	60 ± 2
^{137}Ba	0.97 ± 0.09	3.1 ± 0.2
^{208}Pb	0.12 ± 0.02	0.75 ± 0.04

Isotope	EAFA034#32[a]	AFA034#32[a]
^{25}Mg	1930 ± 324	8511 ± 105
^{55}Mn	0.74 ± 0.10	0.39 ± 0.03
^{57}Fe	11 ± 3	19 ± 1
^{63}Cu	0.032 ± 0.001	0.10 ± 0.02
^{66}Zn	137 ± 40	109 ± 2
^{85}Rb	0.08 ± 0.02	0.14 ± 0.01
^{88}Sr	43 ± 2	61 ± 2
^{137}Ba	0.91 ± 0.2	3.1 ± 0.07
^{208}Pb	0.12 ± 0.02	0.77 ± 0.03

[a]Sample analyzed the same day as an unknown.

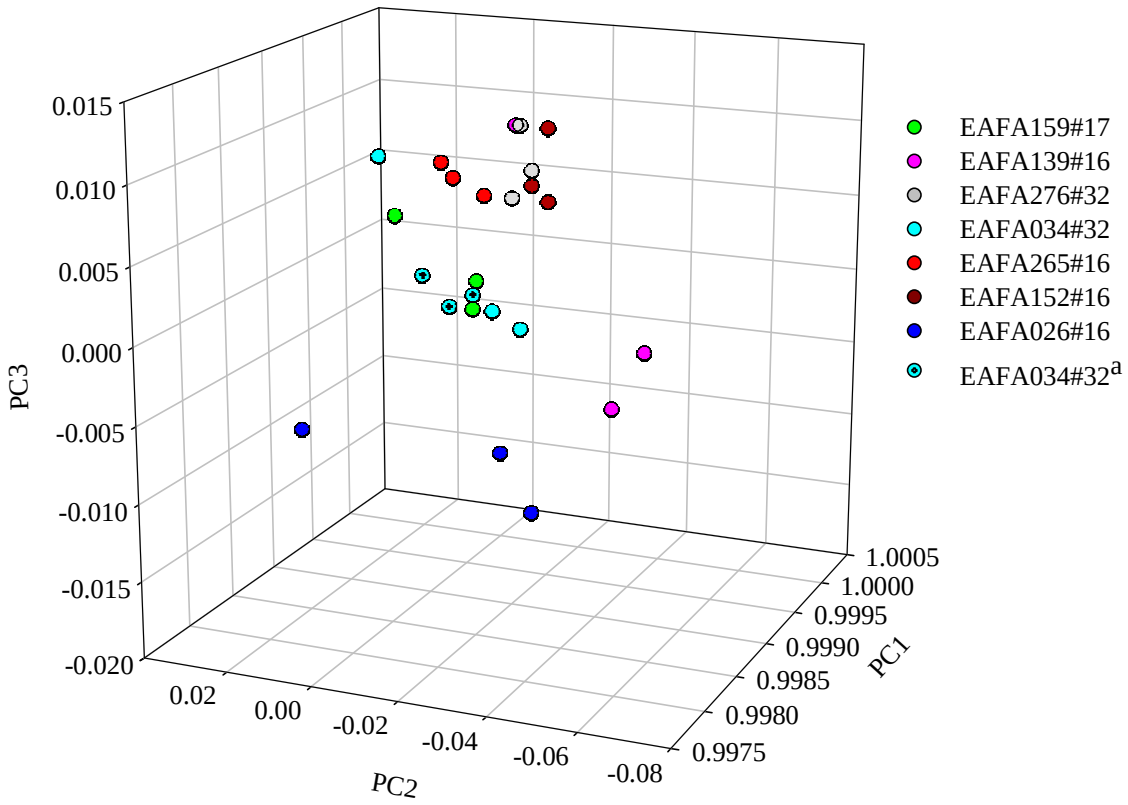

Figure 14. PCA plot of the enamel layer of different individuals.

The PCA analysis of dentine + cementum samples of different individuals showed a correct grouping of the samples and there were more separation of the groups (Figure 15). The sample AFA034#32 was analyzed as an unknown in the same analysis to validate the method. As expected, the groups AFA034#32 and AFA034#32[a] were completely overlapped and separated from the others, therefore the analysis was properly validated. Groups AFA139#16, AFA034#32, AFA034#32[a], and AFA026#16 were considerably separated from the other groups suggesting their elemental composition is significantly different from the other groups.

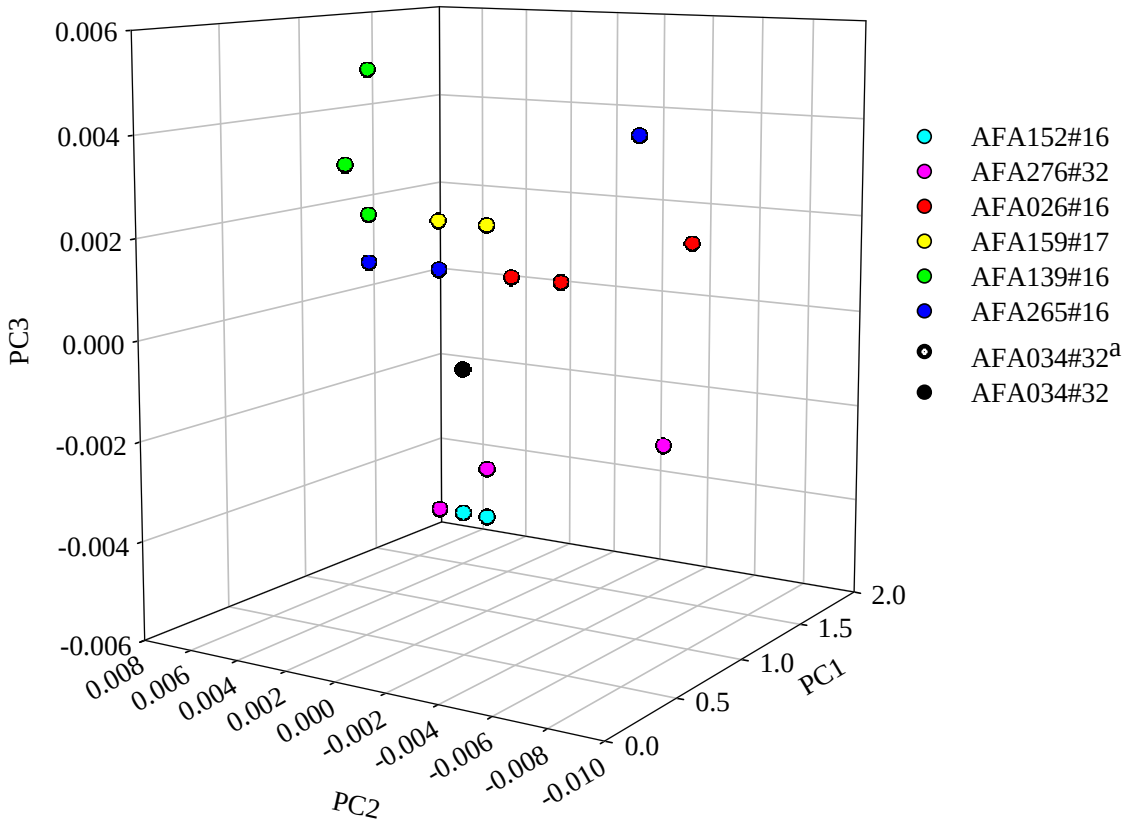

Figure 15. PCA plot of the dentine + cementum layers of different individuals.

3.4.2.3.2 Elemental analysis of whole tooth

Elemental analysis on whole tooth samples was performed using the suggested NITE-CRIME laser ablation method described in Section 3.4.1.4. The same element menu as in the previous section was selected for discrimination analysis. The sample AFA093#17 was measured as an unknown sample in the same analysis to validate the method. Different teeth from the same individual (AFA265 and AFA289) were analyzed to assess the elemental composition within an individual. Each group is comprised of 5 data points representing the elemental composition of an individual. Teeth samples from

the same individual or the sample measured as an unknown were represented with similar identification pattern in the PCA plot (AFA265#17, AF265#32, AFA289#1, AFA289#17, AFA289#32, AFA093#17, and AFA093#17[a]) (Figure 16).

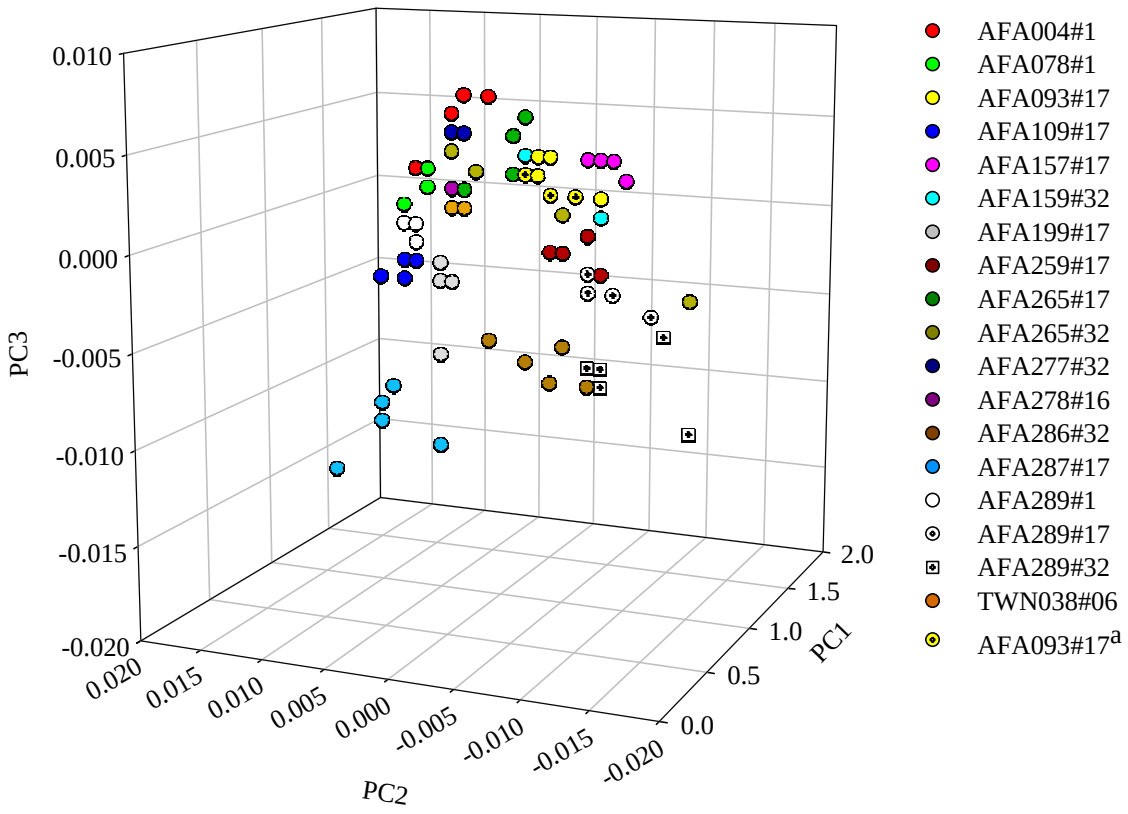

Figure 16. PCA plot of the whole tooth samples of different individuals.

Almost all the individuals' groups were correctly separated, although here was an overlapping between of the groups AFA004#1, AFA 078#1, AFA159#17, AFA265#17, and AFA265#32 (Figure 16). Overlapping of groups AFA265#17 and AFA265#32 was expected since these are samples from the same individual, but these were overlapped with other groups as well. The groups AFA289#1, AFA289#17, and AFA289#32 were

expected to be overlapping one on each other since they are teeth of the same individual. Based on the PCA analysis these three teeth from individual AFA289 seemed to have different elemental composition. Such separation may have to do with the development and the differences in elemental composition on the layers in teeth of the same individual.

3.5 Conclusions

An analytical method using LA-HR-ICP-MS and HR-ICP-MS is suggested for bone and teeth matrices showing accurate and precise measurements of trace elements. Matrix suppression studies demonstrated the utility of using trace elements for discrimination analysis regardless the high content of Ca and P.

The crater morphology and the dimensions of the crater helped to evaluate the performance of the laser and to estimate the amount of mass ablated under the optimized LA conditions. Although the SRMs and the bone samples had different densities, the ablated mass with the experimental set up resulted to be similar. What is more important, regardless the amount of ablated mass the non-matrix match calibration with SRM NIST 612 (glass matrix) provided accurate and precise analyses of bone SRMs.

Trace elemental analysis of buried bones requires careful examination to make sure the biogenic signal is been used for discrimination of individuals. With the approaches used in this study the possibilities of using the diagenetic signal was reduced. When humerus and femur bones are considered together, there is a significant variation within the same individual making unfeasible the separation of individuals by elemental composition using the combination with both bones. When the samples were separated by bone type, discrimination and separation of samples from different origins was

achieved. It was possible to separate bones from different origins if all the bone samples compared were collected from the same anatomical area, although the reasons for the differences are not clear and have not been investigated in this study.

As expected, the elemental composition of the different layers in teeth showed differences in the concentration for some elements. When the elemental composition of the whole tooth was used for the separation of the individuals, there was more overlap between individuals that when the elemental composition of the tooth layers was considered individually. The mixed elemental composition in whole teeth may contribute to the discrepancies found in teeth samples from the same individual. Analysis of more samples teeth samples and the assessment of variation in elemental composition on teeth of the same individual will help to better interpret the results found in this study.

This method has demonstrated the capabilities and the discrimination power of elemental analysis on bone and teeth samples from different origin. Although the discrimination power of this method is satisfactory, increasing the amount of samples analyzed, assessing the heterogeneity of the elemental composition in different anatomical areas (humerus and femur compact bones) of an individual, and creating a database will increase the strength of the discrimination results. The main goal of this study, developing an analytical method for the analysis of these matrices using LA-HR-ICP-MS was successfully accomplished. These results open the possibilities of including trace elements composition for sourcing bones and teeth in forensic analysis.

4 HR-ICP-MS AND LA-HR-ICP-MS FOR THE ANALYSIS OF PLANT MATERIAL

The use of elemental composition for identification and discrimination purposes has been successfully used in matrices such as bone and teeth matrices. The elemental composition in plant depends on the soil conditions and the nutrient availability in this medium; hence it could offer essential isotopic information that will allow the discrimination of plants of the same species originating from different environments.

Elemental analysis of plants has been performed with different instrumental techniques including NAA[158, 159], ICP-AES, and ICP-MS [160, 161]. As mentioned in previous chapters the use of HR-ICP-MS and laser ablation offer several advantages over the other techniques that include excellent sensitivity, shortened analysis time, small sample consumption (in LA) and resolution of polyatomic interferences, especially in complex matrices such as in plants.

In this study, an analytical method was developed for elemental analysis of plant material using the HR-ICP-MS and LA-ICP-MS with the SRM NIST 1515 (apple leaves). The method development included the selection of an element menu based on the major components in plants, the optimization of the analytical instrument using the SRM NIST 1515 (apple leaves), and the comparison of the LA with solution based work for corroboration purposes. Once developed, the analytical method was applied to the analysis of marijuana ashed samples confiscated in different areas of the USA. The results of this study will open the possibility of using elemental analysis to discriminate plants of different origin. To choose an element menu for discrimination it is important to understand the origin, role and distribution of trace elements on plants in general.

4.1 Plant material and its nutrients

Inorganic elements play an important role in the growth and development of plants [162, 163]. Plants have a natural ability for the selection of chemical elements although they are highly dependent on the geochemistry of the environment around them. This biological selection enables the plant controlling its elemental composition but it is limited to the availability of these elements. The nutrition of a plant depends on the supply of essential chemical compounds for the metabolism and growth, and these chemical compounds are called nutrients [162]. Nutrients are transformed to cellular material that then will be used in the form of energy by metabolic processes. The essential nutrients for higher plants are of inorganic origin. The following conditions need to be met in order to consider an element as an essential nutrient: (1) the lack or deficiency of this nutrient will not allow the plant to complete or continue its life cycle; (2) the deficiency in the plant nutrition is specific for that particular element, and (3) the nutrient is directly related to a metabolic process in the plant [162].

Nutrients in plants may be divided in micronutrients and macronutrients, been the macronutrients needed in relatively higher amounts than the micronutrients. The macronutrients (elemental composition) in plants include: C, H, O, N, P, S, K, Ca, Mg, Na, and Si. The micronutrients are: Fe, Mn, Cu, Zn, Mo, B, and Cl. These nutrients classification is not always right since there could be cases where some micronutrients have relatively the same concentration as a macronutrient. In order to have a more appropriate classification the plant nutrients could be classified according to its chemical behavior and physiological function. The plant nutrients are then classified in four groups being the first those elements that are the major constituents in the organic portion

of the plant (Table 21). The second groups consist of P, B, and Si, which share similarities in chemical behavior. The third group includes K, Na, Ca, Mg, Mn, and Cl. These elements are taken from the soil in the form of ions. The last group has the elements that are present in the plant in the form of chelates. The 3rd and 4th groups are not clearly separated since Mn and Ca (present in group 3) are also able to form chelates in the plants [162].

Table 21. Classification of nutrients in living plants [162].

Element	Uptake	Biochmeical Function
1st Group C, H, O, N, S	In the form of CO^2, HCO_3^-, H_2O, O_2, NO_3^-, NH_4^+, N_2, SO_4^{2-}, SO_2 Ions from the soil solution and gases from the atmosphere	Major constituent of organic material. Essential elements of atomic groups which are involved in enzymic processes. Assimilation by oxidation-reduction reactions.
2nd Group P, B, Si	In the form of phosphates, boric acid or borate. Silicate from the soil.	Esterification with native alcohol groups in plants. The phosphate esters are involved in energy transfer reactions.
3rd Group K, Na, Mg, Ca, Mn, Cl	In the form of ions from the soil solution.	Non-specific functions establishing osmotic potentials. More specific reactions in which the ion brings about optimum conformation of an enzyme protein (enzyme activation). Bridging of the reaction partners. Balancing anions. Controlling membrane permeability and electro-potentials.
4th Group Fe, Cu, Zn, Mo	In the form of ions or chelates from the soil solution.	Present predominantly in a chelated from incorporated in prosthetic groups. Enable electron transport by valency change.

Living plant material composition includes organic matter, minerals, and water. The amount of these three may vary according to the plant type, but water will always be the major constituent. In general plant material is about 70% water, 27% organic material, and 3% minerals. Regardless the lower percentages of mineral content, trace elements are essential nutrients for plant growth and development [162].

There are several factors controlling the mineral content on plant material. The primarily factor is the uptake potential for specific mineral nutrients. The second most important factor controlling the mineral content in plants is the nutrient availability in the nutrient medium. There is an increase on the concentration of a particular element following a saturation curve as the nutrient medium increases.

The distribution of nutrients in plants varies according to the plant organs. In general the leaves, roots and stems show higher variability in nutrients' concentration than seeds, tubers, and fruits. The mineral content in plants also varies with age. Older plants tend to have higher concentration of Ca, Mn, and Fe whereas young plants and tissues seem to have higher concentrations of N, K, and P [164].

Most of the time, the mineral content in plant is expressed on a dry weight bias ($\mu g\ g^{-1}$ or ppm); while for physiological considerations it is better to express the nutrients' concentration on a fresh matter bias (mM or me = milli equivalents). Since plant organs have different water content it is important to be cautious when comparing concentration of nutrients on dry material of different organs.

4.2 Soil: nutrient medium for plants

4.2.1 General description of soil

Soil consists of a solid phase, a gas phase, and a liquid phase that affect the supply of nutrients in plants roots. The solid phase is considered the main reservoir of nutrients containing organic and inorganic particles. In the inorganic particles have cations such as K, Na, Ca, Mg, Fe, Mn, Zn, and Cu whereas the organic particles contain P, N, and S. The liquid phase is responsible of the ions transportation into the plant roots. Most of the

nutrients in the liquid phase are in the ionic form although some CO_2 and O_2 could be dissolved in the soil solution. The gaseous phase is responsible for the gas exchange between the organisms in the soil and the atmosphere by supplying O_2 to the living organisms and removing the CO_2 produced from the soil atmosphere. Although the three soil phases seem to have separate functions in plant nutrition, they are all interrelated. The availability of soil nutrients for the plants depends on the relationship of these phases [162].

4.2.2 Nutrients availability

Nutrient availability is related to the plant roots and the physical and chemical state of the nutrients in the soil medium. One of the processes by which the plant gets nutrients from the soil is called root interception. In this process, the close contact of the root with soil colloids allows for the exchange of H^+ released from the plant with cations in the soil. In root interception only cations close to the cell wall will have an exchange with the cations absorbed to the soil, which leads to a small amount of nutrient absorption by the plant. Therefore the root interception process does not provide the plant with the necessary amount of nutrients. Mass flow and dissolution are the main processes by which plants' roots get most of the necessary nutrients. With the mass flow the nutrient is transported to the plant through a flow of water flowing from the soil to the plant's root. The nutrient availability in this case will depend on the water flow rate, the concentration of the nutrient in the water and the capabilities of the plant for water consumption. The diffusion of nutrients on the other hand will depend on the supply from the soil and the plant demand. Diffusion of ions (nutrients) into the roots occurs from high to low

concentration of the nutrient. When nutrients in the soil solution are in high concentration the mass flow takes place allowing the movement of significant amount of water to the roots carrying the solutes. Nutrient depletion around the root occurs when the nutrient uptake is higher than the nutrient transportation into the plants.

The mobility of ions (nutrients) into the plant is highly dependent on the nutrient's concentration in the soil solution. The soil solution varies in composition and concentration and depends mostly on the soil moisture. In wet soil the soil solution is diluted while when the soil dries the soil solution becomes more concentrated.

4.3 Trace elements in soil and plants

There are trace elements essential for the growth and development of all plants, few are only essential for specific species of plants and others are know to stimulate plants growth (Table 22).

4.3.1 Lithium

The Li in earth's crust tend to be more concentrated in felsic igneous rocks and sedimentary aluminosilicates. Lithium is released from the primary mineral in acid and oxidizing media and integrated to the clay minerals and some is fixed to the organic matter. The distribution of lithium in soil depends more on the conditions of the soil formation rather than to the initial content in its parent material [163].

Table 22. Forms and principal functions of trace elements essential for plants [163].

Element	Constituent of	Involved in
Al[a]	----------	Controlling colloidal properties in the cell, possible activation of some dehydrogenases and oxydases
As[a]	Phospholipid (in algae)	Metabolism of carbohydrates in algaeand fungi
B	Phosphogluconates (in algae)	Metabolism and transport of carbohydrates, flavonoid synthesis, nucleicacid synthesis, phosphate utilization, and polyphenol production
Br[a]	Bromophenols (in algae)	----------
Co	Comabide coenzyme	Symbiotic N_2 fixation, possibly also in non-nodulating plants, and valence changes stimulation synthesis of cholophyll and proteins
Cu	Various oxidases, plastocynins, and cenilopasmin	metabolism, possibly involved in symbiotic N_2 fixation, and valence changes
F[a]	Fluoroacetates (in a few species)	Citrate convertions
Fe	Hemo-proteins and nonheme iron proteins, dehydrogenases, and ferrodoxins	Photosynthesis, N_2 fixation, and valence changes
I[a]	Tyrosine and its derivates (in angiosperms and algae)	----------
Li[a]	----------	Metabolism in halophytes
Mn	Many enzyme systems	Photoproduction of oxygen in chloroplasts, and indirectly in NO_3^- reduction
Mo	Nitrate reductase, nitrogenase, oxidases, and molybdoferredoxin	N_2 fixation, NO_3^- reduction, and valence changes
Ni[a]	Enzyme urease (in *Canavalia* seeds)	Possibly in action of hydrogenase and traslocation of N
Rb[a]	----------	Function similar to that of K in some plants
Se[a]	Glycene reductase (in *Clostridium* cells)	----------
Si	Structural components	----------
Sr[a]	----------	Funtion similar to that of Ca in some plants
Ti[a]	----------	Possibly photosynthesis and N_2 fixation
V[a]	Porphyrins, hemoproteins	Lipid metobolism, photosynthesis (in green algae), and possibly in N_2 fixation
Zn	Anhydrases, dehydrogenases, proteinases, and peptidases	Carbohydrate and protein metabolism

[a] Elements known to be essential for some groups or species and whose general essentiality needs confirmation

The lithium in soil is readily available for plants absorption; therefore it is a good reference to determine its content in the soil medium [165]. The lithium in soil is also been found to be strongly associated with Ca and Mg [166]. In plants is seems that

lithium shares the same transport carrier as K^+, which makes it easily transported into the plants. In general, lithium tends to be more concentrated in the leaf tissues than in the root or bulbs. Some evidence suggests that lithium affect the plant growth and development. Soil rich in lithium may cause toxic effects in some plant species such as citrus trees [165]. It is known that Ca inhibits the lithium uptake by plants, thus the addition of calcium could reduce the toxic effect of lithium in the plants.

4.3.2 Rubidium

Rubidium is found in higher concentrations at sedimentary aluminosilicates and felsic igneous rocks. Contrary to lithium, Rb content in soils mainly comes from the parent rock and it is found in higher concentrations at soils over granites and gneisses, and in alluvial soils. Organic matter and micaceous clay minerals favor the sorption of Rb in soil.

Plants easily absorb rubidium from the soil. It seems to take K^+ place in some sites but it can't replace the role of K^+ in metabolic processes. Higher concentrations of rubidium in plants may have a toxic effect, although in potassium deficient plants such as sugar beets the combination of rubidium and sodium can stimulate the plant growth [167].

4.3.3 Copper

Copper is more abundant in intermediate rocks. Copper forms various minerals that are easily soluble in weathering processes releasing Cu ions in acidic environments. It also has the ability of interact with mineral and organic material, and can precipitate when combined with sulfide, carbonate, and hydroxide anions. The variability of copper

in soil profiles is very small. It is believed that Cu in soil is found in the divalent ionic form (2+) but other species may occur. Copper can be fixed in inorganic and organic exchange sites by means of absorption, occlusion and co-precipitation, organic chelation and complexing, and microbial fixation [163].

The Cu content in plants is between 2-20ppm of dry plant material. The uptake of this element seems to be mediate through a metabolic process and some evidence suggests that Cu inhibits the Zn uptake and vice versa [168]. Copper enters the plant roots in a dissociated form, but once in the roots it is found in complex form. The movement of Cu through the different plant organs depends highly on the supply of this element [169]. Copper tends to accumulate in the roots and leaf until the tissues get old, then only small amounts of Cu can move to the younger organs. Also Cu tends to be in higher concentrations at the reproductive organs of plants, although this may vary within plant species.

It is been found that Cu in plants is complexed with low molecular weight organic compounds and proteins. Also it is been found that Cu occurs in enzymes essential in metabolic processes in the plant. Cu is an essential component involved in photosynthesis, respiration, carbohydrate distribution, N reduction and fixation, and protein and cell wall metabolisms. It is also involved in controlling water relationships and in the production of RNA and DNA. Copper deficiency inhibits the reproduction of the plants by decreasing the production of seeds and making the pollen sterile. Sufficient supply of Cu is been related to the plant resistance to fungal diseases [163].

4.3.4 Strontium

Strontium is an element found in intermediate magmatic rocks and in carbonate sediments. It shares similar biochemical characteristics with Ca and sometimes with Mg. The Sr/Ca ratio is fairly stable in the biosphere; therefore it is often used to assess Sr concentrations in the environment. The Sr content in soil is mainly controlled by the parent rock and the climate.

There is a wide range of Sr concentration in plants (<1 ppm-10,000ppm dry weight). Lower concentration of Sr was reported for fruits, grains, and potatoes tubers while higher concentrations were found in legume herbage. The Sr uptake by roots seems to involve exchange diffusion and mass flow mechanisms [170]. The Sr in the roots is not very readily transported to the younger organs, although it is often reported to be in higher concentrations at the top of the plant. Sr is toxic to plants at 30ppm ashed weight [171]. Although a toxicity level has been reported the tolerance of Sr varies within plant species.

4.3.5 Barium

The Ba concentration in earths crust often lies between 400 to 1,200 ppm and tends to be concentrated in intermediate and felsic magmatic rocks. Since Ba has similar ionic radius than K^+ it is often associated with potassium. The barium resulted from rock decomposition precipitates easily as sulfates and carbonates. Barium tends to be in higher concentrations in clays, P and Mn concretions and minerals, and in varnishes of aridic soils. The mobilization of Ba in soil depends on the soil conditions; therefore its concentration varies considerably in the soil solution [163].

Although barium is commonly present in plant at concentrations of 1 to 98 ppm dry weight, it does not show to play an important role in plant growth and development. Higher concentrations of Ba have been reported in leaves of cereal and legumes while lower concentrations were reported in grains and fruits. Barium is readily available for plant uptake in acidic soil. It has been reported as Ba toxic concentrations in plants to be 1-2% dry weight and 220 ppm the highest and moderate toxic levels respectively [171, 172]. Barium toxicity may be reduced in soils rich in Mg, S, and Ca [163].

4.3.6 Zinc

Zinc is often present in soil at concentrations ranging from 10 to 300 ppm in different minerals. A zinc ionic radius is similar to that of Mg^{+} and Fe^{2+}, thus it can replace those ions in mineral structures. The presence of zinc in these mineral structures makes up for most of the zinc present in many soils. Zinc salts are also present in soil although because of their high solubility they will not prevail in the soil for extended periods [173]. Zinc may occur at exchange sites of clays and organic matter or could be found absorbed on the soil surface in the form of Zn^{2+}, $ZnOH^{+}$ or $ZnCl^{+}$. It is been found that the absorption of Zn by goethite increases with the pH increase, therefore the movement of Zn is then restricted in neutral and alkaline soils [174]. The concentration of Zn in soil solution is low ($3x10^{-8}$ to $3x10^{-6}$). The solubility of Zn in soil is restricted by higher pH and by the presence of $CaCO_3$ [162].

There is a general disagreement in whether the plants absorb Zn through passive or active mechanisms. Regardless there is strong evidence that suggests the Zn uptake is carried out mostly by active mechanism [162, 163]. About 90% of the total Zn in plant

roots is likely to happen due to the absorption onto the cell walls surface or on exchange sites. There is a consensus that the absorbed Zn is in the form of both Zn^{2+} and hydrated Zn, although Zn chelates and other complex ions could also be absorbed. It is been reported that Zn is likely to be bounded to soluble low molecular weight proteins and that it also forms insoluble Zn complexes [163].

There is a debate about Zn mobility within the same plant. Some studies suggest Zn is highly mobile throughout the plant while others say it has intermediate mobility. Some plants mobilize significant amounts of Zn from old leaves to new organs, but when deficient the same plant showed little mobility from old leaves to other organs. Baumeister and Ernst in 1978 calculated that about 75% of the total Zn absorbed is found in the top of young plants while only 20-30% happens in the top of old plants [175]. Most of the time Zn is concentrated at the plant roots, although it can me relocated and accumulated at the top of the plant. It is been reported that Zn is located in chloroplasts and likely to be accumulated in the vacuole fluids and in cell membranes [176].

The zinc tolerance varies with plant species. Some plants are able to grow in Zn rich environments. Regardless, concentrations ranging between 150 -200 μg Zn g^{-1} dry weight is considered toxic to the plant [177].

4.3.7 Aluminum

Aluminum is one of the main constituents of earth's crust present in the form of feldspar $CaAl_2Si_2O_8$ [162, 163]. The Al content in soil originates from the parent rock forming a series of Al hydroxides of different charges and composition and becoming the structural components of clay minerals. These Al hydroxides have low solubility in a pH

range of 5-8. The mobility of Al in soil is improved significantly in acidic medium. Therefore Al in acidic soils will be readily available for plants intake. Although aluminum is a common element present in plants, its content varies with plant species and the soil conditions. For higher plants it is been reported that Al happens at around 200ppm dry weight [163]. The physiological role of Al in plants is still unknown but it is been found that at low levels it benefits the plant's growth [178, 179].

In an acidic medium the mobile Al can be easily taken up by the plant causing chemical stress [165]. Aluminum toxicity often results in higher concentrations of Fe and Mn because their availability is increased in an acidic soil. It also results in lower concentrations of Mg and Ca because these tend to leach in this medium [162].

4.3.8 Lead

Lead is found in concentrations of 10-40ppm in the acids series of magmatic rocks and argillaceous sediments and from 0.1 to 10ppm in calcareous sediments and ultramafic rocks. The main occurrence of lead in soil is in the form of 2+ although the 4+ is also known to happen. As the rock decomposes the lead sulfide oxidize turns into carbonates that could be incorporated into the clay minerals, and in the organic matter. Since Pb^{2+} have similar chemical properties as the divalent alkaline earth group, lead can replace Ca, Ba, K, and Sr in sorption sites and in minerals. The natural occurrence of Pb comes mainly form the parent rock and the soil enrichment of this element is associated with lead pollution [163]. The main source of Pb pollution comes from petrol combustion which accounts for up to 80% of the total Pb contamination in the atmosphere [162].

Lead is an element toxic to the plants although it can be found in all plants at low concentrations. Broyer *et al.* reported the necessary Pb levels in a plant to be between 2-6ppb [180]. The absorption of lead thought the roots is through passive mechanism. The rate uptake is decreased when calcium is added to the soil and in lower temperatures [181, 182]. The plant's roots absorb the Pb in the soil solution and it is mostly stored in the cell walls. The Pb takeup rate increases as its concentration in the soil solution increases. Therefore the Pb content in the plant is highly correlated with the Pb concentration in soil. Only 3% of the Pb in the roots is moved to reproductive organs [182]. Airborne lead can be absorbed by the plant's foliage although it is still unclear in which extent the Pb is fixed to the hairy or waxy cuticles of leaves.

4.3.9 Manganese

The manganese concentration in rocks varies from 350-2000ppm. It is one of the most abundant elements in the crust earth. During the rock decomposition process the Mn released forms minerals such as pyrolusite (MnO_2) and manganite [MnO(OH)]. The main occurrence of Mn in soil is in the form of 2+ and Mn oxides. The divalent form is absorbed by the clay minerals, organic matter, and in soil solution. The soil pH, organic matter content, microbial activity and soil moisture are factors that influence the Mn availability as a nutrient [162]. The Mn compounds in the soil play an important role in the plants' nutrition and in controlling other nutrients. Mn concentration varies according to plant species and ranges from 17-334 ppm dry weight. A plant with Mn concentrations between 15 to 25 ppm is considered to be deficient of this element while concentrations around to 500 ppm dry weight have toxic effects in most of the plants [163].

4.3.10 Magnesium

Sandy soils contain about 0.05% of Mg while clay soils have 0.5% of this element. The magnesium present in clay soils is high because it is the product of the weathering of ferromagnesian minerals such as serpentine, olivine, biotite, and hornblende. Higher concentrations of Mg in from of $MgSO_4$ are commonly found at arid and semi-arid soils. The distribution of Mg in soil is divided in exchangeable and non exchangeable and water soluble forms [162]. Although the non-exchangeable Mg is found not to be readily available for plants absorption, there is some evidence that under certain circumstances it could be available. Mg in the exchangeable and soil solution fractions is readily available for plant uptake. These two Mg fractions are the most important supply of this nutrient for plants. The Mg concentration in soil solution is fairly high ranging from 2 to 5 mM, although higher concentrations have been reported (up to 150mM) [162].

Plant roots seem to have a poor Mg^{2+} uptake when compared to K^+. This behavior may have to do with the cation competition (K^+ and NH_4^+) in the passive transport happening in the plant's root. The excess of K^+ can affect the Mg^{2+} uptake in plants. Magnesium can translocate form older to younger leaves or to the apex.

Deficiencies of Mg produce various effects upon the plant species. The effects start at the older leaves and moving to the younger ones. A magnesium deficiency may lead to a delayed reproduction phase of the plant [183].

4.3.11 Nickel

The highest concentration on nickel is found to be high in ultramafic rocks (1400-2000 ppm) while it is decreased in acidic rocks such as granites (5-15 ppm). In sedimentary rocks Ni ranges from 5-90 ppm being the highest at the argillaceous rocks and lower in sandstones [163]. Nickel has affinity for metallic iron and will join whenever they come together. Most of the Ni in terrestrial rocks occurs in sulfides and arsenides and will replace iron in the ferromagnesians. Nickel will also associate to carbonates, silicates, and phosphates. During weathering Ni is easily mobilized and co-precipitated with Mn oxides and iron. Ni^{2+} is fairly stable in aqueous solutions and can move through significant distances.

Most of the Ni at the surface soil is likely to be bonded to an organic phase from which some could be soluble chelates [184]. Also the Ni carried by iron and manganese oxides in soil seemed to be available for plant uptake [185]. Clays and loamy soils, in soils over basic and volcanic rocks, and in organic rich soils are always high Ni content. The world mean Ni concentration is 20 ppm and 19ppm in the USA soil [163].

The normal Ni concentration in dry plant material is between 0.1 to 5 ppm. Nickel seems to be a non essential nutrient in the plant metabolism although some studies have found a close relation of Ni with the enzyme urease [186]. Nickel in soil is readily available and rapidly taken up by plants. There is a positive correlation of the Ni concentration in plants and in soil until the optimal Ni concentration in the plant is achieved. One of the principal factors that affect the Ni uptake is the soil pH. It is been reported a decrease of nickel content in oat grains by increasing the pH from 4.5 to 6.5 [187].

Higher concentrations of Ni can be toxic to plants and in the soil may reduce the uptake of most of the other nutrients [188]. The addition of lime or potassium can reduce the toxic effect of Ni in plants.

4.3.12 Iron

Iron is present in all soils and constitutes about 5% by weight of the earth's crust. The geochemistry of iron in soil depends mostly on the ease of change valence states due to the soil specific chemical conditions. The Fe in oxidizing and alkaline environment will precipitate while the iron in acidic and reducing conditions will promote the solution of iron compounds [163]. The iron in soils is believed to be mostly in the oxides, hydroxides, and chelates forms. The soluble iron content in soil is very low when compared to the total iron. The soluble iron forms include Fe^{3+}, $FeOH^{2+}$, $Fe(OH)_2^{+}$, and Fe^{2+}, being the last the least to contribute to the total soluble inorganic Fe except under high pH soil environment [162].

The absorption of iron by plants is metabolically controlled although plants also absorb the chelates and the divalent and trivalent forms. The plant roots have the capability of reducing Fe^{3+} to Fe^{2+} that allows the absorption of this nutrient. Iron moves through the plant as citrates and soluble ferredoxines. The iron deficiency in plants is observed first at the younger plant parts. The Fe uptake and transport into the plant tissues is strongly affected by the soil pH, the P and Ca concentrations, and the ratios of some heavy metals [163].

4.3.13 Vanadium

Vanadium is more abundant in mafic rocks and in shales with a concentration range of 100 to 250ppm. The behavior and chemical characteristics of vanadium depend greatly on the oxidation state and the pH of the medium. Vanadium can form oxides, hydroxyl oxides, but it does not form its own minerals. Instead vanadium replaces other metals such as Al, Ti, and Fe in crystal structures.

Vanadium tends to be in higher concentrations in organic shales and bioliths since it associates mostly with the organic matter. It has been reported that most of the mobile vanadium is the one held in Fe oxides [185] while in other reports say the VO^{2+}, VO_4^{3-}, and VO_3^- are mobile forms of vanadium in soil. The average world wide V concentration is 90ppm and 84ppm in the U.S. soil [163].

It is still unclear the role of V in plants although it was reported a high concentration of V in some legumes which may suggest that V has a role with the N_2 fixation [189]. Welch and Cary suggested that if V was essential for plants the optimal concentration of this metal will be 2ppb dry weight [190].

The plant roots rapidly take up the soluble V in soil. There are some species that are able to accumulate this element. It was reported in a study that V was passively absorbed in barely roots since the uptake was linearly correlated with the V concentration and also was highly dependent on the pH [191]. The VO^{2+} species in acid conditions seemed to be absorbed more rapidly by the roots than the VO_3^- and HVO_4^{2-} species occurring in neutral and alkaline solutions. The average concentration of V in higher plants is reported to be 1 ppm dry weight, whereas in ashed vegetables it is been reported to be <5-50ppm [163].

Excess amounts of V can be toxic to the plant. The toxicity level can vary according to the plant species. Chlorosis and drawfing in some plants may occur at about 2 ppm dry weight, while in others higher concentrations are needed [163].

4.3.14 Cobalt

Higher concentration of Co earth's crust is found in ultramafic rocks with a range of 100 to 220 ppm while in acid and in sedimentary rocks its concentration ranges are 1 to 15 ppm and 0.1 to 20 ppm respectively. During the rock degradation Co mobilizes in relatively acid media, although due to its high affinity with Fe and Mn oxides and clay minerals this element does not migrate into the soil solution. Therefore the soil organic matter and the clay content are important factors affecting the Co distribution and behavior in soil [163].

The Co uptake on plants is mainly by the roots; although it can be easily take up by the leaves through the cuticle. The ability of the plant to absorb cobalt depends on the mobile Co in soil and the Co concentration in soil solution. In the absorption process the Co behaves like Fe and Mn and it is transported in a form of organic complex compounds [163].

The concentration of cobalt in plants varies upon the species. It is known that legumes accumulate more Co than the grasses. Plants growing in soils rich in Co presented a high accumulation of this metal even though they are not Co accumulators. An excess of Co though can be toxic to some plant species.

4.3.15 Molybdenum

The abundance of molybdenum in earth's crust is mostly associated to granitic and other acidic magmatic rocks ranging from 1 to 2 ppm concentration. In organic rich environments Mo concentration is above 2 ppm. Most of the earth's molybdenum is in the minerals MoO^{2-} anion and MoS_2 (molybdenide), which are often associated to Fe and Ti minerals. In the weathering process the Mo sulfides oxidize leading to MoO_4^{2-} in neutral and basic environments whereas $HMoO_4^-$ is formed in acid environments. Most of the Mo in soil is originated form the parent rock and ranges from 0.013 to 17 ppm in world soils. Soils originated from organic rich shales and granitic rocks are often high in Mo content [163].

The soil pH and the drainage conditions are one of the principal factors governing the Mo solubility in soil and availability to plants. In alkaline environments the Mo is absorbed easily due to the high activity of MoO^{2-} in this medium, while in acidic soils with pH < 5.5 and with high iron oxide content, the Mo is barely available for plants absorption. A common way to increase Mo availability is by liming the acid soil.

Molybdenum is considered an essential nutrient for plants, although the amount required is low. Plants absorb Mo mostly in the form of molybdate ions and its concentration in plants is linearly correlated to the Mo concentration in soil. Molybdenum mobility in plants is moderate although the translocation process is still unclear. Tiffin in 1972 suggested that the translocation could be possible through organic complexing [192]. Molybdenum is an essential component of nitrogenase and nitrate reductase and it is also present in other enzymes (oxidases) that catalyze other reactions where Mo acts as a redox carrier due to the change in valence between Mo^{6+} to Mo^{5+}

[193]. The presence of Mo in these enzymes indicates the Mo is essential in the N_2 fixation or NO_3 reduction process. Plants supplied with NH_4-H do not require as much Mo as the plants that use NO_3-N.

Typical concentrations of Mo in leaves are in the order of 1 ppm dry weight or less, whereas higher concentrations are found in the nodulated roots. Some legumes species accumulate higher quantities of Mo (about 350 ppm dry weight) without showing signs of toxicity. In legumes the average Mo concentration is between 0.73 to 2.3 ppm while in grasses ranges from 0.33 to 1.5 ppm dry weight. Areas contaminated with Mo present higher concentration of this element in plants.

4.3.16 Calcium

On average, the calcium concentration in earth's crust is about 3.64%. Calcium in soil is present in the form of several primary minerals such as calcium phosphates, calcium carbonates, and the Ca bearing Al silicates (feldspars and amphiboles). The calcium concentration in soil varies according to the parent rock and the influence of the weathering and leaching processes during the soil formation. Soils highly leached and weathered are in general low in Ca content whereas soils originated from limestone or chalks usually present high concentrations of Ca [162].

The calcium uptake and translocation in plants appear to be mainly a passive process. Higher plants exhibit considerable concentrations of Ca, although this concentration is mostly attributed to the high Ca levels in the soil solution rather than due to the efficiency of the take up mechanism. Although the Ca^{2+} in soil solution is 10 times higher than K^+, the Ca^{2+} uptake rate is lower than K^+. The lower Ca uptake rate is

attributed to the fact that Ca is absorbed only by young root tips where the cell walls are still not suberized [194]. The calcium uptake is also affected by the presence of other ions such as K^+ and NH_4^+ that are quickly absorbed by the roots. Any factor affecting the growth on new roots such as poor aeration and low temperatures will also affect the Ca uptake.

In plant tissue, Ca is present as a free form of Ca^{2+}, as Ca^{2+} absorbed to carboxylic, phosphorylic and phenolic hydroxyl groups, and as in Ca oxalates, phosphates and carbonates which are often deposited in the vacuoles. On the other hand the Ca is present in seeds as the salt of the inositol hexaphosphoric acid. The majority of the Ca in plant tissue is located at the apoplast and in the vacuoles.

When plants have a poor supply of Ca, most of this element is found at the cell wall fraction or as oxalate [195]. Calcium deficiency in plants characterizes for a reduction in the growing tissue causing deformation in young and new leaves and further on necrosis at the leaf extremes [162].

4.4 Cannabis sativa plant

Marijuana is one of the most commonly used illegal drugs in the United States. *Cannabis sativa* is believed to originate in Central Asia and quickly distributed throughout the world by means of men activities. Whether cultivated or grown in the wild, *Cannabis* plants originating from different geographical environment present different morphological and biochemical properties [196]. *Cannabis* plants are one of the most popular plants for drug preparation especially in the form of marijuana and hashish. Marijuana includes a mix of dry plant tissue while hashish consists of resins extracted

from the flowers [196]. The *Cannabis* plants grow relatively fast and can reach maturity in 60 days. It can be cultivated indoor or outdoor under optimal heat and light conditions. *Cannabis* plants are characterized by finely branched leaves subdivided into lance-shaped leaflets with saw-tooth edge. The *Cannabis* plant could be either male or female and these are produced almost equally. The flowers in male plants are located on small, branched flower stalks, in the leaf axis with a tiny leaf opposite whereas the female flowers are in leafy spikes and clothed in sticky hairs (Figure 17).

Figure 17. Picture *Cannabis* plant.

It is of special interest for the forensic scientist to be able to determine the origin of confiscated plants by law enforcement officers. Trace elements can serve as geographical markers and/or be utilized to differentiate between plants of different origin. Typical elemental analysis of *Cannabis* plants have been done by NAA and Atomic Absorption Spectroscopy (AAS) [159]. More recently LA has been applied for the

forensic analysis different *Cannabis* crops in Australia. Elemental analysis of the plants was used to create elemental profiles of the raw data and used for the discrimination of plants of different origins [80]. Although this data analysis technique seemed to provide favorable results, it is based solely in the comparison of spectral profiles. Laser ablation-ICP-MS have been demonstrated to provide true quantitative analysis for discrimination of different matrices such as glass and paint.

It is known that the elemental composition of different plant organs may vary upon the species [162, 163], thus elemental composition for sourcing purposes should be restricted to a specific organ such as leaves and flowers of *Cannabis* plants. Mixing different plan tissues may introduce another variable that will affect the discrimination process. A method for elemental analysis of plant material and *Cannabis* samples using LA-HR-ICP-MS is been developed in this study.

4.5 Methodology

4.5.1 Method development

4.5.1.1 Solution based analyses

4.5.1.1.1 Sample preparation and digestion procedure

The Standard Reference Material (SRM) NIST 1515 Apple Leaves (National Institute of Standards and Technology, Gaithersburg, MD, USA) was used for the optimization of the digestion procedure. The SRM was dried as indicated in the NIST certificate. After dried, 100 mg of the SRM NIST 1515 were weighed and placed into 50 mL plastic disposable digestion tubes (Environmental Express Inc., USA). Three

milliliters of HNO_3 16 M (Optima grade, Fisher Scientific, Pittsburg, USA) and 1 mL of 30% ultrapure hydrogen peroxide (J.T. Baker, Phillipsburg, NJ, USA) were added to each digestion vessel. The vessels were closed, vortex mixed and sonicated for 2 hours to assist the digestion process. A condensation disc was placed on top of the digestion vessel to avoid evaporation of the acids. The digestion vessels where placed in a heating block at 85°C for 8 hours until no particles residues were observed.

The remaining solution (4 mL) of the digestion process was transferred into a 50 mL volumetric flask. One thousand microliters of a 250 ng g^{-1} rhodium standard solution (CPI International, Santa Rosa, California, USA) were added as internal standard to a final concentration of 5 ng g^{-1} in Solution A. The volume was completed with deionized water (≥18 MΩcm^{-1}) (Nanopore Infinity filtration system (Barnstead)).

An aliquot of 25 μL of Solution A were transferred into a 10 mL volumetric flask. Rhodium was added as internal standard to a final concentration of 5 ng g^{-1} (200 μL of a 250 ng g^{-1} Rh standard solution –CPI International, Santa Rosa, California, USA). The volume was completed with HNO_3 0.8M (Optima grade, Fisher Scientific, Pittsburg, USA) (Solution B).

Twenty-five microliters of Solution A were transferred into a 25 mL volumetric flask with 500 μL of a 250 ng g^{-1} rhodium standard solution (CPI International, Santa Rosa, California, USA) as internal standard (final concentration-5 ng g^{-1}). The volume was completed with HNO_3 0.8 M (Optima grade, Fisher Scientific, Pittsburg, USA).

4.5.1.1.2 External calibration curve

Single element stock solutions of 1000 mg L^{-1} of each element were used to prepare the calibration curve. The following isotopes were measured for quantification: ^{25}Mg, ^{27}Al, ^{55} Mn, ^{56}Fe, ^{57}Fe, ^{85}Rb, ^{88}Sr, ^{137}Ba, and ^{208}Pb.

All solutions were prepared using high purity deionized water (>18 $M\Omega cm^{-1}$) obtained with a Nanopore Infinity filtration system (Barnstead) and ultratrace elemental grade nitric acid (Optima Nitric Acid 70%, Fisher®). Elements were measured against normal ICP-MS calibration. The calibration levels were as follows: 0, 0.5, 1, 3, 5, 7 and 10 ng g^{-1}. A rhodium solution (CPI International, Santa Rosa, California, USA) at a concentration of 5 ng g^{-1} was added as internal standard.

Control verification checks (at 3 ng g^{-1} and 5 ng g^{-1}), including a secondary source standard to validate external calibration, were run with samples in order to evaluate drift and precision over time.

4.5.1.1.3 Recovery study

New ceramic crucibles with lids were cleansed with acid detergent and rinsed with deionized water (>18 $M\Omega cm^{-1}$) obtained with a Nanopore Infinity filtration system, Barnstead. The crucibles were placed in the oven for 2 hours at 150ºC. The crucibles were removed from the oven and let cool down at room temperature for weighing measurements. The crucibles were weighed until constant weight was achieved (±0.005 g). About 300mg of the SRM NIST 1515 Apple leaves (National Institute of Standards and Technology, Gaithersburg, MD, USA) were placed crucibles and the placed in the furnace. Five SRM samples and 3 method blanks were placed in a furnace at 150ºC for 1

hour and then at 300ºC for an additional 5 hours. The crucibles were removed from the furnace and let cool down to room temperature. Once at room temperature the crucibles with the ashes were weighed to determine the mass lost. An average of ~20 mg of ashed samples was recovered.

Then the ashes were reconstituted in the crucibles with 3 mL of $HNO_3$16M (Optima grade, Fisher Scientific, Pittsburg, USA) and 1 mL of 30% ultrapure hydrogen peroxide (J.T. Baker, Phillipsburg, NJ, USA) and transferred to 50 mL digestion tubes (Environmental Express Inc., USA). The samples were submitted to the digestion procedure abovementioned (Section 4.5.1.1.1).

Once the digestion was completed, the solutions were transferred to 50mL volumetric flasks and Rh standard was added as internal standard for a total concentration of 3 ng g^{-1}. The solution was completed with deionized water (>18 $M\Omega cm^{-1}$ obtained with a Nanopore Infinity filtration system, Barnstead). The samples and the method blanks were measured against an external calibration curve described in section 4.5.1.1.2 to asses the recovery.

4.5.1.1.4 Data analysis

The intensities (cps) for the standards and samples were normalized to the rhodium (internal standard) signal (cps). A linear regression line was determined from the plot of the normalized signal (cps) against the concentration of the correspondent standard. The concentrations in the samples were determined by using the slope and intercept of this equation.

4.5.1.2 Laser Ablation Analyses

The LA signal of the sample was acquired for approximately 120 seconds. For the first 30 seconds of the analysis the laser was not fired to acquire a "black" signal that accounts as background. Then the laser is fired for 60 seconds where only the middle 30 seconds were account for signal integration since the first interaction of the laser with the sample produce an unstable signal at the beginning of the ablation. After the laser was turned off, the signal was recorded for an additional 30 seconds to confirm that it returned to its blank value and to help purging the system between samples.

The following isotopes were measured for quantification: ^{25}Mg, ^{27}Al, ^{55} Mn, ^{56}Fe, ^{57}Fe, ^{85}Rb, ^{88}Sr, ^{137}Ba, and ^{208}Pb.

4.5.1.2.1 Sample preparation

Pellets of the SRM NIST 1515 Apple leaves (National Institute of Standards and Technology, Gaithersburg, MD, USA), Cabbage Control 4 (University of Utah cabbage sample) and Control M (FIU marijuana sample) were prepared with a manual pellet press (CARVER, Inc., IN, USA) and a stainless steal 13 mm die.

4.5.1.2.2 Assessment of calcium as internal standard

Calcium is one of the principal nutrients and it is found in % levels in plants, thus it is a good candidate to be used as internal standard for LA analysis. In order to assess the calcium concentration in the ashed marijuana samples, the SRM NIST 1515 and 3 samples were analyzed in replicates of 3 with SEM/EDS to determine an average concentration for this element. The samples were measured in low vacuum with a WD of 10, spot size 5, 20 kV, ~100x, and 100 scans.

4.5.1.2.3 Data analysis

Glass SRM NIST 612 glass matrix (National Institute of Standards and Technology, Gaithersburg, MD, USA) was used as external calibrator for the laser ablation data processing. Calcium of mass 43 was used as internal standard. The concentration of the different elements was determined in the GLITTER V4.1 software (GEMOC, Macquarie University, Australia). The description of the software and how it works is been explained in section 2.3.4.

4.5.1.3 Instrumentation

A HR-ICP-MS system ELEMENT 2 (Thermo Electron Co. Bremen, Germany) was used for solution based and laser ablation analyses. The ICP-MS was coupled to a Nd:YAG laser unit (*New Wave UP- 213* operating at 213nm from New Wave Research, Fremont, CA, USA). The operative principles and a description of the HR-ICP-MS and the laser system were described in Chapter 2, Sections 2.3.2.1 and 2.3.2.3 respectively.

The laser ablation and HR-ICP-MS optimized parameters used in this study are presented in Table 23. Since the amount of the ashed marijuana samples were between 10-70mg it was difficult to do additional homogenization of the ashes due to the high risk of loosing sample in the mixing jars. In order to avoid going thought the pellet and to improve the precision of the analysis and representation of the sample, the ablation mode selected was single line with a 100µm spot size. Helium was used as carrier gas since it has been demonstrated previously that there is an improvement in the sensitivity of LA analyses with glass.

The assessment of calcium as internals standard was performed with a SEM with an EDS detector (JEOL JSM 5900LV, JEOL USA, Inc. Peabody, MA, USA). The operative principles are described in Section 3.3.2.1.

Table 23. LA-HR-ICP-MS optimized parameters.

Laser Ablation System			**HR-ICP-MS System**	
Parameters	***Pre- Ablation***	***Ablation***	**Parameters**	
Wavelength	213 nm		**Auxiliary Gas**	0.80 L min^{-1}
Spot Size	100μm		**Carrier Gas Flow**	(solution) ~0.99 L min^{-1} (laser) ~1.0 L min^{-1}
Ablation Mode	Rastering	Single Line	**Nebulizer Flow**	(solution) 0.80 L min^{-1} (laser) 0.72 L min^{-1}
Scan Rate	75 μm sec^{-1}	15 μm sec^{-1}	**RF Power**	(solution) 1350W (laser) 1300 W
Energy Output	2.4 mJ (100%)	1.4 mJ (40%)	**Plasma Gas Flow**	16 L min-1
Repetition Rate	10 Hz		**Resolution Modes**	(laser) MR (solution) LR, MR, HR
Carrier Gas	He			
Ablation Cell Volume	30.0 mL			

4.5.2 Elemental analysis of ashed marijuana samples

4.5.2.1 Samples description

Ashed marijuana samples donated from University of Utah were submitted for elemental analysis. The samples were confiscated material from different areas of USA (Table 24) and were comprised of plant leaves except sample 569, which was a mix of leaf and flowers.

Samples 372, 402, 409, 415, 428, 433, 434, 453, 456, 466, 473, 474, 479, 483, 484, 502, 503, 504, 510, 516, 518, 529, and 530 were prepared in replicates of 3 when the amount of sample allowed it. The samples were treated and digested following the

abovementioned procedure (Section 4.5.1.1.1) and measured against a normal calibration (Section 4.5.1.1.2). The solutions were analyzed by HR-ICP-MS using the three mass resolutions using the parameters presented in Table 23. The rest of the samples were analyzed by LA-HR-ICP-MS with the optimized parameters described is Section 4.5.1.3.

4.5.2.2 Sample preparation for laser ablation analysis

The SRM NIST 1515 Apple leaves (National Institute of Standards and Technology, Gaithersburg, MD, USA), Cabbage control 4 (University of Utah sample), Control M (FIU sample) and the ashed marijuana samples were pressed into a pellets with a manual pellet press (CARVER, Inc., IN, USA) and a stainless steal 13 mm die. Pre ablation of the samples surface was done prior analysis to avoid any possible contamination from the press (Table 23).

4.5.2.3 Discrimination analysis

The concentration obtained from the data processing was used to do an ANOVA/Pairwise Comparison with Tukey's post hoc test ($p < 0.05$) to determine which pairs of means differed significantly. Pairwise Comparison with Tukey's post hoc test it is a powerful tool for a large number of pair comparisons. For single comparisons of those indistinguishable pairs that were expected to be different a t-test of unequal variances was used. These statistical analyses has been previously reported for the discrimination of glass samples [6, 8].

Table 24. Ashed marijuana samples: Plant component and location were confiscated.

ID	Component	County	State	ID	Component	County	State
245	L	Santa Barbara	CA	632	L	Williamson	IL
264	L	Boone	IN	372	L	Lunenburg	VA
301	L	Washington	MS	402	L	Dickson	TN
314	L	Fulton	IL	409	L	Decatur	TN
315	L	Fulton	IL	415	L	Henry	TN
331	L	Franklin	VA	428	L	Fulton	IL
333	L	Maui	HI	433	L	Morgan	CO
338	L	Benton	WA	434	L	Lewis	MO
339	L	Marathon	MI	453	L	Wilson	TN
352	L	Decatur	IN	456	L	Smith	TN
353	L	Clatsop	OR	458	L	Cumberland	TN
358	L	Jackson	MI	466	L	Fulton	IL
360	L	Franklin	IN	473	L	Jefferson	TN
366	L	Clark	IL	474	L	Fentress	TN
467	L	McDonough	IL	479	L	Knox	TN
482	L	Wells	IN	483	L	Steuben	IN
497	L	Columbia	OR	484	L	Orange	VT
524	L	Lane	OR	502	L	Maui	HI
568	L	Dade	MO	503	L	Nodaway	MO
569	M	Hawaii	HI	504	L	Schoolcraft	MI
570	L	Marion	OR	510	L	Lake	TN
576	L	Coos	OR	516	L	Bennington	VT
590	L	Clackamas	OR	518	L	Morgan	MO
600	L	Jackson	OR	529	L	Massac	IL
				530	L	Pope	IL

L=Leaf

M=Mix of leaf and flower

4.6 Results and Discussion

4.6.1 Solution based analysis

The accuracy and precision of the solution based analysis for plant material was evaluated with the SRM NIST 1515. The accuracy of solution analysis was evaluated with ≤10% bias from the NIST certified value and a precision of ≤10% RSD. To evaluate the performance of the analysis only the certified elements were chosen for comparison. Table 25 presents typical results for solution based analysis of SRM NIST 1515. All the

certified elements showed to be within the acceptable parameters for accuracy, except Fe. Iron in plant matrices has shown low recoveries after open vessel digestion. The recovery of iron has been reported for the SRM NIST 1515 as low as 70% and seems to vary according to the plant type [197]. The recovery of iron also showed to affect the precision of the analysis having 20% RSDs. Other elements with precision above the acceptable parameters were aluminum and barium with 17% and 14% respectively. The higher RSDs for Ba and Al has to do with the slightly enrichment of these elements in one of the replicates. Regardless the accuracy for these elements was good (<10% bias). The method for the analysis of plant material using the SRM NIST 1515 was evaluated successfully.

Table 25. Results of accuracy and precision for solution based analyses of SRM NIST 1515

Isotope	Concentration ± σ, µg g^{-1}	Certified Value, µg g^{-1}	%Bias	%RSD
^{25}Mg	2626 ± 131	2710 ± 8	3	5
^{27}Al	293 ± 50	286 ± 9	2	17
^{55}Mn	55 ± 2	54 ± 3	1	4
^{57}Fe	73 ± 15	83 ± 5	13	20
^{85}Rb	9.7 ± 0.04	10.2 ± 1.5	5	5
^{88}Sr	24.3 ± 0.9	25 ± 2	3	4
^{137}Ba	50 ± 7	49 ± 2	4	14
^{208}Pb	0.487 ± 0.040	0.470 ± 0.027	1	8

4.6.2 Recovery study

For the recovery study the SRM NIT 1515 was submitted to ashing and digestion procedures to evaluate the recovery of the trace elements of interest in plant analysis. The idea is to evaluate the behavior of certain elements in ashed SRM since the marijuana

samples for this study are ashed. Since there is no ashed standard material for plants, the results with the ashed SRM will allow the evaluation of the digestion process with the marijuana samples analyzed by HR-ICP-MS.

After the ashing procedure approximately ~20 mg of the SRM NIST 1515 was recovered. These samples were digested and measured to obtain the concentration. The certified and non certified values provided by NIST were used to determine an estimate of the concentration of the analyzed elements in the ashed SRM NIST 1515. The estimated value then was used to assess the recovery of the trace element in the SRM determined by the %bias.

Elements such as Sm, Ce, La, Ba, Sr, Rb, and Mg had a recovery between 97-89%. Manganese, iron, cobalt, aluminum, vanadium, and chromium had a recovery between 81-69%. Boron, lead, and arsenic had a low recovery of 49%, 37%, and 35% respectively (Table 26). The low recovery of B, Pb and As was expected since these elements are volatile elements and they were may have been lost during the ashing procedure. The elements Cd, Th, and U were below the instrumental detection limits. Zinc showed a significant enrichment resulting in a recovery of 142% for ^{64}Zn and 184% for ^{66}Zn. The high recovery in Zn may be attributed to the fact that the calibration curve of the ^{64}Zn and ^{66}Zn had a correlation coefficient (R^2) of 0.20485 and 0.11376 respectively; therefore the results for this element can't be accounted to evaluate the recovery.

Since the expected concentration values in the ashes are not certified these results serve solely as reference when the SRM NIST 1515 is ashed and submitted to the same digestion procedure as the ashed marijuana samples.

4.6.3 Solution based analysis of ashed marijuana samples

The ashes marijuana samples mentioned in Section 4.5.2.1 and the ashed SRM NIST 1515 were analyzed against a normal calibration curve described in Section 4.5.1.1.2. The elements measured for quantification were determined based on the concentration of the trace element above the instrumental detection limits and the likeliness to be present in all marijuana samples. The elements measured for quantification and discrimination analyses were: ^{25}Mg, ^{27}Al, ^{55} Mn, ^{57}Fe, ^{85}Rb, ^{88}Sr, and ^{137}Ba.

Table 26. Results of the recovery study of the SRM NIST 1515.

Isotope	Concentration ± σ, µg g^{-1}	[a]Expected Value, µg g^{-1}	%Bias	%RSD
^{11}B	182 ± 24	373	51	22
^{25}Mg	34339 ± 714	37467	8	2
^{27}Al	3001 ± 71	3954	24	2
^{51}V	2.6 ± 0.1	3.6	27	4
^{52}Cr	2.9 ± 0.2	[b]4.1	30	7
^{55}Mn	604 ± 14	747	19	2
^{56}Fe	795 ± 25	1148	31	3
^{57}Fe	838 ± 46	1148	27	5
^{59}Co	0.92 ± 0.08	[b]1.2	26	9
^{64}Zn	246 ± 40	173	42	16
^{66}Zn	319 ± 52	173	85	16
^{75}As	0.18 ± 0.09	0.53	65	49
^{85}Rb	127 ± 1	141	10	1
^{88}Sr	315 ± 10	346	9	3
^{111}Cd	[c]----	0.18	[c]----	[c]----
^{137}Ba	606 ± 23	677	11	4
^{139}La	270 ± 41	[b]277	3	15
^{140}Ce	46 ± 1	[b]41	11	3
^{152}Sm	38 ± 2	[b]41	9	5
^{208}Pb	2.4 ± 0.2	6.5	63	10
^{232}Th	[c]----	[b]0.41	[c]----	[c]----
^{238}U	[c]----	[b]0.08	[c]----	[c]----

[a]Expecetd value: mass proportion (~14) times the certified values provided by NIST

[b]Expecetd value: mass proportion (~14) times the non certified values provided by NIST

[c]Below detection limits

The concentration results for the above elements in the SRM NIST 1515 were used to assess the dissolution process of the ashed marijuana samples. The recoveries for these elements in the SRM NIST 1515 are presented in Table 27. The low recovery of lead was expected due to the lost of this volatile element during the ashing procedure. Due to the low recovery of lead and that most of the samples presented Pb concentrations below detection limits; this element was discarded from the discrimination element menu.

Table 27. Results of the recovery of trace elements in ashed SRM NIST 1515 digested with the ashed marijuana samples

Isotope	Concentration ± σ, μg g^{-1}	[a]Estimated Value, μg g^{-1}	%Bias	%RSD	% Recovery
^{25}Mg	28066 ± 4750	37467	25	17	75
^{27}Al	3610 ± 848	3954	9	23	91
^{55}Mn	514 ± 125	747	31	24	69
^{57}Fe	945 ± 19	1148	18	2	82
^{85}Rb	116 ± 21	141	18	18	82
^{88}Sr	292 ± 55	346	15	19	85
^{137}Ba	526 ± 144	677	22	27	78
^{208}Pb	4.1 ± 0.7	6.5	37	17	63

[a]Expecetd value: mass proportion (~14) times the certified values provided by NIST

The concentration of the abovementioned elements for the samples and the SRM were used to carryout an ANOVA/Pairwise comparison with Tukey's Post hoc test. The statistical analysis showed 24 indistinguishable pairs (Table 28) from which 3 pairs were comprised of samples that were confiscated in the same state but in a different county (453 & 510, 474 & 510, and 484 & 516). A t-test of unequal variances was used to corroborate the indistinguishable pairs. All the 24 pairs were distinguished by t-test, including those pairs with samples recovered from in the same state. Table 29 shows the results of the t-test for the pair 372 & 503. The specific geographical location where the

plants were grown will be necessary to confirm the differences found with this study. The discrimination order of the elements was: $^{55}Mn > ^{88}Sr > ^{137}Ba > ^{85}Rb > 27Al, ^{25}Mg > ^{57}Fe$.

Table 28. Results of the ANOVA/Pairwise comparison: Indistinguishable pairs.

Pair #	Pairs Identification	Pair #	Pairs Identification
1	372 & 503	13	484 & 502
2	428 & 474	14	484 & 504
3	428 & 510	15	484 & 510
4	428 & 516	16	484 & 516
5	453 & 510	17	484 & 529
6	453 & 529	18	502 & 504
7	474 & 503	19	502 & 510
8	474 & 510	20	502 & 516
9	474 & 516	21	503 & 510
10	474 & 529	22	504 & 529
11	483 & 484	23	510 & 516
12	483 & 516	24	516 & 529

Table 29. Example of results of a t-test of unequal variances for the pair 372 & 503.

Sample	**^{25}Mg**	**^{27}Al**	**^{55}Mn**	**^{57}Fe**	**^{85}Rb**	**^{88}Sr**	**^{137}Ba**
372	44440	58	660	2374	16	1606	51
	50680	276	757	2685	18	1719	56
503	28307	214	1422	756	3.4	1585	670
	27724	189	1448	775	3.4	1495	652
$t_{Statistics}$	6.2	-0.3	-14.4	11.3	13.5	1.7	-65.1
$t_{Critical}$	12.7	12.7	12.7	12.7	12.7	4.3	12.7

4.6.4 Assessment of Ca as internal standard for LA analysis

The calcium concentration for the SRM NIST 1515 and for the ashed marijuana samples 524, 568, and 569 was determined with SEM/EDS. The analysis was evaluated with the SRM NIST 1515 to verify the accuracy of the calcium measurement. Table 30 shows the results of accuracy and precision of the analysis for the SRM NIST 1515. The

accuracy and precision of Ca concentration was 20% and 12% respectively, which are acceptable result for this technique. The analysis then was validated. The Ca concentration in the ashed marijuana samples used for the laser ablation data processing was 21.75%wt (Table 30). Since the calcium content in the ashed plants was in the percentage level, a slight variation between samples' Ca concentration will not affect significantly the results.

Table 30. Results of the assessment of calcium in ashed marijuana samples for laser ablation data analysis.

Sample	Concentration of Ca, %wt	Sample	Concentration of Ca, %wt
NIST 1515-1	1.23	UT 524	22.71
NIST 1515-2	1.36	UT 568	23.09
NIST 1515-3	1.06	UT 569	19.44
Average, %wt	1.22	Average	21.75
StDev, %wt	0.15	StDev	2.00
%RSD	12.4	%RSD	9.2
Certified Value	1.53		
%Bias	20		

Table 31. Results of accuracy and precision for LA analysis of SRM NIST 1515.

Isotope	Concentration ± σ, µg g^{-1}	Certified Value ± σ, µg g^{-1}	%Bias	%RSD
^{25}Mg	2682 ± 137	2710 ± 8	1	5
^{27}Al	395 ± 5	286 ± 9	38	1
^{55}Mn	55.3 ± 7	54 ± 3	2	12
^{57}Fe	76.2 ± 3.3	83 ± 5	8	4
^{85}Rb	9.4 ± 0.8	10.2 ± 1.5	8	8
^{88}Sr	26.5 ± 0.8	25 ± 2	6	3
^{137}Ba	51.9 ± 2.3	49 ± 2	6	5
^{208}Pb	0.460 ± 0.064	0.470 ± 0.027	0.5	14

4.6.5 Laser ablation analysis

The SRM NIST 1515 pellet was analyzed with the instrumental parameters in Table 23. Only the certified elements by NIST were used to assess the accuracy and precision of the analysis. Acceptable parameters of accuracy and precision for laser ablation analyses were ≤10%Bias and ≤15% RSD respectively.

In terms of accuracy all elements except Al presented a bias of less than 10%, whereas in terms of precision all elements were within the acceptable parameters. Although there was a bias for the Al measurement, the precision was significantly lower than 15% RSD which may suggest there was a contamination with this element (Table 31). Accurate and precise measurements of elements of interest in plant material were evaluated successfully by LA-HR-ICP-MS.

4.6.6 Laser ablation analysis of ashed marijuana samples

The laser ablation method developed for plant analysis was used to determine concentration of the elements Mn, Ni, Ba, Rb, Fe, Sr, Mg, and Pb in the SRM NIST 1515, Cabbage control 4, Control M, and in the ashed marijuana samples. These elements were present in the ashed samples at concentrations above the detection limits, and are generally present in plants.

All the samples were analyzed in three consecutive days; therefore the SRM and the control samples were analyzed each day to validate the analysis. The concentration of these elements then was used to do the discrimination statistical analysis (ANOVA/Pairwise comparison with Tukey's Post hoc test with 95% of confidence level). Seventy-six pairs out of 1128 possible pairs were found to be indistinguishable

from which 49 were correctly identified (Table 32). These correctly identified pairs including ashed marijuana samples measured the on separate days (UT 524, NIST 1515, Control M, and Cabbage control 4) and a sample measured the same day as an unknown (UT 467). A t-test of unequal variances was performed to the 49 pairs correctly identified to confirm the results obtained by the ANOVA/Pairwise comparison. The t-test results showed that pairs: ControlMa & ControlMb, ControlMa & ControlMc were indistinguishable. The pair ControlMb & ControlMc was distinguished by t-test. Heterogeneity of the samples due mixture of leafs and flower may contribute with the differences found on the same sample analyzed in different days. Pairs UT467a1 & UT467a2 and pair UT524a & UT524c were indistinguishable by t-test. All the pairs of the SRM NIST1547 (NIST1547a & NIST1547b, NIST1547a & NIST1547c, and NIST1547b & NIST1547c) were undistinguished by t-test as well. Some pairs of the SRM NIST 1515 were distinguished by t-test just by one element, magnesium. For some of the analyses the Mg concentration in the SRM NIST 1515 was determined with a bias higher than 10%. For the SRM NIST 1547 magnesium was determined with an accuracy of ≤10% bias. Although there was some discrimination between pair of samples from the same origin, the analysis was validated with the SRM NIST 1547, UT524, and UT467. Four pairs (UT315b2 & UT315c2, UT315b2 & UT315c1, UT315b1 & UT315c2, and UT315b1 & UT315c1) were distinguished by ANOVA/Pairwise comparison. The main reason for the discrimination has to do with the heterogeneity of the powdered ashed material. A better homogenization of the ashed marijuana samples, such as in the abovementioned case, may reduce the differences in elemental composition when analyzed as unknown blinds.

The other 27 indistinguishable pairs (Table 33), which were expected to be different in terms of elemental composition, were distinguished by t-test of unequal variances. Table 34 shows the results of one of the t-test analysis performed to one of the indistinguishable pairs incorrectly associated by ANOVA/Pairwise comparison.

In this analysis the most discriminant element resulted to be Ni whereas the least discriminant was Mg. The discrimination order of elements was as follow: ^{60}Ni > ^{208}Pb > ^{55}Mn > ^{85}Rb > ^{56}Fe > ^{88}Sr, ^{137}Ba > ^{25}Mg. The discrimination order may vary with the plant type since some plants may have tendencies to accumulate more elements than others.

Table 32. Results of the ANOVA/Pairwise comparison: Indistinguishable pair correctly identified.

Pair #	Pairs Identification	Pair #	Pairs Identification
1	Control Ma &Control Mb	26	NIST 1515a3 & NIST 1515b1
2	Control Ma & Control Mc	27	NIST 1515a3 & NIST 1515b2
3	Control Mb & Control Mc	28	NIST 1515a3 & NIST 1515b3
4	Cabbage Control4a & Cabb Contro4b	29	NIST 1515a3 & NIST 1515c1
5	Cabbage Control4a & Cabb Contro4c	30	NIST 1515a3 & NIST 1515c2
6	Cabbage Control4b & abb Control c	31	NIST 1515a3 & NIST 1515c3
7	UT 315b1 &UT 315b2	32	NIST 1515b1 & NIST 1515b2
8	UT 315c1 & UT 315c2	33	NIST 1515b1 & NIST 1515b3
9	UT 467a1 & UT 467a2	34	NIST 1515b1 & NIST 1515c1
10	UT 524a & UT 524c	35	NIST 1515b1 & NIST 1515c2
11	NIST 1515a1 & NIST 1515a2	36	NIST 1515b1 & NIST 1515c3
12	NIST 1515a1 & NIST 1515a3	37	NIST 1515b2 & NIST 1515b3
13	NIST 1515a1 & NIST 1515b1	38	NIST 1515b2 & NIST 1515c1
14	NIST 1515a1 & NIST 1515b2	39	NIST 1515b2 & NIST 1515c2
15	NIST 1515a1 & NIST 1515b3	40	NIST 1515b2 & NIST 1515c3
16	NIST 1515a1 & NIST 1515c1	41	NIST 1515b3 & NIST 1515c1
17	NIST 1515a1 & NIST 1515c2	42	NIST 1515b3 & NIST 1515c2
18	NIST 1515a1 & NIST 1515c3	43	NIST 1515b3 & NIST 1515c3
19	NIST 1515a2 & NIST 1515a3	44	NIST 1515c1 & NIST 1515c2
20	NIST 1515a2 & NIST 1515b1	45	NIST 1515c1 & NIST 1515c3
21	NIST 1515a2 & NIST 1515b2	46	NIST 1515c2 & NIST 1515c3
22	NIST 1515a2 & NIST 1515b3	47	NIST 1547a & NIST 1547b
23	NIST 1515a2 & NIST 1515c1	48	NIST 1547a & NIST 1547c
24	NIST 1515a2 & NIST 1515c2	49	NIST 1547b & NIST 1547c
25	NIST 1515a2 & NIST 1515c3		

(a): day 1, (b): day 2, and (c): day 3

Table 33. Results of the ANOVA/Pairwise comparison: Indistinguishable pair incorrectly identified.

Pair #	Pairs Identification
1	Cabb Control4a & NIST 1515a1
2	Cabb Control4a & NIST 1515a2
3	Cabb Control4a & NIST 1515a3
4	Cabb Control4a & NIST 1515b1
5	Cabb Control4a & NIST 1515b2
6	Cabb Control4a & NIST 1515b3
7	Cabb Control4a & NIST 1515c1
8	Cabb Control4a & NIST 1515c2
9	Cabb Control4a & NIST 1515c3
10	Cabb Control4b & NIST 1515a1
11	Cabb Control4b & NIST 1515a2
12	Cabb Control4b & NIST 1515a3
13	Cabb Control4b & NIST 1515b1
14	Cabb Control4b & NIST 1515b2
15	Cabb Control4b & NIST 1515b3
16	Cabb Control4b & NIST 1515c1
17	Cabb Control4b & NIST 1515c2
18	Cabb Control4b & NIST 1515c3
19	Cabb Control4c & NIST 1515a1
20	Cabb Control4c & NIST 1515a2
21	Cabb Control4c & NIST 1515a3
22	Cabb Control4c & NIST 1515b1
23	Cabb Control4c & NIST 1515b2
24	Cabb Control4c & NIST 1515b3
25	Cabb Control4c & NIST 1515c1
26	Cabb Control4c & NIST 1515c2
27	Cabb Control4c & NIST 1515c3

(a): day 1, (b): day 2, and (c): day 3

Table 34. Example of a t-test for one of the indistinguishable pairs incorrectly identified by ANOVA/Pairwise comparison test.

Sample	**^{25}Mg**	**^{55}Mn**	**^{56}Fe**	**^{60}Ni**	**^{85}Rb**	**^{88}Sr**	**^{137}Ba**	**^{208}Pb**
NIST 1515a1	3443	51	78	0.98	9.0	25	41	0.42
	3409	55	75	0.84	9.1	27	52	0.43
	3404	51	74	1.1	9.4	27	57	0.50
	3436	55	[a]----	[a]----	[a]----	[a]----	[a]----	[a]----
Cabb Control 4a	1456	9	27	0.29	7.0	42	1.2	0.012
	1628	16	30	0.36	11	41	1.2	0.039
	1202	15	31	0.27	8.7	45	1.3	0.023
	[a]----	10	[a]----	[a]----	6.9	[a]----	[a]----	0.018
$t_{Statistics}$	16.1	19.8	27.9	9.2	0.9	-12.3	10.2	15.7
$t_{Critical}$	4.3	2.6	2.8	3.2	3.2	3.2	4.3	4.3

[a] Outilers

4.7 Conclusions

An analytical method for the analysis of plant material was developed for solution and laser ablation ICP-MS. The analytical method provided with accurate and precise results allowing to trustfully using elemental composition for possible discrimination of plants of different origins.

Trace elements then were used to develop a strategy using statistical analysis to determine differences between marijuana plants allegedly from of different origin. The discrimination element menu for solution and laser ablation analyses was similar although in laser ablation there were more elements. The differences in the element menu derived from the specific conditions of the dissolution and the laser ablation processes. For example in solution analyses Ni and Pb were below instrumental detection limits whereas in laser ablation these elements were detected with a precision of <10% RSD.

There was discrimination by t-test of some pairs comprised of the same sample measured as blind unknown. Some of the SRM NIST 1515 pairs were not discriminated by t-test and some did. The SRM NIST 1515 pairs were discriminated only by the magnesium concentration. The SRM NIST 1515 was measure three times the same day in three consecutive days. The magnesium concentration for some of the samples was not accurate with respect to the certified value. On the other hand the SRM NIST 1547 was measured one time in each of the three days and all the possible combination pairs of this reference material were indistinguishable by ANOVA/Pairwise comparison and by t-test. Other pairs of the same samples were not distinguished by ANOVA/Pairwise comparion but were discriminated by t-test. The heterogeneity of the ashed marijuana samples and the ControlM may have contributed to the discrepancies in the discrimination of

themselves when measured as unknown blinds. Regardless, the use of elemental composition proved to provide some discrimination of plants from different origin. Knowing the geographical origin of the marijuana plants will provide with a better interpretation of the discrimination results for both solution and laser ablation analyses. This study opens the possibilities of utilizing elemental composition in forensic laboratories for determining the origin of illegal plants such as marijuana.

5 CONCLUSIONS AND RECOMMENDATIONS

The use of ICP-MS has demonstrated to be an excellent tool for elemental analysis determinations in matrices such as glass, bones, teeth, and plant material. The capabilities of the quadrupole (equipped with a dynamic reaction cell) and the high resolution ICP-MS systems were compared for the analysis of Fe which is a good discriminant element to associate glass and a good candidate for discrimination of bone, teeth, and plant matrices of the same origin. The resolution of the polyatomic interferences of Fe in glass was achieved by using the high resolution instrument or by chemical means using the dynamic reaction cell. Method detection limits as low as ~0.03 $\mu g\ g^{-1}$ and 0.14 $\mu g\ g^{-1}$ for laser ablation and solution analyses respectively were achieved with the optimal settings for both ICP-MS systems. The capability of resolving the polyatomic interferences of iron by either a high resolution instrument or a quadrupole with dynamic reaction cell, allows the use of iron in elemental analysis not only for glass discrimination but potentially for other matrices such as bone, teeth and plan material.

Bones and teeth are matrices of interest for the forensic scientists due to the potential information that they can offer about an individual. Evaluating the dietary habits of an individual or population, discrimination between individuals, and the association of an individual to a specific geographical location are the primary applications of elemental composition in the abovementioned matrices, although most of the time the elemental analysis is based solely in light and heavy isotope ratios.

Trace elements in bones and teeth may also provide with complementary information to associate or discriminate between individuals. Elemental composition of trace elements could be especially useful in the separation of commingled human remains

in massive burials. An analytical method for the elemental analysis of bones and teeth samples was developed providing accurate and precise results for the bone SRM NIST 1486 and NIST 1400 for solution and laser ablation analyses. The possibility of suppression of the trace elements due to the high calcium and phosphorus content in bone matrix was evaluated to determine the reliability of using elemental composition for discrimination purposes. There were indications of a slight suppression for some trace elements but it did not affect significantly the accuracy and/or precision of the trace elements analyzed by ICP-MS. Thus the trace elements determinations by ICP-MS were valid and reliable. Two digestion procedures were compared and it was found that the open vessel seems to provide more accurate results for some elements when compared with microwave digestion. For all the other elements both procedures provided with similar results.

For laser ablation analyses, calcium was evaluated in the bone samples to be used as internal standard. The calcium concentration in the different bone samples was around 21%, which is close to the concentration in the SRM NIST 1486. Therefore the calcium was used as internal standard for laser ablation data processing. It was of great importance to find an internal standard present almost uniformly in the matrix, especially since the bone samples should not be ground because it will mix the diagenic and biogenic signals.

A laser ablation method was developed by means of accuracy and precision of the SRM NIST 1486 measurements under different experimental parameters. The optimal instrumental parameters (laser and ICP-MS instruments) were found to be single spot analysis at 10 Hz repetition rate, with a spot size of 100μm and helium as carrier gas.

Additionally, the crater morphology and an estimate of the mass ablated were determined using the optimized laser ablation parameters. The crater morphology on the SRMs NIST 612 (glass matrix) and NIST 1486 (bone meal), and a bone fragment was evaluated with SEM images. Measurements of the craters dimensions and the density of the materials allowed estimating the ablated mass. Although the three samples (NIST 612, NIST 1486 and the compact bone fragment) had different densities, the estimated ablated mass was very similar for all of them when ablated under the same conditions (~8-12 µg).

One of the most significant findings of this study includes the possibility of assessing the biogenic signal in buried bone samples when information of the environmental conditions where the samples were buried is not provided. In order to evaluate the biogenic and the diagenetic signal regions in the bone fragments, different areas of the sample were analyzed in terms of elemental composition to determine where the concentration signal was stabilized. The stability of the signal suggested this area as the one with the biogenic signal. The middle layers of the bone fragments showed the most stable signal for the elements analyzed. The biogenic signal was also confirmed by taking Ca/P ratio measurements of the middle layers of the bone fragments. This ratio can indicate changes in the hydroxyapatite suggesting the area was affected by diagenesis. The middle layers of bone fragments showed a Ca/P ratio within the normal values of unchanged hydroxyapatite confirming the biogenic signal. This new approach to assess biogenic signal with LA-HR-ICP-MS provides with a fast and accurate elemental analysis that can ease the separation process of human remains in cases where no environmental conditions are known.

The optimized laser ablation parameters were used to determine the elemental composition of bones and teeth samples. The elemental composition was used to carryout statistical discrimination analyses to determine the potential use of trace elements to separate samples from different origin and to correctly associate samples from the same origin. In the case of bones, samples from the same individual were associated in groups when only femur or humerus bones were considered separately for discrimination. There was no separation of individuals when both humerus and femur bones were considered. These results revealed the importance of sampling and comparing the same anatomical area since different bones may be exposed to different growing conditions that may affect the elemental composition even within bones of the same individual. Additional studies including analyzing more samples and a heterogeneity study of the elemental composition of different parts of the skeleton may help to assess which bones are more suitable for elemental analysis and provide even more discrimination.

The elemental composition of the different layers in teeth showed differences in the concentration for some elements. When the elemental composition of the whole tooth was used for the separation of the individuals, there was more overlap between individuals that when the elemental composition of the tooth layers was considered individually. The mixed elemental composition in whole teeth may contribute to the discrepancies found in teeth samples from the same individual. Analysis of more samples teeth samples and the assessment of variation in elemental composition on teeth of the same individual will help to better interpret the results found in this study.

The study also contributed to the scientific community with an analytical method capable of separating plant materials allegedly from different origin. Accurate and precise

results were obtained for the SRM NIST 1515 with regular dissolution ICP-MS and with LA-ICP-MS. The use of LA-HR-ICP-MS makes the method suitable for a fast and accurate elemental analysis; which will help to speed up the discrimination process in a forensic laboratory without consuming the evidence. Marijuana ashed samples presumably form different origins were discriminated based on elemental analysis in solution and with LA. For laser ablation analyses the samples and most of reference materials measured the same day or different days as unknown blinds were correctly associated with themselves by ANOVA/Pariwise comparison and with t-test of unequal variances. Pairs expected to be different and were associated by ANOVA/Pairwise comparisons test were separated apart by further statistical analysis with a t-test. As with bone samples it is important to compare elemental composition of plants of the same species and the same plant component to avoid mixing elemental composition signature that may lead to incorrect discriminations or association of plants. Knowing the specific origin where the plants were grown is necessary to better interpret the discrimination results found in this study, thus the source of the differences is still undetermined. This method opens the possibility of including elemental analysis for the separation of plant materials, especially in law enforcement cases when dealing with marijuana plants.

This research and further work will offer forensic scientists with the option of including a fast and easier elemental analysis than isotope ratios for the discrimination of bones, teeth and plant materials using LA-HR-ICP-MS.

LIST OF REFERENCES

[1]. Beard, B. L.; Johnson, C. M., Strontium isotope composition of skeletal material can determine the birth of place and geographic mobility of humans and animals. *J. Forensic Sci.* **2000,** 45, 1049.

[2]. Cox, G.; Sealy, J., Investigating identity and life histories: Isotopic analysis and historical documentation of slave skeletons Found on the Cape Town Foreshore, South Africa. *Int. J. Histor. Archaeol.* **1997,** 1, 207.

[3]. Djingova, R.; Zlateva, B.; Kuleff, I., On the possibilities of Inductively Coupled Plasma Mass Spectrometry for analysis of archaeological bones for reconstruction of paleodiet. *Talanta* **2004,** 63, 785.

[4]. Pye, K., Isotope and trace element analysis of human teeth and bones for forensic purposes. In *Forensic Geoscience - Principles, Techniques and Applications*, Pye, K.; Croft, D. J., Eds. Geological Society Publishing House: London, 2004; pp 215.

[5]. Price, T. D.; Johnson, C. M.; Ezzo, J. A.; Erocksom, J.; Burton, J. H., Residential mobility in prehistoric southwest United States: A preliminary study using strontium isotope analysis. *J. Archeol. Sci.* **1994,** 21, 315.

[6]. Montero, S.; Hobbs, A. L.; French, T. A.; Almirall, J. R., Elemental analysis of glass fragments by ICP-MS as evidence of association: Analysis of a case. *J. Forensic Sci.* **2003,** 48, 1.

[7]. Berends-Montero, S.; Wiarda, W.; de Joodeb, P.; van der Peijl, G., Forensic analysis of float glass using laser ablation inductively coupled plasma mass spectrometry (LA-ICP-MS): validation of a method. *J. Anal. At. Spectrom.* **2006,** 21, 1185.

[8]. Trejos, T.; Montero, S.; Almirall, J. R., Analysis and comparison of glass fragments by laser ablation inductively coupled plasma mass spectrometry (LA-ICP-MS) and ICP-MS. *Anal. Bioanal. Chem.* **2003,** 376, 1255.

[9]. Dickerson, J. W. T., Changes in the composition of the human femur during growth. *Biochem. J.* **1962,** 82, 56.

[10]. Fabig, A.; Herrmann, B., Trace elements in buried human bones: intra-population variability of Sr/Ca and Ba/Ca ratios - diet or diagenesis? *Naturwissenschaften* **2002,** 89, 115.

[11]. Gawlik, D.; Behne, D.; Brätter, P.; Gatschke, W.; Gessner, H.; Kraft, D., The suitability of the iliac crest biopsy in the element analysis of bone and marrow. *J. Clin. Chem. Clin. Bio.* **1982,** 20, 499.

[12]. Lambert, J. B.; Simpson, S. V.; Buikstra, J. E.; D., H., Electron microprobe analysis of elemental distribution in excavated human femurs. *Am. J. Phys. Anthropol.* **1983,** 62, 409.

[13]. Hodson, M. E.; Valsami-Jones, E.; Cotter-Howells, J. D.; Dubbin, W. E.; Kemp, A. J.; Thornton, I.; Warren, A., Effect of bone meal (calcium phosphate) amendments on metal release from contaminated soils - a leaching column study. *Environ. Pollut.* **2001,** 112, 233.

[14]. Shahack-Gross, R.; Bar-Yosef, O.; Weiner, S., Black colored bones in Hayonim Cave, Israel: Differentiating between burning and oxide staining. *J. Archeol. Sci.* **1997,** 24, 439.

[15]. Klepinger, L., Nutritional assessment from bone. *Annu. Rev. Anthropol.* **1984,** 13, 75.

[16]. Simmons, D. J.; Grynaps, M. D., Mechanisms of bone formation in vivo. In *Bone: The Osteoblast and Osteocyte,* Hall, B. K., Ed. The Telford Press: Caldwell, 1989; Vol. 1, pp 193.

[17]. Teitelbaum, S. L., Bone resorption by osteoblasts. *Science* **2000,** 289, 1504.

[18]. Hill, P. A., Bone remodelling. *Br. J. Orthod.* **1998,** 25, 101.

[19]. Parfitt, A. M., The physiological and clinical significance of bone data. In *Bone histomorphometry: Techniques and interpretation*, Recker, R. R., Ed. CRC Press: Boca Raton, FL, 1983; pp 143.

[20]. Woelfel, J. B.; Scheid, R. C., *Dental anatomy. Its relevance to dentistry*. Lippincott Williams & Wilkins: Philadelphia, 2002.

[21]. Koons, R. D.; Fieldler, C.; Rawalt, R. C., Classification and discrimination of sheet and container glasses by Inductively Coupled Plasma-Atomic Emission Spectrometry and pattern recognition. *J. Forensic Sci.* **1988,** 33, 49.

[22]. Ryland, S., Sheet or container?-Forensic glass comparisons with an emphasis on source classification. *J. Forensic Sci.* **1986,** 31, 1314.

[23]. Suzuki, Y.; Sugita, R.; Suzuki, S.; Marumo, Y., Forensic discrimination of bottle glass by refractive index measurement and analysis of trace elements by ICP-MS. *Anal. Sci.* **2000,** 16, 1195.

[24]. Zurhaar, A.; Mullis, L., Characterization of forensic glass samples using inductively coupled plasma mass spectrometry. *J. Anal. At. Spectrom.* **1990,** 5, 611.

[25]. Copley, J.; Almirall, J. R., In *Forensic Examination of Glass and Paint*, Caddy, B., Ed. Taylor and Francis: London, NY, 1999; pp 39.

[26]. Koons, R. D.; Peters, C. A.; Rebbert, P. S., Comparison of refractive index, energy dispersive X-ray fluorescence and inductively coupled plasma atomic emission spectrometry for forensic characterization of sheet glass fragments. *J. Anal. At. Spectrom.* **1991,** 6, 451.

[27]. Duckworth, D. C.; Bayne, C. K.; Morton, D. J.; Almirall, J. R., Analysis of variance in forensic glass analysis by ICP-MS: variance within the method. *J. Anal. At. Spectrom.* **2000,** 15, 821.

[28]. Nonose, N. K., Non-spectral and spectral interferences in inductively coupled plasma high-resolution mass spectrometry Part 2. Comparison of interferences in quadrupole and high resolution inductively coupled plasma mass spectrometries. *J. Anal. At. Spectrom.* **2001,** 16, 560.

[29]. Umpierrez, S.; Trejos, T.; Neubauer, K.; Almirall, J., Determination of iron in glass by solution and laser ablation DRC-ICP-MS. *At. Spectrosc.* **2006,** 27, 76.

[30]. Weyer, S.; J.B., S., High precision Fe isotope measurements with high mass resolution MC-ICP-MS. *Int. J. Mass Spectrom.* **2003,** 226, 355.

[31]. Gürleyük, H.; Brunette, R. C.; Howard, C. R.; Schneider, C.; Thomas, R., Using Dynamic Reaction Cell ICP MS technology to determine the full suite of elements in rainwater samples. *Spectroscopy* **2005,** 20, 22.

[32]. Balcaen, L.; Geuens, I.; Moens, L.; Vanhaecke, F., Determination of ultra-traces of Fe in $AgNO_3$ by means of isotope dilution inductively coupled plasma dynamic reaction cell mass spectrometry. *Anal. Bioanal. Chem.* **2003,** 377, 1020.

[33]. Günther, D.; Hattendorf, A. A., Multi-element analysis of melt and fluid inclusions with improved detection capabilities for Ca and Fe using laser ablation with a dynamic reaction cell ICP-MS. *J. Anal. At. Spectrom.* **2001,** 16, 1085.

[34]. Flem, B.; Larsen, R. B.; Grimstvedt, A.; Mansfeld, J., In situ analysis of trace elements in quartz by using laser ablation inductively coupled plasma mass spectrometry. *Chem. Geol.* **2000,** 182, 237.

[35]. Townsend, A. T., The accurate determination of the first row transition metals in water, urine, plant, tissue and rock samples by sector field ICP-MS. *J. Anal. At. Spectrom.* **2000,** 15, 307.

[36]. Latkoczy, C.; Becker, S.; Ducking, M.; Günther, D.; Hoogewerff, J. A.; Almirall, J. R.; Buscaglia, J.; Dobney, A.; Koons, R. D.; Montero, S.; van der Peijl, G. J. Q.; Stoecklein, W. R. S.; Trejos, T.; Watling, J. R.; Zdanowicz, V. S., Development and evaluation of a standard method for the quantitative determination of elements in float glass samples by LA-ICP-MS. *J. Forensic Sci.* **2005,** 50, 1327.

[37]. American Society for Testing Materials, ASTM Method E2330-04 Standard test method for the determination of trace elements in glass using inductively coupled plasma mass spectrometry. In *ASTM Annual Book of ASTM Standards*, American Society for Testing Materials: West Conshohocken, PA, 2004; Vol. 14.2, p 1.

[38]. Date, A. R.; Gray, A., Development progress in plasma source mass spectrometry. *Analyst* **1983,** 108, 159.

[39]. Heiftje, G. M.; Vickers, G. H., Developments in Plasma Source-Mass Spectrometry. *Anal. Chim. Acta* **1989,** 216, (1/2), 1.

[40]. Beauchemin, D., Inductively Coupled Plasma Mass Spectrometry. *Anal. Chem.* **2002,** 74, 2873.

[41]. Denoyer, E. R.; Tanner, S. D.; Voellkopf, U., A new dynamic reaction cell for reducing ICP-MS interferences using chemical resolution. *Spectroscopy* **1999,** 14, (2), 43.

[42]. Skoog, D. A.; Holler, F. J.; Nieman, T. A., *Principles of Instrumental Analysis*. 5 ed.; Saunders College Publishing: Philadelphia, PA, 1998.

[43]. Tanner, S. D.; Baranov, V. I., A dynamic reaction cell for inductively coupled plasma mass spectrometry (ICPDRC-MS). II. Reduction of interferences produced within the cell. *J. Anal. At. Spectrom.* **1999,** 10, 1083.

[44]. Hattendorf, B.; Günther, D., Characteristics and capabilities of an ICP-MS with a dynamic reaction cell for dry aerosols and laser ablation. *J. Anal. At. Spectrom.* **2000,** 15, 1125.

[45]. Rowan, J. T.; Houk, R. S., Attenuation of polyatomic interferences in Inductively Coupled Plasma Mass Spectrometry by gas-phase collisions. *Appl. Spectrosc.* **1989,** 43, (6), 976.

[46]. Hecht, J., *Understanding Lasers: An Entry-level Guide*. The Institute of Electrical and Electronic Engineers, Inc: New York, 1992.

[47]. Svelto, O., *Principles of Lasers*. 4th ed.; Plenum Publishing Corporation: New York, NY, 1998; p 1.

[48]. Koechner, W., *Solid State of Laser Engineering*. Springer: Germany, 1999; p 47.

[49]. Günther, D.; Mermet, J., Laser Ablation for Inductively Coupled Plasma - Mass Spectrometry. In *Comprehensive analytical chemistry, discrete sample introduction techniques for Inductively Coupled - Mass Spectrometry*, Barcelo, D., Ed. Elsevier: Amsterdam, 2000; Vol. 34.

[50]. Durrant, S. F., Laser Ablation Inductively Coupled Plasma Mass Spectrometry: Achievements, Problems, Prospects. *J. Anal. At. Spectrom.* **1999,** 14, 1385.

[51]. Gamaly, E. G.; Rode, A. V.; Luther-Davies, B., Ultrafast ablation with high-pulse-rate lasers. Part I: Theoretical considerations. *J. Appl. Phys.* **1999,** 85, 4213.

[52]. Rode, A. V.; Luther-Davies, B. E.; Gamaly, G., Ultrafast ablation with high-pulse-rate lasers. Part II: Experiments on laser deposition of amorphous carbon films. *J. Appl. Phys.* **1999,** 85, 4222.

[53]. Mao, S.; Mao, X. L.; Greif, R.; Russo, R. E., Initiation of an early-stage plasma during picosecond laser ablation of solids. *Appl. Phys. Lett.* **2000,** 77, 2464.

[54]. Mao, S. S.; Mao, X. L.; Greif, R.; Russo, R. E., Simulation of a picosecond laser ablation plasma. *Appl. Phys. Lett.* **2000,** 76, 3370.

[55]. Mao, X. L.; Russo, R. E., Observation of plasma shielding by measuring transmitted and reflected laser pulse temporal profiles. *Appl. Phys. A: Mater. Sci. Process.* **1996,** 64, 1.

[56]. Liu, H. C.; Mao, X. L.; Yoo, J. H.; Russo, R. E., Early phase laser induced plasma diagnostics and mass removal during single-pulse laser ablation of silicon. *Spectrochim. Acta, Part B* **1999,** 54, 1607.

[57]. Phipps, C. R.; Dreyfus, R. W., In *Laser Ionization Mass Analysis*, A. Vertes, R. G., F. Adams, Ed. Wiley: New York, 1993.

[58]. Russo, R. E., Laser Ablation. In *Focus on Analytical Spectrometry: A compendium of Applied Spectroscopy Focal Point Articles (1994-1997)*, Holcome, J.; Hieftje, G.; Majidi, V., Eds. Society for AppliedSpectroscopy: 1998; pp 41.

[59]. Winefordner, J. D.; Gornushkin, I. B.; Pappas, D.; Matveev, O. I.; Smith, B. W., Novel uses of lasers in atomic spectroscopy. Plenary Lecture. *J. Anal. At. Spectrom.* **2000,** 15, 1161.

[60]. Eggins, S. M.; Kinsley, L. P. J.; Shelley, J. M. G., Deposition and element fractionation processes during atmospheric pressure laser sampling for analysis by ICP-MS. *Appl. Surf. Sci.* **1998,** 127, 278.

[61]. Günther, D.; Heinrich, C. A., Enhanced sensitivity in laser ablation-ICP mass spectrometry using helium-argon mixtures as aerosol carrier. *J. Anal. At. Spectrom.* **1999,** 14, 1363.

[62]. Horn, I.; Günther, D., The influence of ablation carrier gasses Ar, He and Ne on the particle size distribution and transport efficiencies of laser ablation-induced aerosols: implications for LA-ICP-MS. *Appl. Surf. Sci.* **2003,** 207, 144.

[63]. Günther, D., Laser-Ablation Inductively-Coupled Plasma Mass Spectrometry. *Anal. Bioanal. Chem.* **2002,** 372, 31.

[64]. Russo, R. E.; Mao, X.; Liu, H.; Gonzalez, J.; Mao, S. S., Laser Ablation in Analytical Chemistry-A Review. *Talanta* **2002,** 57, 425.

[65]. Feng, R., In situ trace element determination of carbonates by laserProbe inductively coupled plasma mass spectrometry using nonmatrix matched standardization. *Geochim. Cosmochim. Acta* **1994,** 58, 1615.

[66]. Guillong, M.; Günther, D. G., Quasi 'non-destructive' laser ablation-inductively coupled plasma-mass spectrometry fingerprinting of sapphires. *Spectrochimica Acta Part B* **2001,** 56, 1219.

[67]. Günther, D.; v Quadt, A.; Wirz, R.; Cousin, H.; Dietrich, V. J., Elemental analyses using Laser Ablation-Inductively Coupled Plasma-Mass Spectrometry (LA-ICP-MS) of geological samples fused with $Li_2B_4O_7$ and calibrated without matrix-matched standards. *Microchimica Acta* **2001,** 136, 101.

[68]. Chen, Z. J., Inter-element fractionation and correction in Laser Ablation Inductively Coupled Plasma Mass Spectrometry. *J. Anal. At. Spectrom.* **1999,** 14, 1823.

[69]. Beauchemin, D.; Gregoire, D. C.; Günther, D.; Karanassios, V.; Mermet, J. M.; Wood, T. J., In *Wilson and Wilson's Comprehensive Analytical Chemistry Series: Discrete Sample Introduction Techniques for Inductively Coupled Plasma Mass Spectrometry*, Barcelo, D., Ed. Elsevier: London, 2000; Vol. XXXIV, pp 445.

[70]. Toland, H.; Perkins, B.; Pearce, N.; Keenan, F.; Leng, M. J., A study of sclerochronology by Laser Ablation ICP-MS. *J. Anal. At. Spectrom.* **2000,** 15, 1143.

[71]. Narewski, U.; Werner, G.; Schulz, H.; Vogt, C., Application of Laser Ablation Inductively Coupled Mass Spectrometry (LA-ICP-MS) for the determination of major, minor, and trace elements in bark samples. *Fresenius. J. Anal. Chem.* **2000,** 366, 167.

[72]. Watmough, S. A.; Hutchinson, T. C.; Evans, R. D., Development of solid calibration standards for trace elemental analyses of tree rings by Laser Ablation Inductively Coupled Plasma-Mass Spectrometry. *Environ. Sci. Technol.* **1998,** 32, 2185.

[73]. Craig, C. A.; Jarvis, K. E.; Clarke, L. J., An Assessment of calibration strategies for the quantitative and semi-quantitative analysis of calcium carbonate matrices by Laser Ablation-Inductively Coupled Plasma-Mass Spectrometry (LA-ICP-MS). *J. Anal. At. Spectrom.* **2000,** 15, 1001.

[74]. Jeffries, T. E.; Perkins, W. T.; Pearce, N. J. G., Comparisons of Infrared and Ultraviolet Laser Probe Microanalysis Inductively Coupled Plasma Mass Spectrometry in mineral analysis. *Analyst* **1995,** 120, 1365.

[75]. Trejos, T.; Almirall, J. R., Effect of fractionation on the forensic elemental analysis of glass using Laser Ablation Inductively Coupled Plasma Mass Spectrometry. *Anal. Chem.* **2004,** 76, 1236.

[76]. Stix, J., A critical look at quantitative Laser Ablation ICP-MS analysis of natural and synthetic glasses. *Can. Mineral.* **1995**, 435.

[77]. Schroeder, E., Properties and characteristics of a Laser Ablation ICP-MS System for the quantitative elemental analysis of glasses. *Appl. Surf. Sci.* **1998**, 292.

[78]. Raith, A.; Godfrey, R., Quantitation methods using Laser Ablation ICP-MS. *Fresenius. J. Anal. Chem.* **1996,** 354, 163.

[79]. Potter, D., Semiquantitative analysis of glass by Laser Ablation ICP-MS. *Agilent Technologies* **2000**, 1.

[80]. Watling, J. R., Sourcing the provenance of cannabis crops usinginter-element association patterns ‘fingerprinting’ and laser ablation inductively coupled plasma mass spectrometry. *J. Anal. At. Spectrom.* **1998,** 13, 917.

[81]. Kang, D.; Amarasiriwardena, D.; Goodman, A. H., Application of laser ablation-inductively coupled plasma-mass spectrometry (LA-ICP-MS) to investigate trace metal spatial distributions in human tooth enamel and dentine growth layers and pulp. *Anal. Bioanal. Chem.* **2004,** 378, 1608.

[82]. Ghazi, A. M.; Shuttleworth, S.; Anguloc, S. J.; Pashley, D. H., New applications for laser ablation high resolution ICPMS (LA-HR-ICP-MS): Quantitative measurements of gallium diffusion across human root dentin. *J. Anal. At. Spectrom.* **2000,** 15, 1335.

[83]. Uryu, T.; Yoshinaga, J.; Yanagisawa, Y.; Endo, M.; Takahashi, J., Analysis of lead in tooth enamel by LA-ICP-MS. *Anal. Sci.* **2003,** 19, 1413.

[84]. Helliwell, T. R.; Kelly, S. A.; Walsh, H. P. J.; Klenerman, L.; Haines, J.; Clark, R.; Roberts, N. B., Elemental analysis of femoral bone from patients with fractured neck of femur or osteoarthrosis. *Bone* **1996,** 18, 151.

[85]. Lappalainen, R.; Knuuttila, M., Mg content of healthy and chronically diseased human cancellous bone in relation to age and some physical and chemical factors. *Med. Biol.* **1995,** 63, 144.

[86]. Zhang, Y. X.; Wang, Y. S.; Zhang, Y. P.; Zhang, G. L.; Huang, Y. Y.; He, W., Investigation of elemental distribution in human femoral head by PIXE and SRXRF microprobe. *Nucl. Instrum. Methods Phys. Res., Sect. B* **2007,** 261, 178.

[87]. Shashikiran, N. D.; Subba Reddy, V. V.; Hiremath, M. C., Estimation of trace elements in sound and carious enamel of primary and permanent teeth by atomic absorption spectrophotometry: An in vitro study. *Indian J. Dent. Res.* **2007,** 18, 157.

[88]. Sridharan, T.; Penuka, P., A comparative study of trace elements on dental enamel. *Acta Ciencia Indica* **2000,** XXVIP, (4), 159.

[89]. Tanaka, T.; Maki, K.; Hayashida, Y.; Kimura, M., Aluminum concentrations in human deciduous enamel and dentin related to dental caries. *J.Trace Elem. Med. Bio.* **2004,** 18, 149.

[90]. Arora, M.; Kennedy, B. J.; Elhlou, S.; Pearson, N. J.; Walker, D. M.; Bayl, P.; Chan, S. W., Spatial distribution of lead in human primary teeth as a biomarker of pre- and neonatal lead exposure. *Sci. Total Environ.* **2006,** 371, 55.

[91]. Miner, S. *Preliminary air pollution of barium and its compounds. A literature review*; Public Health Service, National Air Pollution Control Administration: Raleigh, NC, 1969.

[92]. Malleson, T., The accumulation of trace metals in bone during fossilization. In *Trace Metals and Fluride in bones and teeth*, Priest, N. D.; Van De Vyver, F. L., Eds. CRC Press Inc.: Boca Raton, FL, 1990; Vol. 15, pp 344.

[93]. Edward, J. B.; Benfer, R. A.; Morris, J. S., The effect of dry ashing on the composition of human and animal bone. *Biol. Trace Elem. Res.* **1990,** 25, 219.

[94]. Grotti, M.; Abelmoschi, M. L.; Dalla Riva, S.; Soggia, F.; Frache, R., Trace element determinations in human cortical and trabecular bones. *J. Biol. Nucl. Chem.* **2005,** 381, 1395.

[95]. Baranowska, I.; Czernick, K.; Aleksandrowicz, R., The analysis of lead, cadmium, zinc, copper and nickel in bones from the upper silesian industrial district. *Sci. Total Environ.* **1995,** 159, 155.

[96]. Hongue, D.; Johansen, S.; Androchow, E.; Bjertness, E.; Becker, G.; Alexander, J., Determination of aluminum in samples from bone and liver of Elderly Norwegian. *J.Trace Elem. Med. Bio.* **1996,** 10, 6.

[97]. Navario, J. A.; Granadillo, V. A.; Salgado, O.; Rodrigue z-Iturbe, B.; Garcia, R.; Delling, G.; Romero, R., Bone metal content in patients with chronic renal failure. *Clin. Chim. Acta* **1992,** 211, 133.

[98]. Slatzman, B. E.; Gross, S. B.; Yeager, D. W.; Mainers, B. G.; Gartside, P. S., Total body bunders and tissue concentration of lead, cadmium, copper, zinc and ash in 55 human cadavers. *Environ. Res.* **1990,** 52, 126.

[99]. Wittmers, L. E.; Wallgren, J.; Aufderheide, A. C.; Rapp, G., Lead in bone IV. Distribution of Pb in human skeleton. *Arch. Environ. Health* **1988,** 43, 381.

[100]. Tang, S.; Parsons, P.; Slavin, W., Rapid and reliable method for the determination of aluminum in bones by electrothermal. *Analyst* **1996,** 121, 195.

[101]. Zoger, N.; Wobrauschek, P.; Streil, C.; Pepponi, G.; Roschger, P.; Falkenberg, G.; Osterode, W., Distribution of Pb and Zn in slices of human bone by Synchrotron μ-XRF. *X-Ray Spectrom.* **2005,** 34, 140.

[102]. Sun, D. H.; Waters, J.; Mawhinney, T. P., Microwave Digestion and Ultrasonic Nebulization for the Determination of Boron in Animal Tissues by ICP-AES with International Standardization and Addition of Mannitol. *J. Anal. At. Spectrom.* **1997,** 12, 675.

[103]. Assion, A.; Wollenhaupt, M.; Haag, L.; Mayorov, F.; Sarpe-Tudoran, C.; Winter, M.; Kutschera, U.; Baumert, T., Femtosecond Laser-Induced-Breakdown Spectrometry for Ca^{2+} analysis of biological samples with high spatial resolution. *Appl. Phys. B: Lasers Opt.* **2003,** 77, 391.

[104]. Martin, M. Z.; Labbe, N.; Andre, N.; Harris, R.; Ebinger, M.; Wullschleger, S. D.; Vass, A. A., High resolution applications of laser-induced breakdown spectroscopy for environmental and forensic applications. *Spectrochim. Acta, Part B* **2007,** 62, 1426.

[105]. Martin, M. Z.; Wullschleger, S. D.; Garten, C. T.; Palumbo, A. V.; Smith, J. G., Elemental analysis of environmental and biological samples using Laser-Induced Breakdown Spectroscopy and Pulsed Raman Spectroscopy. *J. Dispersion Sci. Technol.* **2004,** 25, 687.

[106]. Samek, O.; Beddows, D. C. S.; Telle, H. H.; Kaiser, J.; Liska, M.; Caceres, J. O.; Gonzalez Urena, A., Quantitative Laser-Induced Breakdown Spectroscopy analysis of calcified tissue samples. *Spectrochim. Acta, Part B* **2001,** 56B, 865.

[107]. Ward, N. D.; Durrant, S. F.; Gray, A., Analysis of biological standard reference materials by LA-ICP-MS. *J. Anal. At. Spectrom.* **1992,** 7, 1139.

[108]. Ward, N. I.; Abou-Shakra, F. R.; Durrant, S. F., Trace elemental content of biological materials: A comparison of NAA and ICP-MS analysis. *Biol. Trace Elem. Res.* **1990,** 26, 177.

[109]. Sanborn, M.; Telmer, K., The spatial resolution of LA-ICP-MS line scans across heterogeneous materials such as fish otoliths and zoned minerals. *J. Anal. At. Spectrom.* **2003,** 18, 1231.

[110]. Wang, S.; Brown, b.; Gray, D. J., Application of Laser Ablation-ICPMS to the spatially resolved micro-analysis of biological tissue. *Appl. Spectrosc.* **1994,** 48, 1321.

[111]. Sillen, A., Diagenesis of inorganic phase of cortical bone. In *The chemistry of prehistoric human bone*, Price, T. D., Ed. Cambridge University Press: Cambridge, 1989; pp 211.

[112]. Hoogewerff, J.; Papesch, W.; Kralik, M.; Berner, M.; Vroon, P.; Miesbauer, H.; Gaber, O.; Künzel, K.-H.; Kleinjans, J., The last domicile of the iceman from Hauslabjoch: a geochemical approach using Sr, C, and O isotopes and trace element signatures. *J. Archaeol. Res.* **2001,** 28, 983.

[113]. Vaughan, J. M. *The physiology of bone*. 3 ed.; Oxford [Eng.] Clarendon Press: New York, 1970.

[114]. Driessens, F. C. M.; Verbeeck, R. M. H., *Biominerals*. CRC Press, Inc: Boca Raton, FL, 1990.

[115]. Spadaro, J. A.; Becker, R. O.; Backman, C. H., The distribution of trace metal ions in bone and tendon. *Calcif. Tissue Int.* **1970,** 6, 49.

[116]. Bratter, P.; Gawlik, D.; Lausch, J.; Rosick, U., On the distribution of trace elements in human skeleton. *J. Radioanal. Chem.* **1977,** 37, 393.

[117]. Dahl, S. G.; Allain, P.; Marie, P. J.; Mauras, Y.; Boivin, G.; Ammann, P.; Tsouderos, Y.; Delmas, P. D.; Christiansen, C., Incorporation and distribution of strontium in bone. *Bone* **2001,** 28, 446.

[118]. Carvalho, M. L.; Marquesa, A. F.; Lima, M. T.; Reuse, U., Trace elements distribution and post-mortem intake in human bones from Middle Age by total reflection X-ray fluorescenc. *Spectrochim. Acta, Part B* **2004,** 59, 1251.

[119]. Yamaguchi, M.; Matsui, R., Effect of dipicinolate, a chelator of zinc, on bone protein synthesis in tissue culture: The essential role of zinc. *Biochem. Pharmacol.* **1989,** 38, 4485.

[120]. Yamaguchi, M.; Oishi, H.; Suketa, Y., Stimulatory effect of zinc on bone formation in tissue culture. *Biochem. Pharmacol.* **1987,** 36, 4007.

[121]. Starcher, B. C.; Hill, C. H.; Madras, J. G., Effect of zinc deficiency on bone collagenase and collagen turnover. *J. Nutr.* **1980,** 110, 2095.

[122]. Lappalainen, R.; Knuuttila, M.; Lammi, S.; Alhava, E. M., Fluoride content related to the elemental composition, mineral density and strength of bone in healthy and chronically diseased persons. *J. Chron. Dis.* **1983,** 36, 707.

[123]. Davis, G. K.; Mertz, W., Copper. In *Trace Elements in Human and Animal Nutrition*, Mertz, W., Ed. Academic Press.: San Diego, CA, 1987; Vol. 1, pp 301.

[124]. Dollwet, H. H.; Sorenson, J. R., Roles of copper in bone maintenance and healing. *Biol. Trace Elem. Res.* **1988,** 18, 39.

[125]. Fell, B. F., The pathology of copper deficiency in animals. In *Copper in Animals and Man*, Howell, J. M.; Gawthorne, J. M., Eds. CRC Press: Bock Raton, FL, 1987; Vol. 2, pp 1.

[126]. Chausmer, A. B.; Wallach, S., Metabolism of trace metals in animals: Part II: Essential trace elements. In *Trace Metals and Fluride in bones and teeth*, Priest, N. D.; Van De Vyver, F. L., Eds. CRC Press Inc: Boca Raton, FL, 1990; Vol. 15, pp 258.

[127]. Wallach, S.; Chausmer, A. B., Metabolism of trace metals in animals and man: Part I: Non-essential pollutant metals. In *Trace Metals and Fluride in Bones and Teeth*, Priest, N. D.; Van De Vyver, F. L., Eds. CRC Press Inc.: Boca Raton, FL, 1990; Vol. 15, pp 233.

[128]. El Solh, N.; Rousselet, F., Effects of stable strontium on calcium metabolism with particular reference to low-calcium diet. In *Handbook of Stable Strontium*, Skoryna, S. C., Ed. Plenum Press.: New York, 1981; p 515.

[129]. Strey, E., Strontium "rickets": bone, calcium and strontium changes. *Australian Ann. Med.* **1961,** 10, 213.

[130]. Tanaka, G.; Kawamura, H.; Nomura, E., Reference Japanese Man-II, Distribution of Strontium in the skeleton and in the mass of mineralized bone. *Health Phys.* **1981,** 40, 601.

[131]. Duckworth, J.; Hill, R., The storage of elements in the skeleton. *Nutr. Abstr. Rev. Ser. Hum. Exp.* **1953,** 23, 1.

[132]. Flinshman, J., Mislene joint disease- A manganese deficiency? *S. Afr. Med. J.* **1981,** 160, 445.

[133]. Rodriguez, M.; Felsenfeld, A. J.; Llach, F., Aluminum administration in the rat separately affects the osteoblast and bone mineralization. *J. Bone Miner. Res.* **1990,** 5, 59.

[134]. Schroeder, H. A.; Tipton, I. H.; Nason, P., Trace metals in man: Strontium and barium. *J. Chron. Dis.* **1972,** 25, 491.

[135]. United States Environmental Protection Agency, Computer printout: Frequency distributions by site/year for barium, the results of samples collected at National Air Surveillance Network sites. In Environmental Monitoring Systems Laboratory: 1984.

[136]. Calabrese, E. J.; Canada, A. T.; Sacco, C., Trace elements and public health. *Annu. Rev. Publ. Health* **1985,** 6, 131.

[137]. Beliles, R. P., The Metals. In *Patty's Industrial Hygiene and Toxicology*, 4 ed.; Clayton, G. D.; Clayton, F. E., Eds. John Wiley & Sons: New York, 1994; p 1925.

[138]. Ellsasser, J. C.; Farnham, J. E.; Marshall, J. H., Comparative kinetics and autoradiography of ^{45}Ca and ^{133}Ba in ten year old beagle dogs. *J. Bone Joint Sur.* **1969,** 51A, 1397.

[139]. Machata, G., Barium. In *Handbook on Toxicity of Inorganic Compounds*, Seiler, H. G.; Sigel, H., Eds. Marcel Dekker, Inc: New York, NY, 1988; pp 97.

[140]. MacDonald, N. S.; Ezmirlian, F.; Spain, P.; McArthur, C., The ultimate site of skeletal deposition of strontium and lead. *J. Biol. Chem.* **1951,** 188, 387.

[141]. Gross, S. B.; Pfitzer, E. A.; D.W., Y.; Kehoe, R. A., Lead in human tissues. *Toxicol. Appl. Pharm.* **1975,** 32, 638.

[142]. Wilson, L.; Pollard, M., Here today, gone tomorrow? Integrated experimentation and geochemical modeling in studies of archaeological diagenetic change. *Acc. Chem. Res.* **2002,** 35, 644.

[143]. Zamata, J.; Perez-Sirvent, C.; Martinez-Sanchez, M. J.; Tovar, P., Diagenesis, not biogenesis: Two late Roman Empire skeletal examples. *Sci. Total Environ.* **2006,** 369, 357.

[144]. Nielsen-Marsh, C. M., Patterns of diagenesis in bone I: The effects of site environments. *J. Archeol. Sci.* **2000,** 27, 1139.

[145]. Collins, M. J.; Nielsen–Marsh, C. M.; Hiller, J.; Smith, C. I.; Roberts, J. P.; Prigodich, R. V.; Wess, T. J.; Csapò, J.; Millard, A. R.; Turner–Walker, G., The survival of organic matter in bone: A review. *Archaeometry* **2002,** 44, 383.

[146]. Hedges, R. E. M., Bone diagenesis: An overview of processes. *Archaeometry* **2002,** 44, 319.

[147]. Ten Cate, A. R., *Oral histology: Development, structure, and function*. 5 ed.; Mosby Inc: Saint Louis, 1998; p 81.

[148]. Cate, A. R. T., *Oral Histology: development, structure, and function*. 5 ed.; Mosby: New York, NY, 1998; p 128.

[149]. Summitt, J. B.; Robbins, J. W.; Hilton, T. J.; Schwartz, R. S., *Fundamentals of operative dentistry*. Quintessence Pub: 2006; p 13.

[150]. Morelli, C.; Russi, R. Morelly-Russi 3D Anatomical Models. http://files.turbosquid.com/Preview/Content_on_2_27_2006_14_11_37/Tooth_4.jpg63625cd6-9964-4a1a-ba38-3ef3c5f19996Large.jpg (July 2008),

[151]. Ross, M. H.; Romrell, L. J.; Kaye, G. I., *Histology: Text and Atlas*. Williams & Wilkins: 1995; p 445.

[152]. Brudevold, F.; Steadman, L. T.; Spinelli, M. A.; Amdur, B. H.; Cron, P., A study of zinc in human teeth. *Arch. Oral Biol.* **1963,** 8, 135.

[153]. Petersson, L. G.; Lodding, A.; Kock, G., Elemental microanalysis of enamel and dentine by secondary ion mass spectrometry (SIMS). *Swed. Dent. J.* **1978,** 2, 41.

[154]. Ahlberg, M.; Akselsson, R., Proton induced x-ray emission in the trace analysis of human tooth enamel and dentine. *Int. J. Appl. Radiat. Is.* **1976,** 27, 279.

[155]. Weihs, C., Canonical discriminant analysis: Comparison of resampling methods and Convex-hull approximation. In *Royal Statistical Society Lecture Note Series 2: Recent Advances in Descriptive Multivariate Analysis*, Krzanowski, W. J., Ed. Oxford University Press: New York, NY, 1995; pp 34.

[156]. Saiki, M.; Takanata, M. K.; Kramarski, S.; Borelli, A., Instrumental neutron activation analysis of rib bone samples and of bone reference materials. *Biol. Trace Elem. Res.* **1999,** 41, 71.

[157]. Cameron, J. R.; Skofronick, J. G.; Grant, R. M., *Physics of the Body*. 2 ed.; Medical Physics Publishing: Madison, WI, 1999; p 96.

[158]. Rajurkar, N. S.; Pardeshi, B. M., Analysis of some herbal plants from India used in the control of diabetes mellitus by NAA and AAS techniques. *Appl. Radiat. Isot.* **1997,** 48, 1059.

[159]. Shinogi, M.; Mori, I., Multielement in Cannabis leaves by instrumental Neutron Activation Analysis- A comparison of Cannabis of various geographical origins in Japan. *Yakugaku Zasshi* **1978,** 98, 1466.

[160]. Borkowska-Burnecka, J., Microwave assisted extraction for trace element analysis of plant materials by ICP-AES. *Fresenius. J. Anal. Chem.* **2000,** 368, 633.

[161]. Masson, P., Matrix effects during trace element analysis in plant samples by inductively coupled plasma atomic emission spectrometry with axial view configuration and pneumatic nebulizer. *Spectrochim. Acta, Part B* **1999,** 54, 603.

[162]. Mengel, K.; Kirkby, E. A., *Principles of plant nutrition*. 4 ed.; International Potash Institute Bern: Switzerland, 1987.

[163]. Kabata-Pendias, A.; Pendias, H., *Trace elements in soils and plants*. CRC Press, Inc.: Boca Raton, FL, 1984.

[164]. Smiths, P. F., Mineal analysis of plant tissues. *Annu. Rev. Plant Phys.* **1962,** 13, 81.

[165]. Gough, L. P.; Shacklette, H. T.; Case, A. A., *Element concentrations toxic to plants, animals, and man*. U.S. Government Printing Office: Washington, D.C, 1979; Vol. 80, p 1466.

[166]. Davey, B. G.; Wheeler, R. C., Some aspects of the chemistry of lithium in soils. *Plant Soil* **1980,** 5, 49.

[167]. El-Sheik, A. M.; Ulrich, A., Interactions of rubidium, sodium, and potassium on the nutrition of sugar beet plants. *Plant Physiol.* **1970,** 46, 645.

[168]. Bowen, G. E., Adsorption of copper, zinc,and manganese by sugar cane tissue. *Plant Physiol.* **1969,** 44, 255.

[169]. Loneragan, J. F., Distribution and movement of copper in plants. In *Copper in soils and Plants*, Loneragan, J. F.; Robson, A. D.; Graham, R. D., Eds. Academic Press: New York, 1981; p 165.

[170]. Elgawhary, S. M.; Malzer, G. L.; Barber, S. A., Calcium and strontium transport to plant roots. *Soil Sci. Soc. Am. J.* **1972,** 36, 794.

[171]. Shacklette, H. T.; Erdman, J. A.; Harms, T. F., Trace elements in plant foodstuffs. In *Toxicity of heavy metals in the environment Part I,* Oehme, F. W., Ed. Marcel Dekker: New York, 1978; p 25.

[172]. Chaudry, F. M.; Wallace, A.; Muller, R. T., Barium toxicity in plants. *Commun. Soil Sci. Plant Anal.* **1977,** 8, 795.

[173]. Lindsay, W. L., Zinc in soils and plant nutrition. *Adv. Agron.* **1972,** 24, 147.

[174]. Grimme, H., Adsorption of Mn, Co, Cu, and Zn to goethite in dilute solutions. *Z. Pflanzenernähr. Bodenk* **1968,** 121, 58.

[175]. Baumeister, W.; Ernst, W., *Mineralstoffe und Pflanzenwachstrum*. Fischer: Stuttgart, 1978; p 416.

[176]. Tinker, P. B., Levels, distribution and chemical forms of trace elements in food plants. *Philosophical transactions of the Royal Society of London B* **1981,** 294b, 41.

[177]. Sauerbeck, D., Which heavy metals concentrations in plants should not be exceeded in order to avoid detrimental effects on their growth. *Landw. Forsch. Sonderh.* **1982,** 39, 108.

[178]. Clark, R. B., Effect of aluminum on the growth and mineral elements of Al-tolerant and Al-intolerant corn. *Plant Soil* **1977,** 47, 653.

[179]. Foy, C. D.; Chaney, R. L.; White, M. C., The physiology of metal toxicity in plants. *Annu. Rev. Physiol.* **1978,** 29, 511.

[180]. Broyer, T. C.; Johnson, C. N.; Paull, R. E., Some aspects of lead in plant nutrition. *Plant Soil* **1972,** 36, 301.

[181]. Hughes, M. K.; Lepp, N. W.; Phipps, D. A., Aerial heavy metal pollution and terrestrial ecosystems. *Adv. Ecol. Res.* **1980,** 11, 217.

[182]. Zimdahl, R. L., Entry and movement in vegetation of lead derived from air and soil source. In *68th Annual Meeting of the Air Pollution Control Association*, Boston, MA, 1975.

[183]. Embleton, T. W., Magnesium. In *Diagnostic criteria of plants and soil*, Chapman, H. D., Ed. University of California, Division of Agricultural Sciences: 1966; pp 225.

[184]. Bloomfield, C., The translocation of metals in soil. In *The Chemistry of Soil Processes*, Greenland, D. J.; Hayes, M. H., Eds. John Wiley & Sons: New York, 1981; p 463.

[185]. Norrish, K., The geochemistry and mineralogy of trace elements. In *Trace Elements in Soil-Plant-Animal Systems*, Nicholas, D. J. D.; Egan, A. R., Eds. Academic Press: New York, 1975; p 55.

[186]. Welch, R. M., The biological significance of nickel, paper. In *International Symposium of Trace Element Stress in Plants*, Los Angeles, CA, 1979.

[187]. Berrow, M. L.; Busrridge, J. C., Sources and distribution of trace elements in soils and related crops. In *Conference on management and control of heavy metals in the environment*, CEP Consultants Ltd: Edinburg, U.K, 1979.

[188]. Crooke, W. M.; Inkson, R. H. E., The relationship between nickel toxicity and major nutrient supply. *Plant Soil* **1955,** 6, 1.

[189]. Dobritskaya, U. I., Distribution of vanadium in natural objects. *Agrokhimiya* **1969,** 3, 143.

[190]. Welch, R. M.; Cary, E. E., Concentration of chromium, nickel, and vanadium in plant materials. *J. Agric. Food Chem.* **1975,** 23, 479.

[191]. Welch, R. M., Vanadium uptake by plants. *Plant Physiol.* **1973,** 51, 828.

[192]. Tiffin, L. O., Translocation of micronutients in plants. In *Micronutrients in Agriculture*, Mortvedt, J. J.; Giordano, P. M.; Lindsay, W. L., Eds. Soil Science Society of America: Madison, WIs, 1972; p 199.

[193]. Nicholas, D. J. D., The functions of trace elements. In *Trace elements in Soil-Plant-Animal Systems*, Nicholas, D. J. D.; Egan, A. R., Eds. Academic Press: New York, 1975; p 181.

[194]. Clarkson, D. T.; Sanderson, J., Sites of absorption and translocation of iron in barley roots: Tracer and microauthoradiographic studies. *Plant Physiol.* **1978,** 61, 731.

[195]. Armstrong, M. J.; Kirkby, E. A., The influence of humidity on mineral composition of tomato plants with special reference to calcium distribution. *Plant Soil* **1979,** 52, 427.

[196]. Landi, S., Mineral nutrition of *Cannabis sativa L*. *J. Plant Nutr.* **1997,** 20, 311.

[197]. Huang, L.; Bell, R. W.; Dell, B.; Woodward, J., Rapid nitric acid digestion of plant material with an open-vessel microwave system. *Commun. Soil Sci. Plant Anal.* **2004,** 35, 427.

APPENDICES

Comparison of High Resolution and Dynamic Reaction Cell ICP-MS Capabilities for Forensic Analysis of Iron in Glass

Waleska Castro, Tatiana Trejos, Benjamin Naes, and José R. Almirall

Department of Chemistry and Biochemistry, Florida International University and International Research Forensic Institute, 11200 SW. 8th Street, Miami, FL 33199

Abstract. Forensic laboratories routinely conduct analysis of glass fragments to determine whether or not there is an association between a fragment(s) recovered from a crime scene or suspect to a particular source of origin. The physical and optical (refractive index) properties of the fragments are compared and, if a "match" between two or more fragments is found, further elemental analysis can be performed to enhance the strength of the association. A range of spectroscopic techniques have been used for elemental analysis of this kind of evidence, including Inductively Coupled Plasma Mass Spectrometry (ICP-MS). Due to its excellent sensitivity, precision and accuracy, several studies have found that ICP-MS methods (dissolution and laser ablation) provide the best discrimination between glass fragments originating from different sources. Nevertheless, standard unit resolution ICP-MS instruments suffer from polyatomic interferences including $^{40}Ar^{16}O^{+}$, $^{40}Ar^{16}O^{1}H^{+}$, and refractory oxide $^{40}Ca^{16}O^{+}$ that compromise the measurement of trace levels of Fe^{56+} and Fe^{57+}, for example. This represents a drawback for the analysis of glass fragments because iron has been previously identified as a good

discriminating element. Currently, there are several techniques available that allow for the reduction of such interferences. However, there is no existing data that compares the detection limits of iron in glass using those techniques.

The aim of this study is to perform a comparison of analytical performance of a standard quadrupole ICP-MS coupled to a Dynamic Reaction Cell (DRC-ICP-MS) and High Resolution Sector Field Inductively Coupled Plasma Mass Spectrometry (HR-SF-ICP-MS) for iron analysis in glass with respect to the method detection limits (MDL), accuracy, and precision. Analyses were conducted using conventional acid digestion and laser ablation methods. For laser ablation analyses a comparison of carrier gases was performed to asses the effect on the detection limits in the detection of iron isotopes. Iron polyatomic interferences were reduced or resolved by using dynamic reaction cell and high resolution ICP-MS. MDLs as low as 0.03 μg g^{-1} and 0.14 μg g^{-1} were achieved in laser ablation and solution based analyses respectively. The use of helium as carrier gas demonstrated improvement in the detection limits of both iron isotopes in medium resolution for the HR-SF-ICP-MS and with DRC in the quadrupole ICP-MS system.

Keywords: glass, elemental analysis, DRC-ICP-MS, HR-SF-ICP-MS, forensic

Introduction

The fragile nature of glass and its abundance in our surroundings make this material a very common type of evidence found in crime scenes such as hit-and-run accidents, burglaries, shootings, and other violent crimes. Vehicle windows, architectural windows, headlamps and containers represent the major sources of glass evidence.

Forensic examiners typically begin by screening the evidence by measuring physical and optical properties such as color, thickness, fluorescence, microscopic examination and refractive index [1-12]. If a match between known and questioned fragments is found in this preliminary stage, elemental analysis is typically conducted in order to improve the discrimination value of the analysis. When two or more fragments share a common elemental profile, they can be considered to originate from the same source of manufacturing origin and provide strong scientific evidence to associate a person to an event or two objects to each other. Fragments that are found to differ by elemental content can be determined to originate from different manufacturing sources and also provide useful information to the court or investigators.

A variety of trace elemental analysis techniques have been used for this purpose, including Atomic Absorption (AAS) [13-15], X-ray Fluorescence (XRF) [16, 17, 19], Neutron Activation (NAA) [18], Scanning Electron Microscopy with Energy Dispersive X-Ray Detection (SEM-EDX) [19, 20], Inductively Coupled Plasma Atomic Emission Spectrometry (ICP-AES) [8,11, 21-24] and Inductively Coupled Plasma Mass Spectrometry (ICP-MS) [25-28]. Each technique has its own advantages and shortcomings. ICP-MS has been shown to be the most effective analytical method for the comparison of trace elements in small glass fragments due to its multi-element capability, excellent sensitivity, high sample throughput and the capability to provide isotopic information.

The physical evidence, especially trace evidence sometimes could provide with a significant breakthrough on a criminal investigation by linking an individual to the crime. This trace evidence is often in the sub-microscopic level (typically 0.1-1mm) and needs

to be carefully analyzed in reliable way without been destroyed to be presented in a court of law. Although conventional digestion methods for ICP-MS have been shown to be excellent tools for elemental analysis of glass, they have the disadvantage of requiring the dissolution of the sample, therefore destroying it prior to introduction to the ICP-MS and increasing the contamination risk. During the last two decades, laser ablation (LA) has increasingly been used and preferred as a sample introduction method in forensic laboratories due to the advantages it offers over dissolution of the glass prior to analysis [29-32]. The most significant advantages of LA sampling technique include the capability of doing spatial resolution and in situ spot analysis, small sample consumption, reduction in sample preparation time, shortened analysis time, and a reduced risk of contamination. These advantages make LA a suitable sampling technique for the analysis of trace evidence such as glass and paint in forensic cases.

Variations in elemental profiles within glass populations are due to differences in elemental composition of the raw materials used and/or those contributed by the manufacturing processes. Although some of the raw materials used in glass manufacturing are relatively pure, a glass product may contain impurities, such as iron oxide, that could produce undesirable color and alter furnace temperatures. Only one-part-per-thousand of iron oxide in sand can impart a green color on the glass and therefore manufacturers usually use decoloring agents to remove or mask the tint. Iron oxide is typically present at concentrations that range from 0.07 to 0.16% wt in float glass, 0.03 to .015 %wt in containers, 0.05% wt in borosilicate glass, and 0.01%wt in lead crystal glass while in optical and insulating lead glasses, iron oxide content is reduced to trace levels [33].

The elements used for the discrimination of glasses by ICP-MS had been critically selected from previous studies in which precision, accuracy and discrimination potential of these elements were evaluated at major, minor and trace levels [25, 26]. Iron has been identified in previous studies as an excellent discriminating element and it has been successfully used for classification and discrimination of glasses by X-ray fluorescence [8, 16, 34] and ICP-AES [8, 34]. Nevertheless, the concentration of iron in some glass populations may be close to or lower than the limits of detection of XRF and ICP-AES. Although standard ICP-MS methods provide better sensitivity than the aforementioned techniques, the analytical performance of iron represents a challenge due to inherent interferences. In 2000, Duckworth *et al*. reported that elements measured by ICP-MS without good bias (≤10%) and precision (≤10%RSD) were closely inspected before using them as discriminating elements in a database for float glass. In this study iron presented a bias and precision higher than 10% [6]. The poor precision and accuracy of iron measurements in glass standards do not allow its use in glass databases and limits its use in casework.

The analytical challenges of iron in glass by ICP-MS are the result of polyatomic isobaric interferences such as $^{40}Ca^{16}O^{+}$ and $^{40}Ar^{16}O^{+}$ on $^{56}Fe^{+}$, and $^{40}Ca^{16}O^{1}H^{+}$, $^{40}Ar^{16}O^{1}H^{+}$, and $^{41}K^{16}O^{+}$ on $^{57}Fe^{+}$, respectively. Fortunately, there are several ICP-MS techniques capable of resolving polyatomic interferences. These interferences can be suppressed by using either DRC or HR respectively [35-37]. A solution based analysis using DRC-ICP-MS reports a comparison of MDLs in 2% HNO_3, in rain water/ HNO_3/HF matrix and the reporting limits generated by Frontier Geosciences Laboratories (Seattle, WA) with detection limits as low as 9 ng L^{-1} for the 2% HNO_3 and 383 ng L^{-1} in

the rainwater sample [38]. Balcaen *et al.* performed determinations of Fe in $AgNO_3$ solutions with isotope dilution using the DRC-ICP-MS with NH_3 as a reactant gas. They reported lower iron detection limits with the isotope dilution (0.013 μg g^{-1}) than with external calibration (1.2 μg g^{-1}) [39]. In 2001 Günther *et al.* reported a comparison of detection limits of $^{56}Fe^+$ and $^{57}Fe^+$ using the standard (STD) mode and the DRC mode with hydrogen and neon as reactant and buffer gases, respectively for laser ablation experiments. The limits of detection were determined for a spot size of 40μm using the gas blank and the ablation of the SRM NIST 610 glass. In that study, the limits of detection were improved from 5.9 μg g^{-1} in STD mode to 2.1 μg g^{-1} using DRC mode for $^{57}Fe^+$, while for $^{56}Fe^+$ the limits of detection were reported to be 0.3 μg g^{-1} [40].

A study of trace elements in quartz by LA-HR-ICP-MS using an external calibration with the three SRMs NIST 612, NIST 614, and NIST 616 reported limits of detection for $^{56}Fe^+$ of 2.6 μg g^{-1} in medium mass resolution [41]. Iron detection limits on the order of pg g^{-1} were reported for analyses of water, plant, tissue, and rock samples in medium mass resolution by a HR-SF-ICP-MS. The MDLs for iron in oyster tissue/tomato leaves and rock sample digestion blanks were reported to be 113 pg g^{-1} and 3940 pg g^{-1} for $^{56}Fe^+$, and 580 pg g^{-1} and 10600 pg g^{-1} for $^{57}Fe^+$ respectively [42].

Although there are reports of iron detection limits with both ICP-MS systems, at the present there is no existing data that compares the detection limits for $^{56}Fe^+$ and $^{57}Fe^+$ in glass samples using those techniques utilizing both laser ablation and solution introduction methods. The capability of resolving or reducing the iron polyatomic interferences by using the DRC and high resolution systems will allow for a more optimized use of Fe for the discrimination of glass samples.

This work was conducted to evaluate the method detection limits (MDL) that can be achieved for Fe using different ICP-MS systems (Quadrupole, Dynamic Reaction Cell and High Resolution) for solution and laser ablation sampling introduction methods of glass standard reference materials (SRMs). This work includes the assessment of precision and accuracy for iron measurements to evaluate the possibility of including iron in routine forensic analyses of glass samples by ICP-MS.

Experimental

Laser Ablation Analyses. Glass standard reference material (SRM) NIST 612 (National Institute of Standards and Technology, Gaithersburg, MD, USA) was used for laser ablation analyses with both ICP-MS systems using all configurations. SRM NIST 610 (National Institute of Standards and Technology, Gaithersburg, MD, USA) and the FGS glass standards, described elsewhere [43] , were used as external calibrators for some experiments using a NewWave UP 213 laser ablation system (Fremont, CA, USA) and argon as the carrier gas. Method detection limits were calculated for $^{56}Fe^{+}$ and $^{57}Fe^{+}$ using SRM NIST 612. Standard reference materials (SRMs) NIST 1831, NIST 614 and the FGS standards were analyzed to evaluate the accuracy and precision of the method. For a proper assessment of LA experiments using the ELEMENT 2 high resolution ICP-MS (Thermo Electron Co. Bremen, Germany) and the ELAN DRC II (PerkinElmer, LAS, Shelton, CT, USA), other SRMs were used in place of SRM 612 since the former was used as an external calibrator in the data reduction analyses. For practical purposes only the results of the SRM FGS1 will be presented for all the laser ablation ICP-MS systems.

The total analysis time was of approximately 170 seconds. During the first 55 seconds the laser was blocked (via the use of a shutter) and the signal of the "blank" was acquired in order to account for the background level. The laser was then fired for 60 seconds, but only the middle-latter 40 seconds of the ablation signal were used for measurements due to the inherent instability caused when the laser first interacts with a sample. Following these 60 seconds the laser was turned off and the signal was recorded for an additional 55 seconds to purge any signal carryover between samples. Seven sample replicates of either SRM NIST 612 on two non-consecutive days were used to determine the MDLs of LA analyses. Figure 1 shows the transient signal of $^{56}Fe^{+}$ during a typical analysis. The Glitter software (GLITTER, GEMOC, Macquarie University, Australia) was used for data reduction to determine concentration and the MDLs. Glittter software enables plotting the transient signal collected from the LA analysis and to select the background and signal intervals for data reduction. To determine the concentration the Glitter software uses Equation 1, where $conc_{ni}$ is the concentration of element **i** in analysis **n**, cps_{nij} is the mean count rate (background subtracted) of isotope **j** of **i** in analysis **n**, $abundance_j$ is the natural abundance of isotope **j**, and $yield_{ni}$ is the cps per ppm of element **i** in analysis **n**. The $yield_{ni}$ is calculated using Equation 2, where $yield_{ns}$ is the cps per ppm of the internal standard **s** in analysis **n**, $Int(yield_{ni}/yield_{ns})^{std}$ is the ratio of the yield of element **i** in analysis **n** to the yield of the internal standard **s** in analysis **n** interpolated over the standard analyses.

$$conc_{ni} = (cps_{nij} / abundance_j) / (yield_{ni}) \qquad \textbf{Eq.1}$$

$$yield_{ni} = yield_{ns} * Int(yield_{ni} / yield_{ns})^{std} \qquad \textbf{Eq.2}$$

Glitter software uses Equation 3 to calculate the limits of detection with 99% confidence level based on Poisson counting statistics. In the Equation 3 B is the total counts in the background interval.

$$MDL = 2.3 * \sqrt{2B} \qquad \textbf{Eq. 3}$$

The LA data analysis were performed using SRM NIST 612, SRM 610 or SRM FGS2 as a single point external calibrator. For all the analytical determinations ^{29}Si was used as the internal standard, except for the DRC experiments where ^{24}Mg was chosen as the internal standard.

The glass SRMs were rinsed with high purity deionized water and dried overnight prior the LA analysis

Solution Analyses. High purity standards (CPI International, Santa Rosa, California, USA) were used for the preparation of the external calibration curves. Optima grade nitric acid (HNO_3), hydrofluoric acid (HF), hydrochloric acid (HCl) [Fisher Scientific Pittsburg, USA], and high purity deionized water (>18MΩcm^{-1}) was used for samples dilutions, and for the preparation of the calibration curve solutions. Rhodium was used as an internal standard for all solutions analyzed.

Standard reference materials (SRMs) NIST 612, NIST 1831, NIST 614 (National Institute of Standards and Technology, Gaithersburg, MD, USA), and the standards FGS1 and FGS2 were digested following the ASTM E2330-04 standard method for trace elemental analysis of glass using ICP-MS to determine the accuracy and precision of the analysis [27]**.**

The samples were washed first in methanol for 10 minutes, then with HNO_3 1.6 mol L^{-1} for 30 minutes, followed by rinsing with high purity water (>18 MΩ cm^{-1}). After rinsing, they were left to dry overnight. Glass samples were crushed and weighed to approximately 2 mg ± 1 μg into 5 mL polypropylene tubes. Trace elemental grade (optima grade) nitric (HNO_3), hydrofluoric acid (HF) and hydrochloric acid (HCl) [Fisher Scientific Pittsburg, USA] were used for the digestion of glass. Samples were sonicated for 2 hours before the drying process into the dry heater block (Dry Digital Bath Incubator, Boekel Scientific, Feasterville, PA, USA). After the samples were taken to complete dryness, they were reconstituted with 0.8 mol L^{-1} HNO_3, the internal standard and high purity water. Dilutions of the reconstituted digested glass samples were prepared and measured along with seven reagent blanks that were treated in the same way as the glass samples.

The calibration curves were prepared from single element high purity standards (1000 μg g^{-1}) [CPI International, Santa Rosa, California, USA]. Rhodium was added as internal standard to a final concentration of 3 ng g^{-1}, 3 ng g^{-1} and 50 ng g^{-1} for the HR-SF-ICP-MS, DRC mode ICP-MS and standard mode ICP-MS calibration curves respectively. Calibration curves had seven calibration points in a range of 0-10 ng g^{-1} for the ELEMENT 2 and ELAN DRC Mode, and from 0-100 ng g^{-1} for ELAN STD mode analyses. Two control verification checks (at 3 and 5 ng g^{-1} for ELEMENT 2 and ELAN DRC mode and at 7 and 25 ng g^{-1} for the ELAN standard mode) were run with samples in order to evaluate drift and precision over time. All sample preparations and analyses were performed in a normal laboratory environment.

The glass samples were measured against an external calibration curve. The intensities (cps) for the standards and samples were normalized to the rhodium (internal standard) signal (cps). A linear regression line was determined from the plot of the normalized signal (cps) against the concentration of the correspondent standard and the concentrations in the samples were determined by using the slope and intercept of this equation.

The iron MDLs on solution analyses of SRM NIST 612 were determined by using the standard deviation of the blank's signal and the slope of the calibration curve. MDLs were determined with at least 7 replicates of reagent blanks measured in two non-consecutive days in order to account for inter-day variations.

In order to compare the MDLs obtained from laser and solution work, the MDLs for solution are referred to the concentration on glass assuming and average weight of 2mg of glass diluted into 4mL after acid digestion [27]. Therefore, MDL obtained in $\mu g\ L^{-1}$ were multiplied by a factor of 2 to be reported in $\mu g\ g^{-1}$ on glass.

Precision and accuracy of LA and solution analyses. The accuracy of the analyses was determined by comparing the SRMs NIST 612, NIST 1831, standards FGS1 and FGS2 experimental values of iron with the certified and/or consensus values. Precision was determined by calculating the relative standard deviation (%RSD) of 5 sampling replicates on each glass sample. The method was evaluated with an accuracy of $\leq$10% bias from the consensus or certified value, and a precision of $\leq$10% RSD.

Instrumentation

Laser systems. Two different Nd:YAG laser units were used for this work: 1) a *New Wave UP- 213* operating at 213nm (New Wave Research, Fremont, CA, USA) and 2) a *CETAC LSX 200+* (CETAC Technologies, Omaha, NE, USA) operating at 266nm. Laser ablation parameters are further described in Table 1. The laser ablation systems were operated under different parameters using both helium and argon as a carrier gas, and different ablation cell volumes. The experimental parameters were optimized for each system.

ICP-MS systems. The ICP-MS instruments used for this study were an ELAN DRC II ICP-MS (PerkinElmer, LAS, Shelton, CT, USA) and a HR-SF-ICP-MS ThermoFinnigan ELEMENT 2 (Thermo Electron Co. Bremen, Germany). The DRC-ICP-MS was equipped with a quartz cyclonic spray chamber and a concentric tube pneumatic nebulizer. The sample intake rate into a concentric nebulizer and cyclonic spray chamber was 1 mL min^{-1} An ASX 510 autosampler (CETAC Technologies, Omaha, NE, USA) was coupled to the ICP-MS for the solution analyses. For laser ablation analyses, the laser systems were connected to the torch intake of the ICP-MS. The DRC-ICP-MS was operated in STD mode and DRC mode. The removal of $^{56}Fe^{+}$ polyatomic interferences was achieved by using methane as a reactant gas in the DRC mode. Methane is often used as reactant gas for the removal Fe interferences [44-45]. Preliminary results in our laboratory showed better sensitivity on the detection of $^{56}Fe^{+}$ with methane as reactant gas. The removal of the refractory interference CaO^{+} was improved significantly with methane than with other gases in glass matrix. It seems that methane works better for the

removal of $^{56}Fe^{+}$ interference CaO^{+} in Ca –rich matrices. Additionally for safety reasons it is more convenient to work with methane than with ammonia gas. For solution analyses the HR-SF-ICP-MS sample introduction setup included a quartz cyclonic spray chamber with a microflow PFA-ST nebulizer (400 µL min^{-1} intake flow) [ESI Scientific, NE, USA] and a 1.5 mm quartz injector connected to a quartz torch CD-type for removable injector (ESI Scientific, Omaha, NE, USA). The laser systems were connected to a 1.75 mm quartz injector inserted into the torch. The HR-SF-ICP-MS system was used in the three mass resolutions available: low (R~ 300), medium (R~ 4000) and high (R~10000).

Before conducting each experiment, the instruments were optimized for sensitivity (maximum counts per second) and for doubly charged species (≤3%) and oxides (≤0.3%). An additional optimization in LA analyses of the ratio U/Th on SRM 612 was also conducted as a measure of fractionation levels (with ~1 ± 0.2 determined to be acceptable).

Results and Discussion

Three main ICP-MS configurations were used to evaluate the method detection limits of iron in glass analysis: ICP-MS STD mode, ICP-MS DRC mode and HR-SF-ICP-MS, where the latter two were used to reduce the polyatomic interferences associated with Fe measurements. MDLs were evaluated with laser ablation and solution modes since these are the two major sampling introduction methods routinely used in forensic laboratories for elemental analysis. Two laser systems were operated with helium and argon separately as carrier gases in order to account for the effects of laser wavelengths on the sensitivity. The ablation process and the efficiency of particles

transportation into the ICP-MS are important factors affecting the sensitivity and limits of detection. It is been reported that the use of helium as carrier gas have improved the sensitivity and limits of detection of several trace elements [46-47]. Table 1 shows the experimental parameters used for each ICP-MS configuration.

Both isotopes $^{56}Fe^{+}$ and $^{57}Fe^{+}$ were analyzed, however the target isotope in this study was $^{56}Fe^{+}$ since it has a greater abundance than $^{57}Fe^{+}$ (91.72% vs 2.2%). Iron interferences represent an analytical challenge for standard ICP-MS systems because polyatomic interferences containing argon (a property of the ICP) and calcium (a major component in glass) are present at very high levels.

Method Evaluation for Solution Based and Laser Ablation Analyses

Analytical performance of DRC vs. STD mode

Analytical performance of the method was evaluated in terms of limits of detection, accuracy and precision. For solution analysis in STD mode, $^{57}Fe^{+}$ concentration on the standard FGS1 was considerably high compared to the consensus value meaning the interferences produced were not efficiently removed in this mode possibly due to high abundances of argon hydroxide interferences. This effect of the interferences in standard mode is more pronounced at low concentration levels of iron such as in the case of SRM 612 were iron is only present at 56.3 $\mu g\ g^{-1}$. By using the DRC mode, the iron interferences were properly reduced leading to an accurate measurement of $^{56}Fe^{+}$ when compared to the consensus value ($580 \pm 60\ \mu g\ g^{-1}$) with a bias and a precision of less than 10 % (Table 2). The target mass to reduce interferences on DRC with methane is iron of mass 56 for its possible application on routinely forensic

analysis of glass. Iron of mass 57 was not measured in the DRC mode; therefore the effect on reducing the main interferences on this mass was not optimized. In the LA analyses with the STD mode and different carrier gases, $^{57}Fe^{+}$ produced better accuracy than in solution based analyses. This is because in LA mode, a dry plasma contains much less hydroxide interferences such as $^{40}Ca^{16}O^{1}H^{+}$, $^{40}Ar^{16}O^{1}H^{+}$. For the analysis of $^{56}Fe^{+}$ in the DRC Mode the interferences were efficiently reduced leading to a good accuracy of <10% bias and a precision of the measurements of < 10%RSD (Table 3).

Analytical performance of HR-SF-ICP-MS in different resolution modes

Interferences of $^{57}Fe^{+}$ were not properly resolved for solution analyses with the ELEMENT 2 in low resolution mode due to the larger amount of hydroxides present in wet plasma. Hydroxides species $^{40}Ca^{16}O^{1}H^{+}$ and $^{40}Ar^{16}O^{1}H^{+}$ in solution based analyses of $^{57}Fe^{+}$ in LR mode were a contribution factor for the significant increase in its measured concentration with respect to the consensus value for FGS1. Therefore the results for iron of mass 57 in LR mode were not reported. The accuracy and precision of $^{57}Fe^{+}$ measurements were improved in medium resolution (MR) and high resolution (HR) with less than 10 % bias and less than 10 % RSD for precision (Table 2).

For most of the laser ablation experiments using HR-SF-ICP-MS with the three mass resolutions, the polyatomic interferences of $^{56}Fe^{+}$ and $^{57}Fe^{+}$ were properly resolved providing accurate concentration measurements of iron in the standard FGS1. Accuracy and precision of the analyses in all the mass resolutions were within the acceptable parameters (≤10% bias and ≤10% RSD) (Table 3).

In general, solution based and laser ablation accuracy and precision results with the different ICP-MS configurations were in agreement. The results showed improved accuracy on the DRC and HR-SF ICPMS being medium resolution the optimum resolution and optimal setting for $^{56}Fe^{+}$ measurement. The method was properly assessed giving validity to the MDLs results obtained during these experiments.

Method Detection Limits of Solution Based and Laser Ablation Analyses

The iron method detection limits in DRC mode were significantly lower than in standard mode (0.03 vs 9.5 µg g^{-1} for laser ablation and 0.33 vs 1.9 µg g^{-1} for solution based analyses). This demonstrates the ability of DRC with eliminating interferences, reducing the limits of detection and allowing for more certainty in iron determinations in glass matrices. Higher background levels in solution and laser ablation analyses in the STD mode contribute to higher detection limits of $^{57}Fe^{+}$.

The use of a high resolution sector field ICPMS resolved the polyatomic interferences in iron. Low MDLs for both iron isotopes were achieved in laser ablation analyses using the ELEMENT 2, particularly in medium resolution for $^{56}Fe^{+}$. Higher MDLs in HR could be attributed to the increase in resolution which decreases the sensitivity, therefore affecting the limits of detection (Table 4). When comparing the MDLs results in MR and HR using the two laser systems, higher detection limits were observed with the NW UP213 laser system. The differences in the ablation process (ie. amount of mass ablated) due to the lasers energies and spot size could contribute to these variations in MLDs. Regardless, the MDL values are comparable (Table 4). In the low resolution mode, high background levels contributed to the increase in the detection

limits. This pattern was also observed for the STD mode in the quadrupole instrument.

The solution-based analyses with the HR-SF-ICP-MS showed an improvement in the MDLs of both iron isotopes in medium and high resolutions vs. low resolution. In the quadrupole system the use of DRC allowed to achieve MDLs of 0.30 μg g^{-1} for $^{56}Fe^{+}$ (Table 5). In MR and HR, the interference signals are properly separated from the iron signals, while in the DRC mode, the polyatomic interferences are significantly reduced by chemical reaction but may not be completely removed.

In solution based analyses higher MDLs for $^{56}Fe^{+}$ were obtained than with laser ablation. Differences in the MDLs could be attributed to the dilution factor and the possible increase in background contribution due to the digestion process in solution analyses.

Carrier Gas Effect on Laser Ablation MDLs with the ELEMENT 2 and ELAN DRC II ICP-MS Systems

MDLs for both iron isotopes obtained with the CETAC LSX 200+ laser coupled to the HR-SF-ICP-MS were not significantly different at low and high resolutions when argon or helium were used as the carrier gas. Slightly lower MDLs were obtained for $^{56}Fe^{+}$ and $^{57}Fe^{+}$ when helium carrier gas was used in medium resolution. Experiments performed with the New Wave UP 213 laser coupled to the HR-SF-ICP-MS showed similar MDLs for $^{57}Fe^{+}$ and $^{56}Fe^{+}$ with helium and argon carrier gases in medium and high resolution. In low resolution higher MDLs were obtained when using argon as carrier gas because of the higher background produced with this laser of lower energy (2.4mJ vs. 4.8mJ for the CETAC LSX 200+).

With the ELAN DRC II, the carrier gas effect was more significant. Lower detection limits are achieved when helium was used as the carrier gas. MDLs determined for iron isotopes in the ELAN DRC II with both carrier gases were comparable with what was observed in MR with the ELEMENT 2 with both laser ablation systems/carrier gas combinations.

For laser ablation analysis in glass matrix, helium as carrier gas has proven to increase the sensitivity in the detection of elements. The improvement in sensitivity is attributed to a more efficient particle removal and transportation into the ICP-MS [46-47]; therefore lower detection limits are achievable.

Conclusions

Polyatomic interferences for iron were significantly reduced or resolved with both DRC-ICP-MS and HR-SF-ICP-MS. Method limits of detection as low as ~0.03 µg g^{-1} were achieved with both DRC and the SF instruments using laser ablation mode in glass matrices (Table 4). DRC-ICP-MS provided an excellent tool to achieve low MDLs for Fe in both laser ablation and solution analyses, but it is limited to the analysis of few elements in the DRC mode since the suppression of interferences is chemically dependent and other interferences could be formed in the cell that affect the analysis. From a practical point of view, this limitation requires separate measurements for Fe and for the other elements typically used in glass comparisons, especially when LA is involved since the transition from DRC to non-DRC mode is not fast enough for transient signals. The need of performing separate analysis for Fe and for the rest of the elements used in glass analysis is not only time consuming but also requires more sample. An advantage of

DRC-ICP-MS over HR-SF-ICP-MS is its lower costs and ease of use.

HR-SF-ICP-MS allowed for the resolution of iron interferences in both medium and high resolutions. In laser ablation, the lower MDLs were achieved using medium resolution since in high resolution the sensitivity is significantly reduced, affecting the detection limits. In solution analyses, the HR-SF-ICP-MS system at MR provides lower detection limits than DRC-ICP-MS (0.14 $\mu g\ g^{-1}$ vs. 0.30 $\mu g\ g^{-1}$ respectively). Advantages of HR-SF-ICP-MS vs. DRC-ICP-MS instruments include its capability to achieve lower MDLs for Fe (particularly in laser ablation introduction method) and its capability to conduct multielemental analysis using laser ablation. Nevertheless, the fast transient signal measured in laser ablation does not allow to switch from different resolution modes in the same method, therefore the multielemental analysis is restricted to one resolution mode in the sector field instrument. The detection limits of some elements may be affected in medium and high resolution because an increasing the resolution results in sacrificing the analytical sensitivity. These are important factors when considering using laser ablation with the sector field instrument.

Solution and LA analyses with the different ICP-MS instrumental setups provide accurate and precise measurements of the iron isotopes. The accuracy and precision in a multielemental analysis could be affected when the DRC-ICP-MS is used. The reactant gas could react with other isotopes of interest within the glass matrix causing problems in their detection. Although similar MDLs can be achieved with helium or argon as carrier gas in the LA-HR-SF-ICP-MS systems, lower detection limits could be obtained with helium.

This work demonstrates the capabilities of these ICP-MS systems and setups to

resolve and/or reduce polyatomic interferences allowing for accurate and precise measurements of iron isotopes in glass matrices. Although there were some differences in MDLs for each of the LA setups and ICP-MS systems, these results open the possibilities of doing elemental analysis which includes the use of iron isotopes in routine casework analysis of glass.

Acknowledgments

This work was supported by the National Institute of Justice (NIJ), grant 2005-IJ-CX-K069. The HR-SF-ICP-MS was acquired with a National Science Foundation (NSF) Major Research Instrumentation (MRI) award 0420874 to Florida International University. The Florida International University and the FIU Dissertation Year Fellowship are also acknowledged.

References

1. Pearce NJ, Perkins WT, Westgate JA, Gorton MP, Jackson SE, Neal CR and Chenery SP (1997) Geostandard Newslett 21:115-144

2. Brown G (1985) J Forensic Sci 39:806-813

3. Almirall JR, Cole M, Gettinby G, Furton K (1998) Science & Justice 38:93-100

4. American Society for Testing Materials (E1967-98 R03)- Standard test method for the automated determination of refractive index of glass samples using the oil immersion method and a phase contrast microscope; In *ASTM Annual Book of ASTM Standards*, Vol 14.2; American Society for Testing Materials: West Conshohocken, PA; p664; 2003

5. Locke J (1987) Microscope 35:151

6. Duckworth DC, Bayne CK, Morton DJ, Almirall JR (2000) J Anal At Spectrom 15: 821

7. Montero S, Hobbs AL, French TA, Almirall JR (2003) J Forensic Sci 48:1101-1107

8. Koons RD, Peters CA, Rebbert PS (1991) J Anal At Spectrom 6:451

9. Parouchais T, Warner IM, Palmer LT, Kobus II (1996) J Forensic Sci 41:351

10. Almirall JR, Manslaughter caused by a hit and run: glass as evidence of association; In Ilouck M(Ed): *Mute Witness: Trace evidence analysis*; Academic Press: San Diego, CA, p139; 2001

11. Buscaglia J (1994) Anal Chim Acta 288:17-24

12. Thornton JI, Langhauser C, Kehane D (1984) J Forensic Sci 29:711

13. Catterick T, Wall C (1978) Talanta 25:573-577

14. Catterick T, Hughes J, Southeard G (1976) J Forensic Sci 8:217-227

15. Almirall JR: Elemental Analysis of glass fragments; In Caddy B (Ed.): *Forensic Examination of Glass and Paint*, Taylor and Francis: London, NY; p65-83; 2001

16. Ryland S (1986) J Forensic Sci 31:1314

17. Dudley RJ, Howden CR, Taylor TJ, Smalldon KW (1980) X-ray Spectrom 9:119

18. Coleman RF, Goode GC (1973) J Radioanal Chem 15:367-388

19. Jembrih D, Schreiner M, Peev M, Krejsa P, Clausen C (2000) Mikrochimica Acta 133(1-4): 151-157

20. Brozek-Mucha Z, Zadora G (1998) Institute of Forensic Research, Z Zagadnien Nauk Sadowych 37:68-89

21. Andrasko J, Maehly A (1978) J Forensic Sci 23(2):250-262

22. Hickman DA (1981) Forensic Sci Int 17:265

23. Hickman DA (1987) Forensic Sci Int 33:23

24. Almirall JR: The evaluation of glass evidence by statistical analysis of inductively coupled plasmaatomicemission spectroscopy and refractive index data- Ph.D. dissertation; University of Strathclyde: Glasgow, U.K.;1998

25. Suzuki, Y.; Sugita, R.; Suzuki, S.; Marumo, Y. *Anal. Sci.* **2000**, 16, 1195.

26. Zurhaar A, Mullis L (1990) J Anal At Spectrom 5:611

27. American Society for Testing Materials (E2330-04)- Standard test method for the determination of trace elements in glass using inductively coupled plasma mass spectrometry. In *ASTM Annual Book of ASTM Standards*, Vol 14.2 ; American Society for Testing Materials: West Conshohocken, PA; p1; 2004

28. Beary ES, Paulsen P (1993) Anal Chem 65:1602-1608

29. Trejos T, Montero S, Almirall JR (2003) Anal Bioanal Chem 376(8):1255-1264

30. Latkoczy C, Becker S, Ducking M, Günther D, Hoogewerff JA, Almirall JR, Buscaglia J, Dobney A, Koons RD, Montero S, van der Peijl GJQ, Stoecklein WRS, Trejos T, Watling JR, Zdanowicz VS (2005) J Forensic Sci 50(6):1327-1341

31. Watling RJ, Lynch BF, Herring D (1997) J Anal At Spectrom 12(2):195-203

32. Bajic SJ, Aeschliman DB, Saetveit NJ, Baldwin DP, Houk RS (2005) J Forensic Sci 50(5):1123-1127

33. Copley J, Almirall JR: In Caddy B (Ed): *Forensic Examination of Glass and Paint*, Taylor and Francis: London, NY; pp 39, 67 (chapter 2 and 4); 1999

34. Koons RD, Fieldler C, Rawalt RC (1988) J Forensic Sci 33(N1):49-67

35. Nonose NK (2001) J Anal At Spectrom 16:560-566

36. Weyer S, Schwieters JB (2003) Int J Mass spectrom 226:355-368

37. Umpierrez S, Trejos T, Neubauer K, Almirall J (2006) At Spectr 27(3): 76-79

38. Gürleyük H, Brunette RC, Howard CR, Schneider C, Thomas R (2005) Spectrosc 20(1):22-29

39. Balcaen L, Geuens I, Moens L, Vanhaecke F (2003) Anal Bioanal Chem 377:1020-1025

40. Günther D, Hattendorf, Audétat A (2001) J Anal At Spectrom 16:1085-1090

41. Flem B, Larsen RB, Grimstvedt A, Mansfeld J (2002) Chem Geol 182:237-247

42. Townsend AT (2000) J anal At Spectrom 15:307-314

43. Becker S, Ducking M, Watzke P, Stoecklein W (2003) Forensic Sci Int 136:361

44. Hill SJ, Ford MJ, Ebdon L (1992) J Anal At Spectrom 7:1157-1165

45. Rowan JT, Houk RS (1989) Appl Spectrosc 43(6):976-980

46. Günther D, Heinrich CA (1999) J Anal At Spectrom 14:1363-1368

47. Horn I, Günther D (2003) Applied Surface Sci 207(1-4): 144-157

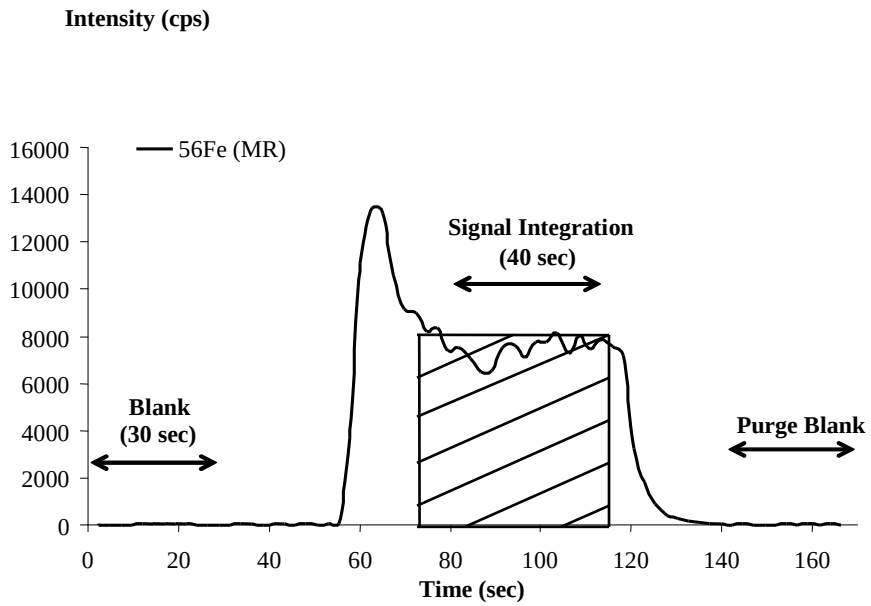

Figure 1. A typical laser ablation transient signal of iron in SRM NIST 612 analyzed with the ELEMENT 2.

Table 1. Instrumental parameters used for the MDL experiments.

LASER SYSTEMS			ICP-MS SYSTEMS			
Parameters	***CETAC LSX 200+***	***New Wave UP 213***	**Parameters**	***ELAN DRC II (STD mode)***	***ELAN DRC II (DRC mode)***	***ELEMENT 2***
Wavelength	266 nm	213 nm	**Auxiliary Gas**	1.1 L min^{-1}	1.0 L min^{-1}	0.8 L min^{-1}
Spot Size	100 μm	100 μm	**Ablation Cell Carrier gas**	0.90 L min^{-1} (laser, He) 0.80 L min^{-1} (laser, Ar)	0.90 L min^{-1} (laser, Ar)	0.60-0.72 L min^{-1} (laser, Ar) 1.0-1.1 L min^{-1} (laser, He)
Energy Output	4.8 mJ	2.4 mJ	**Nebulizer Flow**	1.0 L min^{-1} (solution)	1.0 L min^{-1} (solution)	1.0 L min^{-1} (solution)
Repetition Rate	10 Hz	10 Hz		0.98 L min^{-1} (laser)	0.98 L min^{-1} (laser)	0.62-0.70 L min^{-1} (laser)
Carrier gas	Ar or He	Ar or He	**RF Power**	1500 W (solution) 1550 W (laser)	1501 W (solution) 1550 W (laser)	1300 W (solution) 1350 W (laser)
Ablation Cell Volume	50.2 mL	30.0 mL	**Reaction Gas**	-	CH_4	-
			Reaction Gas Flow	-	0.5 L min^{-1}	-
			RPq	-	0.5 (laser) 0.6 (solution)	-
			Resolution Modes	-	-	Low, Medium and High

-Not applicable.

Table 2. Results of accuracy (%bias) and precision (%RSD) for solution based analyses for standard FGS1.

	ELAN STD Mode			ELAN DRC Mode		
Isotope	**Average ± σ**	**%RSD**	**[a] %Bias**	**Average ± σ**	**%RSD**	**[a] %Bias**
^{57}Fe	699 ± 9	1.3	21	-	-	-
^{56}Fe	-	-	-	554 ± 58	10	5

	E2 in MR			E2 in HR		
Isotope	**Average ± σ**	**%RSD**	**[a] %Bias**	**Average ± σ**	**%RSD**	**[a] %Bias**
^{57}Fe	544 ± 52	10	6	529 ± 13	3	9
^{56}Fe	542 ± 61	11	7	521 ± 10	2	10

[a] Bias was determined using the consensus value of Fe: 580 ± 60 μg g^{-1} [30]

-Not determined.

Table 3. Results of accuracy (%bias) and precision (%RSD) for LA analyses for standard FGS1.

(ELEMENT 2 -New Wave UP213 laser)

	E2 in LR (Ar)			E2 in MR (Ar)			E2 in HR (Ar)		
Isotope	**Average ± σ**	**%RSD**	**[a] %Bias**	**Average ± σ**	**%RSD**	**[a] %Bias**	**Average ± σ**	**%RSD**	**[a] %Bias**
^{57}Fe	557 ± 25	5	4	619 ± 5	1	7	630 ± 8	1	9
^{56}Fe	-	-	-	629 ± 11	2	8	636 ± 22	3	10

(ELEMENT 2 -New Wave UP213 laser)

	E2 in LR (He)			E2 in MR (He)			E2 in HR (He)		
Isotope	**Average ± σ**	**%RSD**	**[a] %Bias**	**Average ± σ**	**%RSD**	**[a] %Bias**	**Average ± σ**	**%RSD**	**[a] %Bias**
^{57}Fe	631 ± 15	6	9	602 ± 17	3	4	561 ± 39	3	3
^{56}Fe	-	-	-	609 ± 23	2	5	556 ± 8	2	4

(ELEMENT 2 -CETAC LSX 200+)

	E2 in LR (Ar)			E2 in MR (Ar)			E2 in HR (Ar)		
Isotope	**Average ± σ**	**%RSD**	**[a] %Bias**	**Average ± σ**	**%RSD**	**[a] %Bias**	**Average ± σ**	**%RSD**	**[a] %Bias**
^{57}Fe	613 ± 14	2	6	650 ± 13	2	12	565 ± 4	1	3
^{56}Fe	-	-	-	641 ± 3	0.5	11	648 ± 5	1	12

(ELEMENT 2 -CETAC LSX 200+)

	E2 in LR (He)			E2 in MR (He)			E2 in HR (He)		
Isotope	**Average ± σ**	**%RSD**	**[a] %Bias**	**Average ± σ**	**%RSD**	**[a] %Bias**	**Average ± σ**	**%RSD**	**[a] %Bias**
^{57}Fe	561 ± 16	3	3	613 ± 22	4	6	544 ± 40	7	6
^{56}Fe	-	-	-	547 ± 16	3	6	636 ± 12	2	10

[a] Bias was determined using the reference value of Fe: 580 ± 60 μg g^{-1} [30]

-Not determined.

Table 4. MDLs for SRM NIST 612 laser ablation analyses of $^{56}Fe^{+}$ and $^{57}Fe^{+}$ using the different ICP-MS configurations.

MDLs ± σ for Laser Ablation Analyses in μg g^{-1} (ELEMENT 2 -LSX 200+ laser)

Isotope	E2 in LR (Ar)	E2 in MR (Ar)	E2 in HR (Ar)	E2 in LR (He)	E2 in MR (He)	E2 in HR (He)
^{57}Fe	2.3 ± 0.1	0.40 ± 0.04	1.5 ± 0.5	2.4 ± 0.1	0.23 ± 0.06	1.2 ± 0.6
^{56}Fe	-	0.055 ± 0.003	0.15 ± 0.01	-	0.037 ± 0.003	0.11 ± 0.03

MDLs ± σ for Laser Ablation Analyses in μg g^{-1} (ELEMENT 2 -New Wave UP213 laser)

Isotope	E2 in LR (Ar)	E2 in MR (Ar)	E2 in HR (Ar)	E2 in LR (He)	E2 in MR (He)	E2 in HR (He)
^{57}Fe	8.3 ± 0.9	0.9 ± 0.4	3.6 ± 0.6	3.5 ± 0.3	0.8 ± 0.2	3.9 ± 1.2
^{56}Fe	-	0.12 ± 0.01	0.3 ± 0.1	-	0.085 ± 0.007	0.29 ± 0.05

MDLs ± σ for Laser Ablation Analyses in μg g^{-1} (ELAN DRC II -New Wave UP213 laser)

Isotope	ELAN STD mode (He)	ELAN STD mode (Ar)	ELAN DRC mode (He)	ELAN DRC mode (Ar)
^{57}Fe	9.5 ± 1.0	9.6 ± 2.0	-	-
^{56}Fe	-	-	[a] 0.025 ± 0.003	0.6 ± 0.2

[a] Data published from a previous study [37]

-Not determined.

Table 5. MDLs results for solution analyses of $^{56}Fe^{+}$ and $^{57}Fe^{+}$ using the different ICP-MS systems.

MDLs ± σ for Solution Analyses in μg g^{-1} (ELEMENT 2)

Isotope	E2 in MR	E2 in HR
^{57}Fe	0.19 ± 0.12	0.58 ± 0.10
^{56}Fe	0.14 ± 0.06	0.62 ± 0.11

MDLs ± σ for Solution Analyses in μg g^{-1} (ELAN DRC II)

Isotope	ELAN STD mode	ELAN DRC mode
^{57}Fe	1.9 ± 1.2	-
^{56}Fe	-	0.30 ± 0.04

-Not determined.

VITA

WALESKA CASTRO

October 1977	Mayagüez, Puerto Rico, USA
December 2002	M.Sc. in Chemistry University of Puerto Rico Mayagüez Campus Mayagüez, Puerto Rico, USA
Jan 2003	Lecturer of General Chemistry Department Chemistry University of Puerto Rico Mayagüez Campus Mayagüez, Puerto Rico, USA
July 2008	Research Associate Materials Characterization Laboratory Earth and Environmental Systems Institute The Pennsylvania State University University Park, PA, USA

PUBLICATIONS

Castro, W.; Trejos, T.; Naes, B.; Almirall, J. Comparison of high-resolution and dynamic reaction cell ICP-MS capabilities for forensic analysis in glass. *Anal Bioanal Chem* **2008**, *392*, 663–672

Almirall, J.R.; Umpierrez, S.; Castro, W.; Gornushkin, I.; Winefordner, J. Forensic elemental analysis of materials by laser induced breakdown spectroscopy (LIBS). *Proceedings of SPIE-The International Society for Optical Engineering* **2005**, 5778, 657-666.